Check for updates

EcoMat

WILEY

EcoMat
FUNCTIONAL MATERIALS FOR GREEN ENERGY AND ENVIRONMENT

REVIEW OPEN ACCESS

Recent Trends in Conjugated Polymer-Based Thermoelectrics From Materials to Device

Daegun Kim[1] | Hoimin Kim[2] | Jeong-Min Seo[2] | Il Jeon[2,3,4,5,6] | Hansol Lee[1] | Boseok Kang[2,5,6]

[1]School of Chemical, Biological and Battery Engineering, Gachon University, Seongnam, Republic of Korea | [2]SKKU Advanced Institute of Nanotechnology (SAINT), Sungkyunkwan University (SKKU), Suwon, Republic of Korea | [3]SKKU Global Research Center (SGRC), Sungkyunkwan University, Suwon, Republic of Korea | [4]New Industry Creation Hatchery Center (NICHe), Tohoku University, Sendai, Japan | [5]Department of Nano Engineering, Sungkyunkwan University, Suwon, Republic of Korea | [6]Department of Semiconductor Convergence Engineering, Sungkyunkwan University, Suwon, Republic of Korea

Correspondence: Il Jeon (il.jeon@skku.edu) | Hansol Lee (hlee22@gachon.ac.kr) | Boseok Kang (bskang88@skku.edu)

Received: 1 July 2025 | **Revised:** 20 August 2025 | **Accepted:** 30 August 2025

Funding: This work was supported by National Research Foundation of Korea (RS-2023-NR076607, RS-2024-00403639, RS-2025-00516030, RS-2025-25413074, RS-2025-23523476).

Keywords: conjugated polymers | doping | flexible thermoelectric generators | molecular engineering | organic thermoelectrics

ABSTRACT

This comprehensive review provides an in-depth examination of recent advances in thermoelectric (TE) materials based on conjugated polymers (CPs), emphasizing strategies aimed at enhancing their performance for energy harvesting applications. CP-based TE materials have garnered significant interest due to their inherently low thermal conductivity, mechanical flexibility, lightweight nature, and the easy tunability of molecular structures. Despite these advantages, their commercialization remains limited by challenges such as modest TE performance and insufficient long-term stability. This review explores key progress in molecular design, structural engineering, and doping strategies that have led to notable improvements in critical parameters such as electrical conductivity, Seebeck coefficient, and power factor, collectively enhancing the TE figure of merit (ZT). In addition, the article traces the historical development of CP-based flexible TE generators for wearable and portable electronics, underscoring the importance of bridging the gap between material TE properties, mechanical properties, and device realization.

1 | Introduction

The thermoelectric (TE) effect refers to a direct conversion of thermal energy to electricity and vice versa in a single material, the phenomena of which are called the Seebeck effect and the Peltier effect, respectively. The Seebeck effect, discovered by Thomas J. Seebeck in 1821, generates an electrical potential difference as a result of a temperature difference which induces a thermal diffusion of charge carriers in a conductor or semiconductor [1]. Thermoelectric generators (TEGs) generate electricity based on the Seebeck effect, harnessing thermal energy. TEGs are considered a promising candidate for clean energy generation for converting waste heat, which is the product of any energy conversion processes in plants, factories, and even the other energy harvesting technologies such as photovoltaics, piezoelectrics, and triboelectrics [2].

A typical TEG consists of alternating p-type and n-type semiconductor legs thermally connected in parallel and electrically in series [3], enabling the conversion of a temperature gradient into a unidirectional electric current by harnessing the opposing Seebeck voltages. When a temperature difference is loaded across the device, a potential difference (ΔV) occurs due to the Seebeck effect, and electrical energy is generated as current

Daegun Kim and Hoimin Kim contributed equally to this study.

This is an open access article under the terms of the Creative Commons Attribution License, which permits use, distribution and reproduction in any medium, provided the original work is properly cited.

© 2025 The Author(s). *EcoMat* published by The Hong Kong Polytechnic University and John Wiley & Sons Australia, Ltd.

flows by connecting a load. The efficiency in the conversion of input thermal energy to output electrical energy by a TEG is governed by a TE figure of merit (ZT) of TE materials. ZT is a dimensionless value defined as $ZT = S^2\sigma T/\kappa$, where S is the Seebeck coefficient ($S = \Delta V/\Delta T$), σ is the electrical conductivity, and κ is the thermal conductivity. The product $S^2\sigma$ is also called the power factor (PF) [4]. Therefore, a TE material should have high electrical conductivity and Seebeck coefficient and low thermal conductivity to have a high ZT. Various efforts are being made to develop materials that meet these conditions.

Traditional TE materials were primarily developed by alloying inorganic heavy metals, whose high concentration of free electrons and heavy nucleus has advantages in achieving high electrical conductivity and low thermal conductivity. However, inorganic materials often have drawbacks such as toxicity, limited processability, heaviness, and low mechanical flexibility. Recently, organic materials have been considered as promising candidates for TE materials because of their advantages over inorganic TE materials: non-toxicity, solution processability, lightweight, and mechanical flexibility [1]. With the growing interest and demand for wearable electronic devices, organic-based TEGs have gained attention as lightweight and flexible power supply devices to operate wearable electronics [5]. Additionally, organic TE materials inherently have low thermal conductivity, and their electrical properties can be freely adjusted through molecular design, suggesting their potential for high TE performance [4]. In this review article, we aim to introduce recent achievements in organic TE materials, especially those based on conjugated polymers (CPs). Compared to other small organic molecules, CPs offer significant advantages in TE applications. Small organic molecules typically suffer from poor electrical conductivity due to their discrete molecular nature, resulting in inefficient charge transport [6]. The limited solubility and brittle polycrystalline domains of small organic molecules also hinder solution processing and flexible device fabrication [7]. Furthermore, their small molecular size and limited delocalization make them more susceptible to oxidative degradation in ambient conditions. In contrast, CPs exhibit extended π-conjugation, enabling efficient charge delocalization, structural tunability, and mechanical flexibility. These features allow CPs to be processed into large-area, bendable films using scalable techniques such as spin-coating, printing, or roll-to-roll processing, making them ideal candidates for flexible TE applications. By examining recent achievements in TE performance in CPs, we aim to discover strategies for molecular design to achieve high TE performance in CPs. Material engineering is also closely related to device structure, thus flexible and stretchable TEGs reported to date are also reviewed.

2 | CP-Based TE Materials

The efficiency η of heat-electricity conversion by a TE material is given by a function of temperature and ZT value:

$$\eta = \left(\frac{T_H - T_C}{T_H}\right)\left[\frac{\sqrt{1+Z\overline{T}}-1}{\sqrt{1+Z\overline{T}}+T_C/T_H}\right] \quad (1)$$

where T_H and T_C are temperatures at hot side and cold side, respectively, and $\overline{T}$ is their average. The front part of the Equation (1) is just the Carnot efficiency, so the TE conversion efficiency approaches to the ideal Carnot efficiency as $Z\overline{T} \to \infty$. However, it is challenging to realize a high ZT value, because of tradeoffs between TE parameters: Seebeck coefficient, electrical conductivity, and thermal conductivity [8, 9]. The trade-off relation between the electrical conductivity and the thermal conductivity in traditional inorganic TE materials is formulated according to the Wiedemann-Franz law, which states a linear relationship between these parameters:

$$\frac{\kappa}{\sigma} = LT \quad (2)$$

where $L = 2.44\times10^{-8}\,V^2K^{-2}$ is Lorenz number. The Wiedemann-Franz law does not effectively work in organic materials due to a significant contribution of lattice scattering to thermal conduction. However, a negative correlation between the Seebeck coefficient and the electrical conductivity is generally observed for various organic materials. Such a trade-off relation between the Seebeck coefficient and the electrical conductivity primarily arises from the fact that they have opposing dependencies on charge carrier concentration. That is, increasing carrier concentration through molecular doping to achieve high electrical conductivity causes a decrease in the Seebeck coefficient. Such a trade-off relation between the Seebeck coefficient and the electrical conductivity onto molecular doping typically exhibits a relation $S \propto \sigma^{-1/4}$ for various organic materials, limiting the ZT value. Thus, the material engineering of organic TE materials has aimed to improve both the Seebeck coefficient and the electrical conductivity, overcoming the trade-off relations between TE parameters.

The thermal conductivity of CPs typically is on the order of $0.1\,W\,m^{-1}K^{-1}$, which is far lower than that of traditional inorganic TE materials, and it often deviates from the Widemann-Franz law due to the thermally-activated hopping-based charge transport mechanism [10]. The major drawback of using CPs for TE applications is their low electrical conductivities, which limit the ZT value to less than 1 [11, 12]. Thus, many works on CP-based TE materials have focused on enhancing the electrical conductivity of CPs through doping, which effectively generates charge carriers via redox reactions between CP and the added dopant [11]. Consequently, recent research on TE materials based on CPs is primarily focused on understanding how doping efficiency and electrical conductivity vary depending on the structure of the CP, the type of dopant, and the doping mechanism (Figure 1a,b) [13–19]. On the other hand, studies on the Seebeck coefficient of the CP-dopant system are also vital, though research on the correlation between the structure and thin-film microstructure of CPs and their Seebeck coefficients is still in relatively early stages and has not been systematically established (Figure 1c) [20–22].

In the following content, we intend to examine the molecular structure design of various CPs reported in recent organic TE device fields and their corresponding TE properties, aiming to understand the structure–property relationship of CPs for TE devices. The TE properties of CPs can vary significantly depending on the characteristics of doping, such as the type of dopants used, the doping process, and post-treatment, but this article

25673173, 2025, 10, Downloaded from https://onlinelibrary.wiley.com/doi/10.1002/eom2.70029 by Hansol Lee - Gachon University Global Campus , Wiley Online Library on [29/09/2025]. See the Terms and Conditions (https://onlinelibrary.wiley.com/terms-and-conditions) on Wiley Online Library for rules of use; OA articles are governed by the applicable Creative Commons License

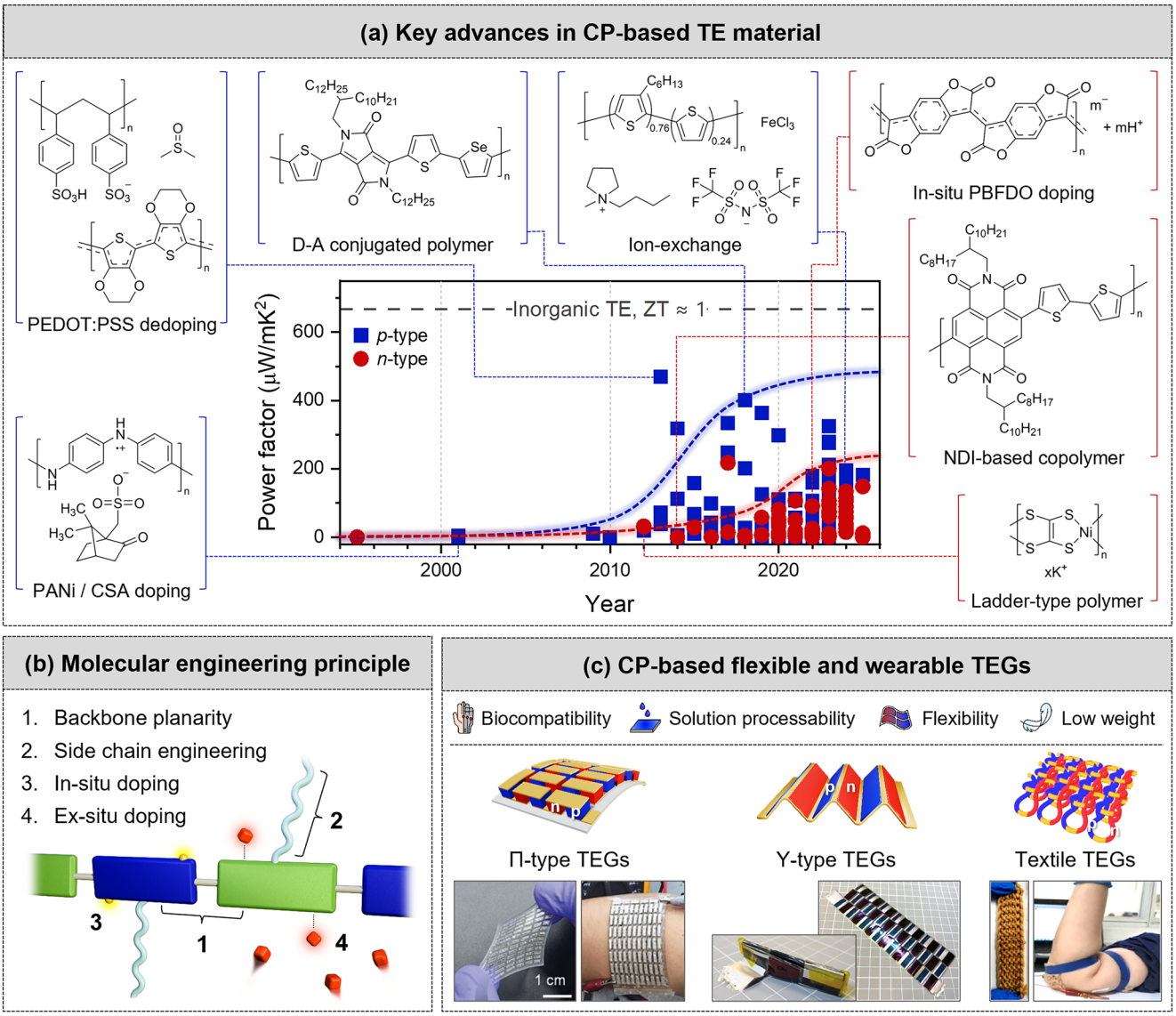


FIGURE 1 | (a) Chronology of key achievements in polymer-based TEs over the past two decades. (b) Conceptual schemes illustrating molecular engineering principles for conjugated polymers. (c) Key properties of CP-based TE material and the corresponding types of flexible and wearable TGEs. Panel c reproduced from 20 with permission (Copyright 2025, Wiley), 21 with permission (Copyright 2025, Wiley), and 22 with permission (Copyright 2020, Springer Nature).

will focus solely on the reported structures of CPs and the optimum TE performance achieved in these polymers.

2.1 | P-Type CPs

The early development of CP-based TE materials predominantly focused on p-type systems, where holes serve as the primary charge carriers (Figure 1a). The advancement of p-type CP-based TE materials is largely attributed to the availability of well-designed electron-donating polymer backbones and effective electron-withdrawing dopant molecules. In contrast, achieving n-type doping in CPs remains challenging due to the limited availability of suitable electron-deficient polymer backbones, which require low lowest unoccupied molecular orbital (LUMO) levels, high planarity, and good air stability for efficient doping, as well as a lack of efficient electron-donating dopants. Therefore, it would provide a comprehensive overview of the historical progress in CP-based TE materials to introduce p-type CPs prior to n-type CPs.

Conjugated polymers used as thermoelectric materials can be broadly categorized into two types, homopolymers and copolymers, depending on the composition of their building blocks. In the field of thermoelectric polymers, as in other areas of organic electronics, early studies primarily focused on classical homopolymers. A representative example is poly(3-alkylthiophene), a well-known p-type polymer. These classical polymers have been extensively studied due to their relatively simple synthesis and high processability. However, the uniformly distributed charge density along the backbone of homopolymers often results in limited charge transport properties, which are insufficient to achieve high thermoelectric performance [23]. Therefore, the development of polymers with more

25673173, 2025, 10, Downloaded from https://onlinelibrary.wiley.com/doi/10.1002/eem2.70029 by Hansol Lee - Gachon University Global Campus , Wiley Online Library on [29/09/2025]. See the Terms and Conditions (https://onlinelibrary.wiley.com/terms-and-conditions) on Wiley Online Library for rules of use; OA articles are governed by the applicable Creative Commons License

efficient charge transport and thermoelectric properties has been necessary.

One representative strategy for designing such polymers is to copolymerize electron-rich and electron-deficient conjugated units to form donor–acceptor (D–A) type conjugated copolymers. As widely explored in other organic electronic devices such as organic field-effect transistors and organic photovoltaics, D–A type conjugated copolymers can exhibit significantly improved charge transport and electronic properties compared to homopolymers. This is attributed to intra- and intermolecular charge transfer between the donor and acceptor building blocks (commonly known as the push-pull effect) which promotes stronger π-π stacking and enhanced structural order [23]. Moreover, the electronic structure and π-conjugation length of D–A type conjugated copolymers can be finely tuned through the selection, modification, and functionalization of various donor and acceptor units. These advantages have driven extensive research on D–A type conjugated copolymers as thermoelectric materials and have contributed to their high thermoelectric performance. In the following subsections, we will examine representative thermoelectric polymers in the order of p-type homopolymers and copolymers (Table 1).

2.1.1 | Poly(3,4-Ethylenedioxythiophene) (PEDOT)

PEDOT is one of the most widely studied p-type CPs in the field of organic TE materials and currently reports the highest PF among CP-based TE materials due to its high electrical conductivity [3]. Commercial products of PEDOT often contain poly(-styrene sulfonic acid) (PSS) which plays roles of solubilizer as well as counter-ion. PSS possesses a bunch of sulfonate groups, a portion of which stabilizes polarons in PEDOT chains while the rest endows PEDOT:PSS with solubility in water. Aqueous PEDOT:PSS solution has been reported to have colloidal dispersion, which has a core-shell structure of hydrophobic PEDOT-rich core and hydrophilic PSS shell [45]. Such a unique colloidal structure is often projected to solid-state morphology after the film formation, resulting in pancake-like morphology where PEDOT-rich grains are surrounded by PSS layers, which impede charge transport by establishing electrically insulating layers. Therefore, removing the PSS shell through solvent post-treatment using polar solvents, such as ethylene glycol, dimethyl sulfoxide, or sulfuric acid, has been reported to facilitate charge transfer between PEDOT cores. For example, in one study, ethylene glycol treatment on PEDOT:PSS films effectively reduced the PSS content within the PEDOT:PSS film, as evidenced by S 2p X-ray photoelectron spectroscopy spectra, resulting in improved electrical conductivity and PF values of 900 $S\,cm^{-1}$ and 470 $\mu W\,m^{-1}\,K^{-2}$, respectively, whereas the untreated film exhibited only about 600 $S\,cm^{-1}$ and 70 $\mu W\,m^{-1}\,K^{-2}$ for electrical conductivity and PF, respectively (Figure 2a) [14]. It is noteworthy that the Seebeck coefficient of the PEDOT:PSS film also increased from ~30 $\mu V\,K^{-1}$ in the untreated film to ~70 $\mu V\,K^{-1}$ after ethylene glycol treatment. Similarly, treating PEDOT:PSS with sulfuric acid effectively reduces the PSS content in the film, yielding a remarkable electrical conductivity of 4000 $S\,cm^{-1}$. Such a dramatic increase in the electrical conductivity upon sulfuric acid treatment originates from a high concentration of sulfonate anion ($[HSO_4]^-$), which preserves polaron by replacing sulfonate groups of PSS during the post-treatment (Figure 2b). In addition, the removal of PSS induced significant structural rearrangement within the film, where PEDOT crystallized into a nanofibril morphology, and the increased crystallinity of PEDOT contributed greatly to the enhancement of electrical conductivity [46]. When a sulfuric acid-treated PEDOT:PSS film is exposed to a sodium hydroxide (NaOH) solution, ion exchange occurs between PSS ions in the film and OH^- ions in the solution. This ion exchange reduces the doping level of the PEDOT:PSS film, subsequently enhancing the Seebeck coefficient. The reduced oxidation level of PEDOT caused by NaOH treatment was confirmed through changes in the film's absorption spectrum in the visible light region, which was also evident from the visually observable color change of the film. A PEDOT:PSS film treated only with sulfuric acid exhibited an electrical conductivity of 2156 $S\,cm^{-1}$, a Seebeck coefficient of 16.5 $\mu V\,K^{-1}$, and a resulting PF of 58.7 $\mu W\,m^{-1}\,K^{-2}$. However, after NaOH treatment, while the electrical conductivity decreased to around 1000 $S\,cm^{-1}$, the Seebeck coefficient increased to over 35 $\mu V\,K^{-1}$, leading to a maximum reported PF of ~200 $\mu W\,m^{-1}\,K^{-2}$. Further optimization of process conditions has resulted in a maximum PF of 334 $\mu W\,m^{-1}\,K^{-2}$ (Figure 2c) [24].

Furthermore, the TE performance of PEDOT:PSS has been improved by controlling the interaction between PEDOT and PSS. When alkyl sulfonate anions are added to PEDOT:PSS, the interactions between the alkyl sulfonate anions and PEDOT competitively hinder interactions between PSS and PEDOT. This leads to a reduction in electrostatic interactions between PEDOT and PSS (Figure 2d) [25]. Such a reduction increases the planarity and inter-chain interactions of PEDOT. Consequently, the structure of PEDOT in the film changes from a core-shell to a fibrous form, promoting efficient charge transport pathways and enhancing electrical conductivity. The decrease in interactions between PEDOT and PSS also reduces PEDOT's doping level, which in turn elevates the Seebeck coefficient. As a result, through optimization of the alkyl chain length of alkyl sulfonate, a maximum PF of 700 $\mu W\,m^{-1}\,K^{-2}$ was reported, whereas the PF was below 100 $\mu W\,m^{-1}\,K^{-2}$ when no alkyl sulfonate anion was added [25]. Similarly, replacing the PSS anion in PEDOT:PSS with other anions also led to changes in PEDOT's planarity and crystallinity depending on the strength of electrostatic forces between PEDOT and the anions, thereby allowing for modulation of electrical conductivity and the Seebeck coefficient. By replacing PSS with thiocyanate (TC), dicyanoamide (DCA), tricyanomethanide (TCM), and tetracyanoborate (TCB), the electrical conductivity was effectively tuned within the range of 600 to 2200 $S\,cm^{-1}$, and the Seebeck coefficient within the range of 50 to 75 $\mu V\,K^{-1}$, resulting in an optimal PF of 630 $\mu W\,m^{-1}\,K^{-2}$ when PSS was replaced with TCB [26].

2.1.2 | Poly(3-Hexylthiophene) (P3HT) and Poly(2,5-Bis(3-Tetradecylthiophen-2-Yl)thieno[3,2-b]Thiophene) (PBTTT)

P3HT and PBTTT are semiconducting CPs based on thiophene and have been widely researched as p-type organic TE materials along with PEDOT. These polymers possess a high highest occupied molecular orbital (HOMO) level due to the electron-rich characteristics of the thiophene units, thereby facilitating

25673173, 2025, 10, Downloaded from https://onlinelibrary.wiley.com/doi/10.1002/eom2.70029 by Hansol Lee - Gachon University Global Campus , Wiley Online Library on [29/09/2025]. See the Terms and Conditions (https://onlinelibrary.wiley.com/terms-and-conditions) on Wiley Online Library for rules of use; OA articles are governed by the applicable Creative Commons License

TABLE 1 | Summary of key thermoelectric parameters of representative p-type thermoelectric conjugated polymers.

Polymer	Dopant	Maximum PF [$\mu W\,m^{-1}\,K^{-2}$]	References	Remarks
PEDOT:PSS	—	70	[14]	No treatment
	—	470	[14]	Ethylene glycol treatment
	—	58.7	[24]	Sulfuric acid treatment
	—	200	[24]	Sulfuric aicd + NaOH treatment
	—	700	[25]	Addition of alkyl sulfonate
	—	630	[26]	Addition of tetracyanoborate
P3HT	F4TCNQ	0.2	[27]	Low crystallinity
	F4TCNQ	2.7	[27]	High crystallinity
	$FeCl_3$	21	[28]	Aligned by rubbing
PBTTT	$FeCl_3$	1940	[29]	Aligned by rubbing
PDPP3T	$FeCl_3$	276	[30]	
PDPPS-12	$FeCl_3$	126	[15]	
PDPPSe-12	$FeCl_3$	300	[15]	
EHT6-20DPP	$FeCl_3$	56.7	[31]	
PDPP-4T-EDOT	$FeCl_3$	298.2	[32]	
PDPP-5T	$FeCl_3$	11.1	[32]	
PDTP-DPP	$FeCl_3$	10.8	[33]	
PCZ-DPP	$FeCl_3$	1.8	[33]	
C6-ICPDPP	$FeCl_3$	1.32	[34]	
PIDF-BT	F4TCNQ	35	[35]	
PIDF-BSe	F4TCNQ	39.7	[36]	
	$AuCl_3$	30.9	[36]	
PIDT-TBTT	$FeCl_3$	4.91	[37]	
PIDT-BBT	F4TCNQ	1.47	[38]	At 400 K
PIDTT-BBT	F4TCNQ	4.04	[38]	At 382 K
PBDTDTBTF-1	$FeCl_3$	0.037	[39]	At 106°C
PBDTDTBTF-2	$FeCl_3$	0.177	[39]	At 97°C
PBDTDTBTF-3	$FeCl_3$	1.12	[39]	At 70°C
P(BDT-EDOT)	$FeCl_3$	0.37	[40]	At room temperature
	$FeCl_3$	0.9	[40]	At room temperature
P(BDTTT-EDOT)	$FeCl_3$	2.19	[40]	At room temperature
	$FeCl_3$	101.3	[40]	At 350 K
P(BDT-DPP)	$FeCl_3$	0.26	[41]	At room temperature
	$FeCl_3$	0.95	[41]	At 390 K
P(BDTTT-DPP)	$FeCl_3$	6.50	[41]	At room temperature
	$FeCl_3$	10.50	[41]	At 350 K
PCPDTBT	$B(C_6F_5)_3$	4.41	[42]	
PCPDTSBT	$B(C_6F_5)_3$	7.73	[42]	

(Continues)

25673173, 2025, 10, Downloaded from https://onlinelibrary.wiley.com/doi/10.1002/eem2.70029 by Hansol Lee - Gachon University Global Campus , Wiley Online Library on [29/09/2025]. See the Terms and Conditions (https://onlinelibrary.wiley.com/terms-and-conditions) on Wiley Online Library for rules of use; OA articles are governed by the applicable Creative Commons License

TABLE 1 | (Continued)

Polymer	Dopant	Maximum PF [$\mu W\,m^{-1}\,K^{-2}$]	References	Remarks
	$FeCl_3$	49.8	[42]	
PCDTPT	F4TCNQ	21.8	[43]	
PCDTFBT	F4TCNQ	31.5	[43]	
DPP-MeDTP	F4TCNQ	85.2	[12]	
DTP-T2	F4TCNQ	12.4	[12]	
DTP-TT	F4TCNQ	3.63	[12]	
PDFD-T	$FeCl_3$	31.8	[44]	Low molecular weight
PDFD-T	$FeCl_3$	79.5	[44]	High molecular weight
PDFD-TT	$FeCl_3$	28.3	[44]	
PDFD-DTT	$FeCl_3$	8.1	[44]	

electron transfer with dopants [9]. Doping by dopants such as 2,3,5,6-tetrafluoro-7,7,8,8-tetracyanoquinodimethane (F4TCNQ) and $FeCl_3$ has achieved exceptional TE properties for these CPs. Polythiophenes have been well-studied as semiconducting materials for transistors and solar cells as well as TE materials. Hence, the structural and electrical characteristics of polymer films are relatively well-known [4]. In a study observing the change in TE properties depending on the crystallinity of F4TCNQ-doped P3HT films, it was observed that electrical conductivity increased with increasing crystallinity, while the Seebeck coefficient remained relatively unchanged (Figure 3a) [27]. The increase in electrical conductivity originates from the carrier mobility enhancement accompanied by improved crystallinity, which barely affects charge carrier density and, thereby, the Seebeck coefficient. In the P3HT film with the lowest crystallinity, the electrical conductivity, Seebeck coefficient, and PF were approximately $0.7\,S\,cm^{-1}$, $51\,\mu V\,K^{-1}$, and $0.2\,\mu W\,m^{-1}\,K^{-2}$, respectively, whereas in the P3HT film with the highest crystallinity, these values reached $12.7\,S\,cm^{-1}$, $46\,\mu V\,K^{-1}$, and $2.7\,\mu W\,m^{-1}\,K^{-2}$, respectively, demonstrating that the TE performance can be enhanced by nearly tenfold through increasing the crystallinity of P3HT [27, 47]. Techniques for aligning P3HT chains in one direction have also been reported to significantly improve the TE performance [28, 29]. At high temperatures, the polymer film can be aligned parallel to the direction in which the polymer chains are rubbed. Such aligned P3HT films showed improved electrical conductivity and Seebeck coefficient when doped with $FeCl_3$ compared to unaligned films (Figure 3b). At the $FeCl_3$ concentration that yielded the highest PF, the electrical conductivity along the rubbing direction was $570\,S\,cm^{-1}$, which was more than 10 times higher than that in the direction perpendicular to rubbing ($48\,S\,cm^{-1}$). The Seebeck coefficient along the rubbing direction was $5.4\,\mu V\,K^{-1}$, more than twice that of the perpendicular direction ($2.3\,\mu V\,K^{-1}$). As a result, the P3HT film aligned by rubbing exhibited a maximum PF of $21\,\mu W\,m^{-1}\,K^{-2}$ along the rubbing direction. Similarly, this method was applied to PBTTT. Since PBTTT includes thienothiophene and possesses a more rigid chain than P3HT, it showed a higher degree of molecular alignment and improvement in electrical conductivity. Aligned PBTTT doped with $FeCl_3$ was reported to have an electrical conductivity of $2\times10^5\,S\,cm^{-1}$, a Seebeck coefficient of $9.4\,\mu V\,K^{-1}$ and a PF of $1.94\,mW\,m^{-1}\,K^{-2}$ [29].

In most cases, the electrical conductivities of P3HT films upon doping were limited to the value below $100\,S\,cm^{-1}$ regardless of doping concentration, indicating poor doping efficiency in the P3HT films. Shanahan et al. recently achieved high electrical conductivity in polythiophene films by implementing cleavable side chains. The acrylic side chain with a bulky alkyl group was attached to polythiophene (POET-T2), so that the bulky alkyl group can be cleaved when exposed to heat or triflic acid (TfOH) (Figure 3c) [48]. The long side chain can improve the doping efficiency by allowing the diffusion of dopants into polymer crystallites, minimizing the structural distortion in the π-π stacking ordering. However, when the polymer is fully doped, the long side chains form insulating layers in the lamellar crystallites, impeding the charge transport. The in situ cleavage by TfOH transformed the acrylic side chain to −COOH, leaving TfO^- anion. The anion exchange between ionized $F4TCNQ^-$ and TfO^- was observed upon doping with F4TCNQ + TfOH, achieving both high carrier concentrations and carrier mobilities. The polymer doped with F4TCNQ and subsequently subjected to side chain cleavage using TfOH achieved an electrical conductivity of ~$10\,S\,cm^{-1}$, which is more than 10^4 times higher than that of the polymer doped with F4TCNQ without side chain cleavage. This result implied that the long side chain inhibited both the intercalation of dopant and the charge transport in the highly doped state.

PBTTT was used as a model polymer to examine the impact of the dopant position within the CP film on doping efficiency and TE properties [49]. The distribution of the F4TCNQ dopant within the amorphous or crystalline regions of the PBTTT film was controlled depending on whether the doping process was performed via vapor doping or solution sequential doping. Vapor doping led to a greater distribution of F4TCNQ in the crystalline regions, as evidenced by the change in d-spacing of the crystals with increasing dopant concentration. It was observed that the presence of dopants in crystalline regions led

25673173, 2025, 10, Downloaded from https://onlinelibrary.wiley.com/doi/10.1002/eom2.70029 by Hansol Lee - Gachon University Global Campus , Wiley Online Library on [29/09/2025]. See the Terms and Conditions (https://onlinelibrary.wiley.com/terms-and-conditions) on Wiley Online Library for rules of use; OA articles are governed by the applicable Creative Commons License

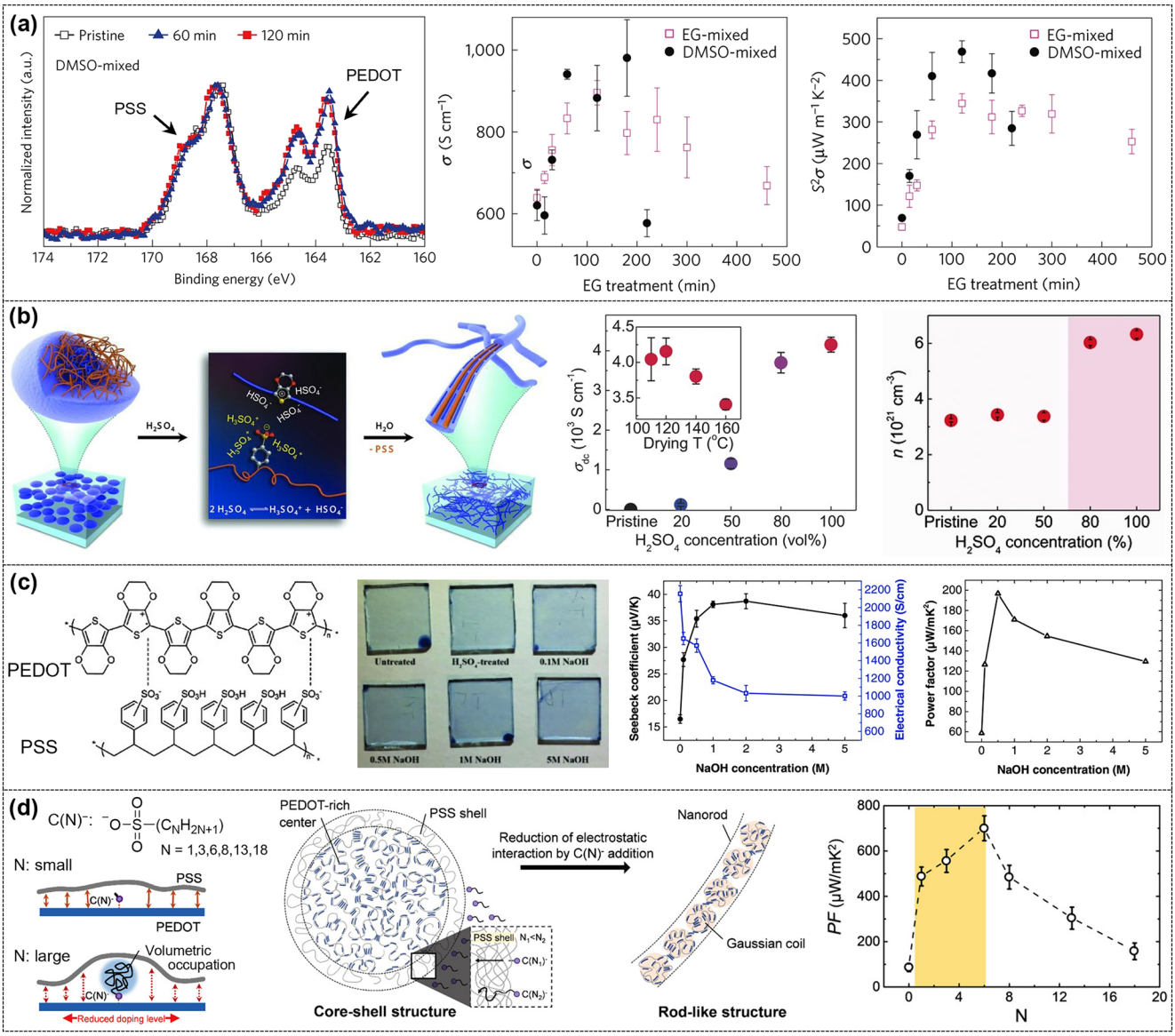


FIGURE 2 | PEDOT:PSS for p-type TE materials. (a) A decrease in PSS/PEDOT ratio in XPS S 2p spectra was induced through selective removal of PSS from the PEDOT:PSS film using ethylene glycol (EG) dipping treatment (Left), which improved both the electrical conductivity (σ) and the power factor ($S^2\sigma$) (Right). Reproduced from 14 with permission (Copyright 2013, Springer Nature). (b) PEDOT:PSS treated by H_2SO_4 to replace PSS with HSO_4^- ion (Left), which increased the carrier concentration (n) and the electrical conductivity (σ_{dc}) (Right). Reproduced from 25 with permission (Copyright 2014, Wiley). (c) PEDOT:PSS treated by H_2SO_4 was dedoped by NaOH treatment, which increased the opacity, the Seebeck coefficient and the power factor and decreased the electrical conductivity of the PEDOT:PSS film. Reproduced from 26 with permission (Copyright 2017, Wiley). (d) The anion exchange-induced solution-state colloidal morphology change in PEDOT:PSS solution (Center), resulting in an improved power factor (*PF*). Reproduced from 27 with permission (Copyright 2019, Wiley).

to higher doping efficiency than in amorphous regions. The charge carriers are more delocalized in the crystalline regions, allowing the dopant to ionize more effectively. The charge delocalization mitigated the trade-off between electrical conductivity and the Seebeck coefficient, resulting in a more gradual slope in the Seebeck coefficient versus electrical conductivity plot and a steeper slope in the power factor versus electrical conductivity plot. Though the theoretical backgrounds have not been clearly elucidated, the decrease in the Seebeck coefficient due to the increase in electrical conductivity appeared to be relatively limited when dopants were located in the crystalline region (Figure 3d) [49].

The Seebeck coefficient depends on the difference between the Fermi energy level and the charge transport energy level, so the Seebeck coefficient can be improved by mixing CPs with different HOMO levels [50, 51]. When CPs with deeper HOMO levels were added, the charge transport energy level of the mixed thin film decreased. Optimization of the composition enhanced the Seebeck coefficient by maximizing the difference between the Fermi energy level and the charge transport energy level. Mixing P3HT with poly(3-thiothiophene) (P3HTT) increased a Seebeck coefficient of up to 700 $\mu V K^{-1}$ [51], and mixing P3HT with poly[[4,8-bis[(2-ethylhexyl)oxy]benzo[1,2-b:4,5-b']dithiophene-2,6-diyl][3-fluoro-2-[(2-ethylhexyl)carbonyl] thieno[3,4-b]thiophenediyl]]

25673173, 2025, 10, Downloaded from https://onlinelibrary.wiley.com/doi/10.1002/eom2.70029 by Hansol Lee - Gachon University Global Campus , Wiley Online Library on [29/09/2025]. See the Terms and Conditions (https://onlinelibrary.wiley.com/terms-and-conditions) on Wiley Online Library for rules of use; OA articles are governed by the applicable Creative Commons License

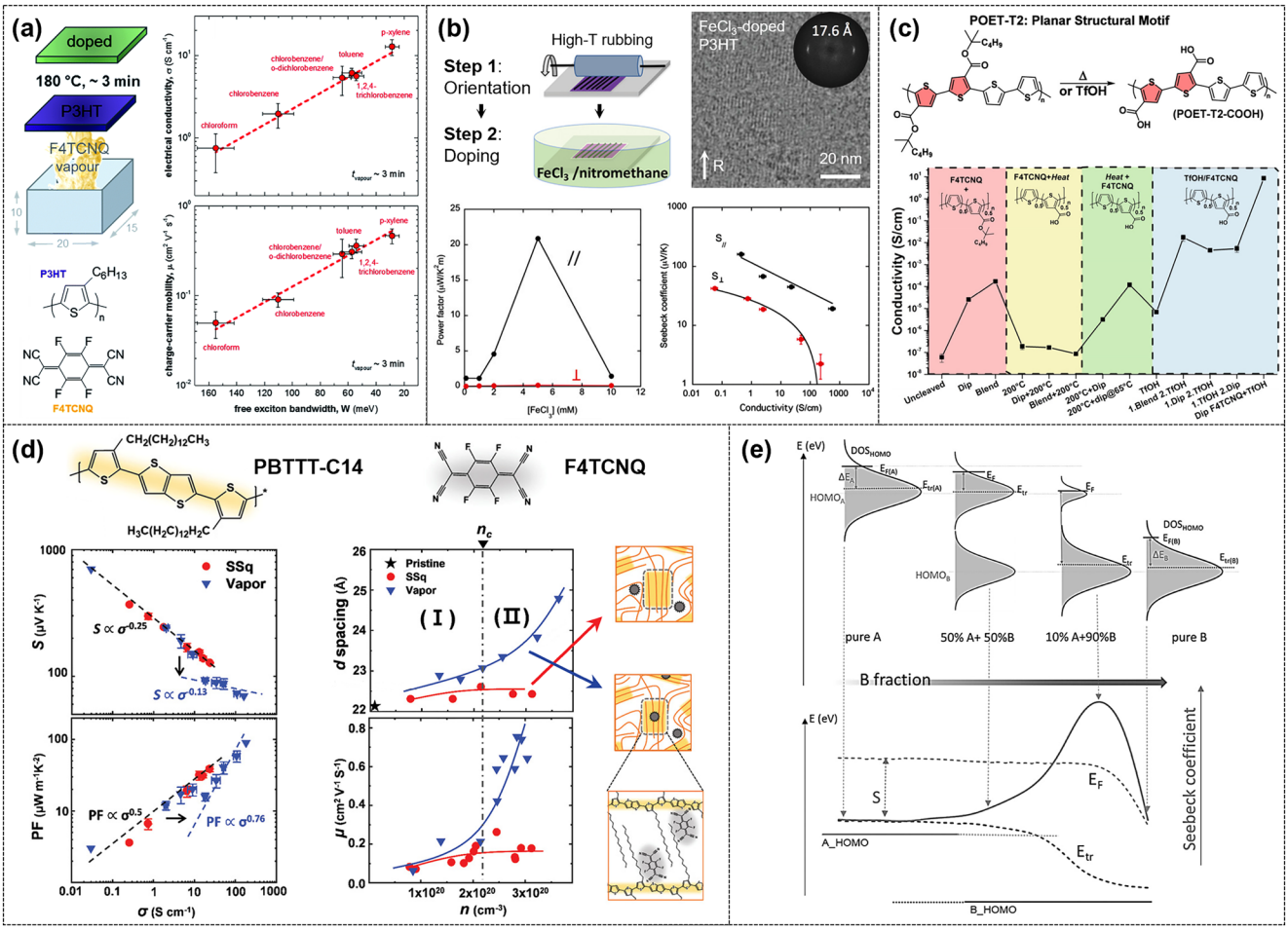


FIGURE 3 | P3HT and PBTTT for p-type TE materials. (a) P3HT-based TE materials with F4TCNQ vapor doping with various solvent. The solvent affected the free exciton bandwidth (W), which was proportional to the carrier mobility (μ) and the power factor ($S^2\sigma$). Reproduced from 29 with permission (Copyright 2018, The Royal Society of Chemistry). (b) Rubbing-induced anisotropy in the power factor and the Seebeck coefficient in $FeCl_3$-doped P3HT film with respect to $FeCl_3$ concentration. Reproduced from 32 with permission (Copyright 2019, Wiley). (c) The effect of various cleavable side chain and cleavage mechanisms on electrical conductivity during the doping process in POET-T2. Reproduced from 33 with permission (Copyright 2024, American Chemical Society). (d) Comparison of solution-sequential (SSq) doping and vapor doping in TE properties and microstructure of PBTTT films as a function of electrical conductivity (σ) or carrier concentration (n). Reproduced from 34 with permission (Copyright 2022, Wiley). (e) The density of states (DOS) distribution of mixed system and accompanying changes in the fermi level (E_F) and transport level (E_{tr}). Reproduced from 35 with permission (Copyright 2018, Wiley).

(PTB7)orpoly[[2,3-bis(3-octyloxyphenyl)-5,8-quinoxalinediyl]-2,5-thiophenediyl] (TQ1) yielded Seebeck coefficients of 1100 and 2000 μVK^{-1}, respectively (Figure 3e) [50].

2.1.3 | Conjugated Copolymers Containing Diketopyrrolopyrrole (DPP)

The DPP unit possesses a low LUMO level and strong electron-withdrawing character, making it a widely used electron acceptor unit in the synthesis of D–A type conjugated copolymers. Structurally, the DPP unit is based on a π-conjugated bicyclic dilactam ring, with substitutable positions at the 3 and 6 sites that allow the introduction of aromatic flanking groups and alkylatable nitrogen atoms at the 2 and 5 positions (Figure 4a). Through appropriate control over these positions, the physical and electronic properties of DPP-containing conjugated polymers can be finely tuned [52–56]. For example, the LUMO level can be effectively modulated by varying the flanking groups, while the solubility and microstructure of the polymers can be influenced by the nature of the alkyl groups introduced at the nitrogen atoms. Owing to its high coplanarity and strong π–π stacking ability, the DPP unit promotes strong interchain ordering and facilitates high charge carrier mobility in conjugated polymers incorporating it [57]. Therefore, polymers incorporating the DPP unit are expected to achieve high electrical conductivity through doping, which is essential for attaining high TE performance in conjugated polymers. A D–A type polymer poly(2,2′-[(2,5-bis(2-hexyldecyl)-3,6-dioxo-2,3,5,6-tetrahydropyrrolo[3,4-c]pyrrole-1,4-diyl)dithiophene]-5,5′-diyl-alt-thiophen-2,5-diyl) (PDPP3T), comprising DPP and thiophene as electron acceptor and electron donor, respectively, exhibited enhanced planarity and intermolecular interactions compared to P3HT, and showed up to twice the electrical conductivity of P3HT when doped with $FeCl_3$ (Figure 4b) [30]. In the case of P3HT, a maximum PF of ~56 $\mu W\,m^{-1}\,K^{-2}$ was observed only at a relatively high $FeCl_3$ concentration of 9 mM, whereas PDPP3T exhibited

25673173, 2025, 10, Downloaded from https://onlinelibrary.wiley.com/doi/10.1002/eom2.70029 by Hansol Lee - Gachon University Global Campus , Wiley Online Library on [29/09/2025]. See the Terms and Conditions (https://onlinelibrary.wiley.com/terms-and-conditions) on Wiley Online Library for rules of use; OA articles are governed by the applicable Creative Commons License

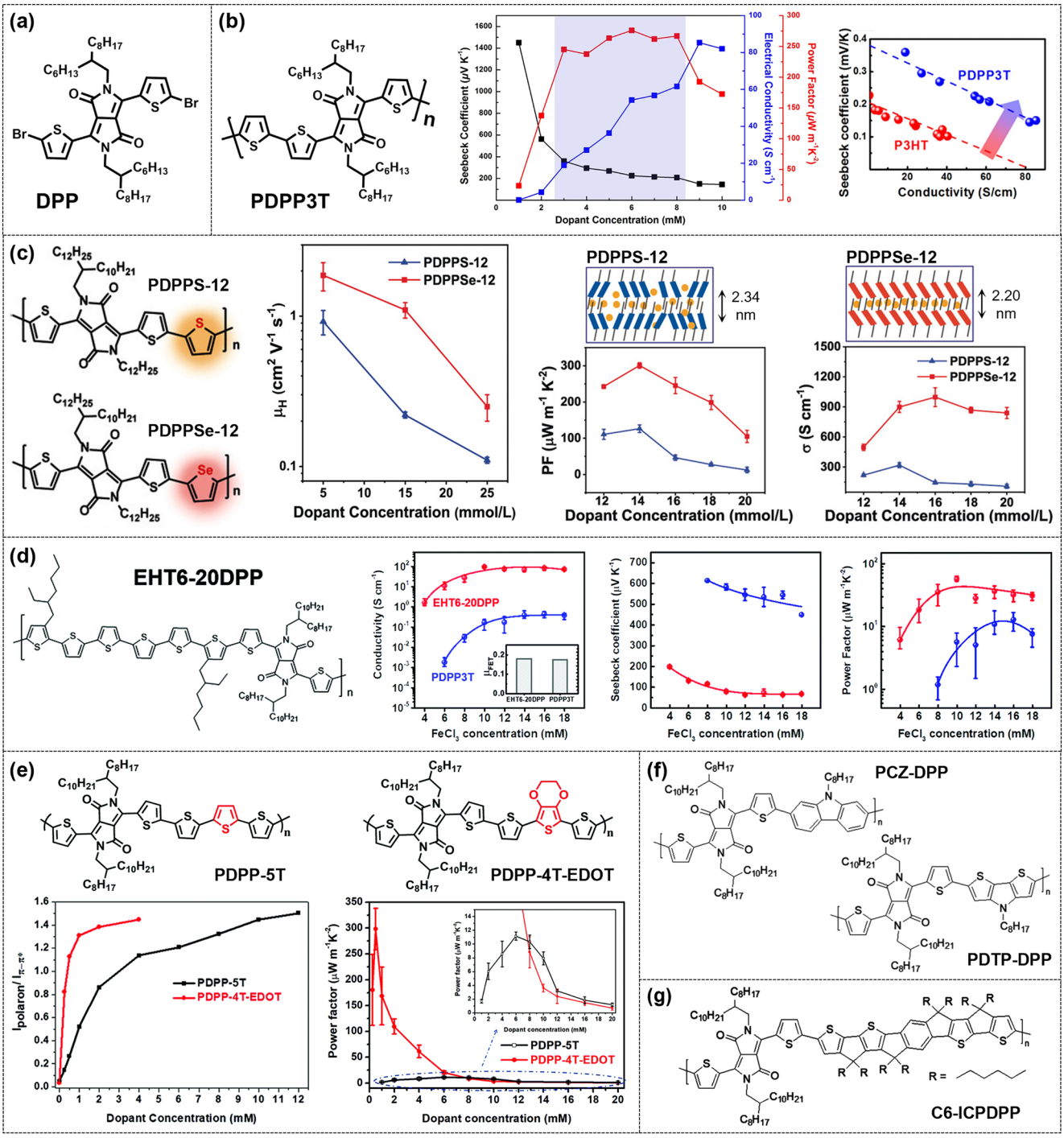


FIGURE 4 | DPP copolymers for p-type TE materials. (a) The chemical structure of DPP moiety. (b) TE properties of PDPP3T with respect to dopant concentration and their comparison with those of P3HT. Reproduced from 43 with permission (Copyright 2017, Springer Nature). (c) The hall mobilities (μ_H) of PDPPS-12 and PDPPSe-12 films as a function of dopant concentration. The structural disorders engaged with doping caused decreases in both μ_H and the power factor at high doping level. Reproduced from 15 with permission (Copyright 2019, Wiley). (d) The repeat unit of EHT6-20DPP contained 8 thiophene rings that induced extended doping efficiency compared to that obtained in PDPP3T, resulting in high electrical conductivities and high power factors for all $FeCl_3$ concentrations. Reproduced from 44 with permission (Copyright 2021, The Royal Society of Chemistry). (e) Replacement of thiophene ring in PDPP-5T with EDOT (PDPP-4T-EDOT) enhanced the polaron absorption ($I_{polaron}$) to absorption by neutral chain segment ($I_{\pi-\pi^*}$) at the same dopant concentration, indicating an improved doping efficiency, which yielded a high power factor. Reproduced from 45 with permission (Copyright 2020, The Royal Society of Chemistry). Chemical structures of (f) PCZ-DPP, PDTP-DPP, and (g) C6-ICPDPP.

consistently high PFs across a broad concentration range of 3 to 8 mM, with a maximum PF reaching 276 $\mu W\,m^{-1}\,K^{-2}$. Moreover, since PDPP3T exhibited high electrical conductivity even with relatively small amounts of dopant, it achieved higher Seebeck coefficients than P3HT over a wide range of electrical conductivities [30].

25673173, 2025, 10, Downloaded from https://onlinelibrary.wiley.com/doi/10.1002/eom2.70029 by Hansol Lee - Gachon University Global Campus , Wiley Online Library on [29/09/2025]. See the Terms and Conditions (https://onlinelibrary.wiley.com/terms-and-conditions) on Wiley Online Library for rules of use; OA articles are governed by the applicable Creative Commons License

A comparative study was conducted on the TE properties of poly[2,5-bis(2-decyltetradecyl)pyrrolo[3,4-c]pyrrole-1,4(2H,5H)-dione-alt-5,5′-bis(2-thienyl)-2,2′-bithiophene] (PDPPS-12), a D–A type polymer composed of DPP units and thiophene, and PDPPSe-12, a polymer in which one of the thiophene units of PDPPS-12 is replaced with selenophene (Figure 4c) [15]. PDPPSe-12 exhibited markedly improved molecular packing compared to PDPPS-12. In addition, while the crystallinity of PDPPS-12 greatly decreased upon doping with $FeCl_3$, PDPPSe-12 maintained its crystallinity even after doping. This was interpreted as being due to the relatively large atomic radius of Se, leading to a larger π-π stacking distance in PDPPSe-12, hence reducing damage to the π-π overlap caused by dopant penetration. PDPPSe-12 exhibited higher charge carrier mobility and electrical conductivity compared to PDPPS-12, along with better retention of electrical conductivity at increasing dopant concentrations. At the optimal dopant concentration, PDPPSe-12 showed an electrical conductivity of approximately 900 $S\,cm^{-1}$, whereas PDPPS-12 exhibited around 320 $S\,cm^{-1}$. At this dopant concentration, both polymers displayed similar Seebeck coefficients of about 60 $\mu V\,K^{-1}$. As a result, PDPPSe-12 achieved a significantly enhanced TE performance, with a maximum power factor of 300 $\mu W\,m^{-1}\,K^{-2}$, compared to a maximum of 126 $\mu W\,m^{-1}\,K^{-2}$ for PDPPS-12 [15].

In PDPP3T, it was reported that further increasing the number of thiophene units in the donor unit improved the doping efficiency by the dopant (Figure 4d) [31]. For the polymer EHT6-20DPP, which has an increased number of 8 thiophene units, there was an enhanced doping efficiency compared to PDPP3T when doped with $FeCl_3$. This was interpreted as being due to EHT6-20DPP having more thiophene units as donor units, thus enhancing electron-donor characteristics toward the dopant. Additionally, EHT6-20DPP showed a higher affinity to the dopant compared to PDPP3T, facilitating the penetration of the dopant into the polymer film, which also contributed to improving doping efficiency. As a result, EHT6-20DPP exhibited over 100 times higher electrical conductivity (with a maximum value of 93.3 $S\,cm^{-1}$) than PDPP3T across all $FeCl_3$ concentrations. Despite the two polymers showing nearly identical field-effect mobilities in their undoped states, this large difference in electrical conductivity clearly indicates that the additional thiophene units in EHT6-20DPP played a crucial role in enhancing doping efficiency. On the other hand, the Seebeck coefficient of $FeCl_3$-doped EHT6-20DPP was below ~200 $\mu V\,K^{-1}$, which is significantly lower than the value of 450 to 600 $\mu V\,K^{-1}$ observed in PDPP3T. Nevertheless, due to its much higher electrical conductivity, EHT6-20DPP exhibited a superior PF, reaching up to 56.7 $\mu W\,m^{-1}\,K^{-2}$, compared to a maximum PF of 12.8 $\mu W\,m^{-1}\,K^{-2}$ for PDPP3T [31].

In D–A type polymers composed of DPP units and thiophene, it was reported that the introduction of ethylenedioxythiophene (EDOT) to the donor unit improved both doping efficiency and TE performance (Figure 4e) [32]. The TE properties of PDPP-5T, a polymer made up of DPP units and five thiophene units, were compared with PDPP-4T-EDOT, in which one of the five thiophene units in PDPP-5T is replaced with EDOT. EDOT, being more electron-rich than thiophene, resulted in a higher HOMO level when introduced into the polymer, thus enhancing charge transfer to the $FeCl_3$ dopant. The enhanced charge transfer was confirmed by the UV–vis–NIR absorption spectra, where PDPP-4T-EDOT exhibited a higher ratio of polaronic absorption to neutral state absorption compared to PDPP-5T, despite being treated with the same dopant concentration. In addition, the alkoxy groups increased the planarity of the polymer chains through noncovalent O···S interactions, improving charge transport characteristics. Upon doping with $FeCl_3$, at the optimized dopant concentration, PDPP-5T exhibited an electrical conductivity of 62.5 $S\,cm^{-1}$, a Seebeck coefficient of 42.2 $\mu V\,K^{-1}$, and a power factor of 11.1 $\mu W\,m^{-1}\,K^{-2}$, whereas PDPP-4T-EDOT showed an electrical conductivity of 99.2 $S\,cm^{-1}$, a Seebeck coefficient of 174.2 $\mu V\,K^{-1}$, and a power factor of 298.2 $\mu W\,m^{-1}\,K^{-2}$, demonstrating more than 25 times higher TE performance compared to PDPP-5T [32].

A comparison was also made between DPP-based D–A type polymers incorporating either carbazole (PCZ-DPP) or dithienopyrrole (PDTP-DPP) as the donor unit (Figure 4f) [33]. Upon doping, the electrical conductivity of PDTP-DPP was observed to be higher than that of PCZ-DPP. This was interpreted as PDTP-DPP having a larger planarity and more delocalized electronic orbitals compared to PCZ-DPP. Specifically, the delocalization of electrons reduced the Coulomb binding energy from the ionized dopants and enhanced planarity reduced the energy disorder. As a result, the activation energy required for charge transport in PDTP-DPP was found to be smaller than that in PCZ-DPP. The optimized electrical conductivity of PDTP-DPP was reported to be 66.8 $S\,cm^{-1}$, which is more than ten times higher than that of PCZ-DPP, and the PF of PDTP-DPP was also reported to be approximately 5 times higher at 10.8 $\mu W\,m^{-1}\,K^{-2}$ [33].

Research was also conducted on the use of extended donor units where multiple fused heterocycles are combined (Figure 4g) [34]. The polymer C6-ICPDPP used a long monomer unit as a donor, in which thiophene and cyclopentadithiophene (CPDT) are attached on both sides of benzene. Such a donor unit had a high planarity and well-delocalized HOMO over the entire chain. Interestingly, as the doping concentration increased, the Seebeck coefficient gradually decreased and exhibited a polarity switching behavior, changing from positive to negative values. C6-ICPDPP achieved a maximum PF of 1.32 $\mu W\,m^{-1}\,K^{-2}$ when p-type and 0.410 $\mu W\,m^{-1}\,K^{-2}$ when n-type [34].

2.1.4 | Conjugated Copolymers Containing Isoindoloindole (IDID)

Indole and its derivatives, due to their planar-fused aromatic structure and rich electron density, can be used as electron donors favorable for p-doping [58]. IDID has a fused structure composed of indole units. Specifically, indolo[3,2-*b*]indole, in which two pyrrole rings are fused at the center and two benzene rings are positioned on the outer sides, forming a fully fused, centrosymmetric structure, is often used for optoelectronic applications [59, 60]. Structural derivatization is possible at the (N,N-), (2,7-), and (3,8-) positions of indolo[3,2-*b*]indole, allowing for the modulation of the electrical properties and microstructure of CPs incorporating this unit [59]. Therefore, CPs containing this IDID unit were also studied as TE materials. F atoms are often introduced to IDID (IDIDF or IDF)

25673173, 2025, 10, Downloaded from https://onlinelibrary.wiley.com/doi/10.1002/eom2.70029 by Hansol Lee - Gachon University Global Campus , Wiley Online Library on [29/09/2025]. See the Terms and Conditions (https://onlinelibrary.wiley.com/terms-and-conditions) on Wiley Online Library for rules of use; OA articles are governed by the applicable Creative Commons License

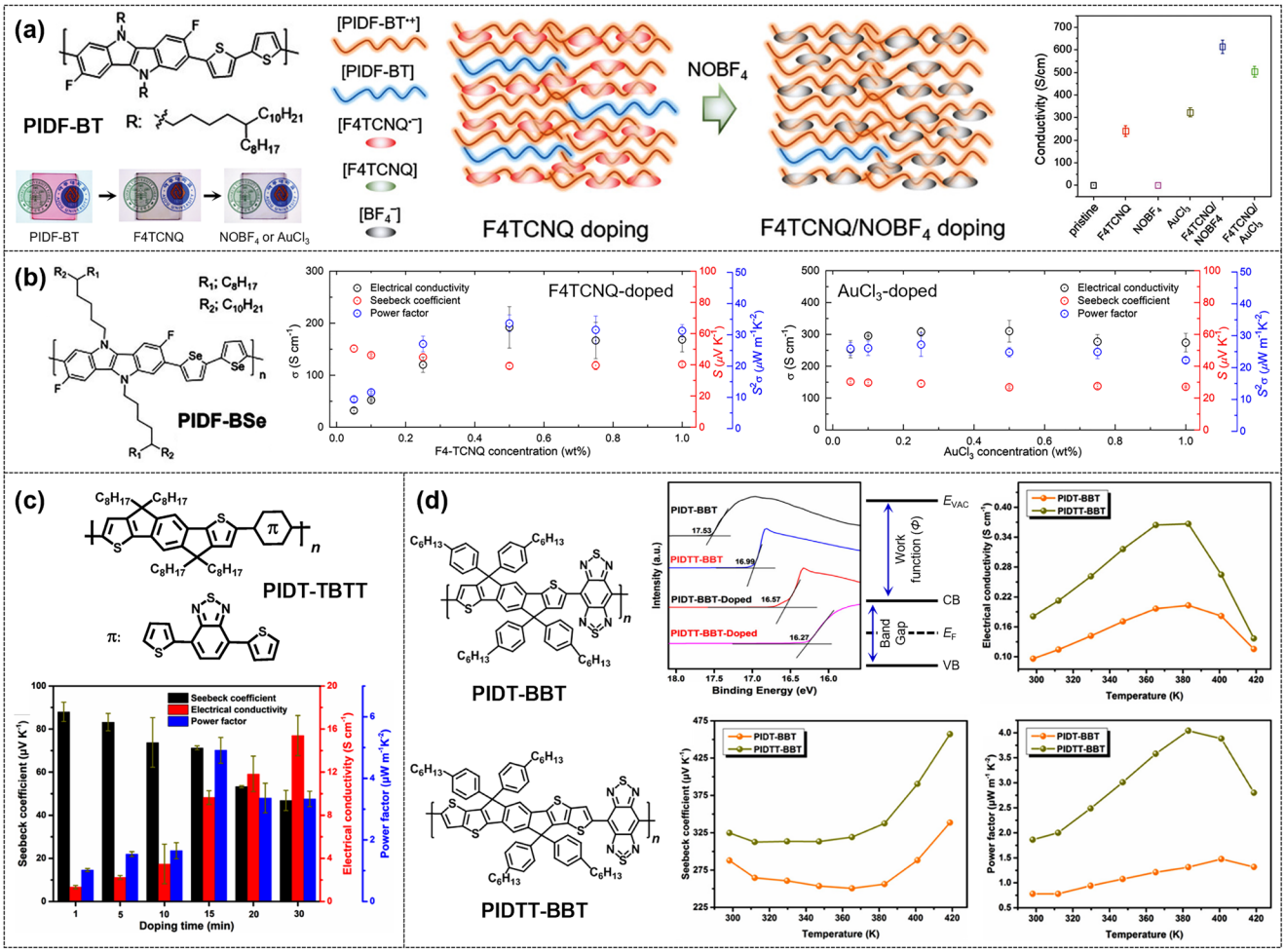


FIGURE 5 | IDID- and IDT-based copolymers for p-type TE materials. (a) Sequential doping of F4TCNQ and $NOBF_4$ on PIDF-BT films. Reproduced from 52 with permission (Copyright 2020, Wiley). (b) Structure of PIDF-BSe and its TE properties as a function of dopant concentration when doped with either F4TCNQ or $AuCl_3$. Reproduced from 53 with permission (Copyright 2022, Elsevier). (c) Chemical structure and TE properties of PIDT-TBTT with respect to the doping time. Reproduced from 56 with permission (Copyright 2020, MDPI). (d) Comparison of TE properties and the Fermi level (E_F) shifts between PIDT-BBT and PIDTT-BBT upon doping of F4TCNQ (25 mol%). Reproduced from 57 with permission (Copyright 2021, MDPI).

to control its electron-donating characteristics. For example, the CP PIDF-BT, consisting of IDF and bithiophene (BT) as a donor-donor type, aimed to enhance carrier mobility by increasing the chain planarity through inducing S-F interactions by introducing F atoms into the IDID unit (Figure 5a) [58]. Effective integer charge transfer was observed between the IDID unit and F4TCNQ. Interestingly, the doping efficiency of PIDF-BT showed a tendency to increase as the crystallinity of the PIDF-BT thin film decreased. This was interpreted as more effective diffusion of the dopant within the film when the crystallinity was lower. Through optimization of doping conditions and PIDF-BT crystallinity, a maximum electrical conductivity of over 210 $S\,cm^{-1}$ and a PF of 35 $\mu W\,m^{-1}\,K^{-2}$ were reported [35]. Later, for the same polymer, a "cascade doping" method was attempted, doping successively with different dopants such as $NOBF_4$ or $AuCl_3$ after primary doping with F4TCNQ. In this method, the diffusion of the second dopant, $NOBF_4$, into the polymer was facilitated by the increased interchain spacing induced by the first dopant, F4TCNQ. As the second dopant penetrated the polymer, the doping level was further increased. As a result, a significantly enhanced electrical conductivity of 610 $S\,cm^{-1}$ was achieved through F4TCNQ/$NOBF_4$ cascade doping, compared to the electrical conductivities obtained by doping with F4TCNQ or $NOBF_4$ alone, which were 243 $S\,cm^{-1}$ and 0.03 $S\,cm^{-1}$, respectively (Figure 5a) [61].

Studies on the TE properties of the polymer PIDF-BSe, which has the same molecular structure as PIDF-BT but introduces biselenophene (BSe) instead of bithiophene, were also conducted (Figure 5b) [36]. Selenophene has stronger electron-donating properties than thiophene, so the HOMO level of PIDF-BSe was found to be higher than that of PIDF-BT, enhancing the p-doping efficiency. Also, the Se–Se interactions increased intermolecular interactions, further enhancing charge transport characteristics. PIDF-BSe achieved a maximum electrical conductivity of 237 $S\,cm^{-1}$ and a PF of 39.7 $\mu W\,m^{-1}\,K^{-2}$ when doped with F4TCNQ, which is slightly higher than that of PIDF-BT doped with the same dopant. When doped with $AuCl_3$, PIDF-BSe exhibited a maximum electrical conductivity of 303 $S\,cm^{-1}$ and 30.9 $\mu W\,m^{-1}\,K^{-2}$ [36].

25673173, 2025, 10, Downloaded from https://onlinelibrary.wiley.com/doi/10.1002/eom2.70029 by Hansol Lee - Gachon University Global Campus , Wiley Online Library on [29/09/2025]. See the Terms and Conditions (https://onlinelibrary.wiley.com/terms-and-conditions) on Wiley Online Library for rules of use; OA articles are governed by the applicable Creative Commons License

2.1.5 | Conjugated Copolymers Containing Indacenodithiophene (IDT)

IDT serves as one of the representative donor units in D–A type conjugated copolymers. It features a fused structure of five aromatic rings, comprising a central benzene core and two thiophene rings at the ends. The presence of bridging atoms connecting the benzene and thiophene rings leads to a fused five-membered ring structure, which enhances the planarity of the conjugated backbone and extends the effective conjugation length [62, 63]. This structural feature promotes strong π–π interactions and reduces conformational disorder. Therefore, it has been utilized in the development of D–A type polymers with high carrier mobilities [37]. The bridging atoms also offer convenient sites for the introduction of side chains, allowing for modulation of solubility and control over polymer microstructure. Owing to these advantages, the IDT unit is widely employed as a building block in CPs for various electronic applications, including TE applications.

The TE properties of PIDT-TBTT, which has the IDT unit as the donor and the benzothiazole (BT) unit as the acceptor, were reported. As the immersion time of the polymer film in the dopant ($FeCl_3$) solution increased, the electrical conductivity gradually increased while the Seebeck coefficient decreased. At the optimal immersion time (15 min), an electrical conductivity of 9.65, a Seebeck coefficient of 71.26, and a PF of 4.91 $\mu W\,m^{-1}\,K^{-2}$ were achieved (Figure 5c). This PF was significantly higher than those of polymer copolymerized with thiophene instead of BT, demonstrating the importance of high carrier mobility attributed to the D–A type structure [37].

The influence of additional thiophene introduction to the IDT unit was studied in D–A type polymers composed of IDT and benzobisthiazole (BBT) units (Figure 5d) [38]. Comparing the PIDT-BBT, which has IDT as the donor unit, with PIDTT-BBT, where thiophene is further attached to both sides of IDT (forming the IDTT donor unit), it was found that PIDTT-BBT had higher chain planarity compared to PIDT-BBT. Upon solution-mixed doping with F4TCNQ, both polymers exhibited a significant increase in work function, indicating that they were effectively p-doped by F4TCNQ. When electrical conductivity and Seebeck coefficient were measured over the temperature range of 300 to 420 K, PIDTT-BBT exhibited higher values than PIDT-BBT across the entire range. The significantly higher electrical conductivity of PIDTT-BBT was attributed to its much greater hole mobility (274 $cm^2\,V^{-1}\,s^{-1}$), compared to that of PIDT-BBT (4.52 $cm^2\,V^{-1}\,s^{-1}$). PIDTT-BBT achieved a maximum power factor of 4.04 $\mu W\,m^{-1}\,K^{-2}$ at 382 K, while PIDT-BBT reached a maximum power factor of 1.47 $\mu W\,m^{-1}\,K^{-2}$ at 400 K [38].

2.1.6 | Conjugated Copolymers Containing Benzodithiophene (BDT)

The BDT unit is a widely recognized donor moiety, noted for its strong electron-donating capability and high molecular planarity, which collectively contribute to the formation of polymers with high carrier mobility and narrow bandgaps [41]. Additionally, the optical and electrical properties of BDT-based polymers can be fine-tuned through the strategic modification of side chains attached to the central benzene ring. Owing to these favorable characteristics, BDT-based D-A polymers have been extensively investigated for their potential application as TE materials.

The TE properties of PBDTDTBTF, a polymer composed of BDT as the donor unit and benzothiadiazole (BT) as the acceptor unit, were systematically compared by modifying the side chains on the BDT unit. Specifically, alkoxy, alkylthiophene, and alkylthienothiophene side chains were introduced in PBDTDTBTF-1, PBDTDTBTF-2, and PBDTDTBTF-3, respectively (Figure 6a) [39]. Among these, PBDTDTBTF-3 exhibited enhanced crystallinity because incorporating an alkylthienothiophene side chain improved the planarity of the polymer backbone and effectively extended the conjugation length. The room temperature electrical conductivity of the $FeCl_3$-doped polymers increased in the order of PBDTDTBTF-1 (0.002 $S\,cm^{-1}$) < PBDTDTBTF-2 (0.349 $S\,cm^{-1}$) < PBDTDTBTF-3 (1.519 $S\,cm^{-1}$), consistent with the increasing degree of side chain conjugation. The electrical conductivity of these polymers decreased with increasing temperature, which was attributed to the disruption of intermolecular stacking at elevated temperatures. At room temperature, the Seebeck coefficients of PBDTDTBTF-1, PBDTDTBTF-2, and PBDTDTBTF-3 were 240.72 $\mu V\,K^{-1}$, 36.09 $\mu V\,K^{-1}$, and 60.83 $\mu V\,K^{-1}$, respectively. The Seebeck coefficient increased with temperature, and the rate of increase was significantly higher in PBDTDTBTF-2 and PBDTDTBTF-3 than in PBDTDTBTF-1. This indicates that polymers with two-dimensional conjugated side chain structures exhibited higher Seebeck coefficients at elevated temperatures compared to those without. The maximum power factors for each polymer were 0.037 $\mu W\,m^{-1}\,K^{-2}$ at 106°C for PBDTDTBTF-1, 0.177 $\mu W\,m^{-1}\,K^{-2}$ at 97°C for PBDTDTBTF-2, and 1.12 $\mu W\,m^{-1}\,K^{-2}$ at 70°C for PBDTDTBTF-3, demonstrating that the incorporation of conjugated side chains can significantly enhance the TE performance of BDT-based conjugated polymers [39].

Donor-donor type polymers comprising BDT and EDOT units were also investigated for their TE properties (Figure 6b) [40]. In this study, P(BDT-EDOT) featured an alkoxy side chain on the BDT unit, while P(BDTTT-EDOT) incorporated an alkylthienothiophene side chain, enabling two-dimensional (2D) conjugation in the latter polymer. The introduction of 2D conjugation in P(BDTTT-EDOT) enhanced the polymer's crystallinity, resulting in an electrical conductivity of 1.64 $S\,cm^{-1}$, approximately double that of P(BDT-EDOT) (0.81 $S\,cm^{-1}$). Furthermore, P(BDTTT-EDOT) exhibited a higher Seebeck coefficient of 115.58 $\mu V\,K^{-1}$, which was attributed to a steeper increase in the density of states near the Fermi energy level upon doping, as indicated by ultraviolet photoelectron spectroscopy, compared to P(BDT-EDOT). The temperature-dependent electrical conductivity measurements of the two doped polymers followed the variable range hopping (VRH) model more closely than the Arrhenius-type hopping model, indicating that charge transport in these materials occurs via a quasi-one-dimensional hopping mechanism. Furthermore, the analysis revealed that P(BDTTT-EDOT) possesses a higher density of states (DOS) at the Fermi level, a shorter average hopping distance, and a lower average hopping energy compared to P(BDT-EDOT), further confirming that P(BDTTT-EDOT) enables greater charge generation and more efficient charge transport. The optimized PF

25673173, 2025, 10, Downloaded from https://onlinelibrary.wiley.com/doi/10.1002/eom2.70029 by Hansol Lee - Gachon University Global Campus , Wiley Online Library on [29/09/2025]. See the Terms and Conditions (https://onlinelibrary.wiley.com/terms-and-conditions) on Wiley Online Library for rules of use; OA articles are governed by the applicable Creative Commons License

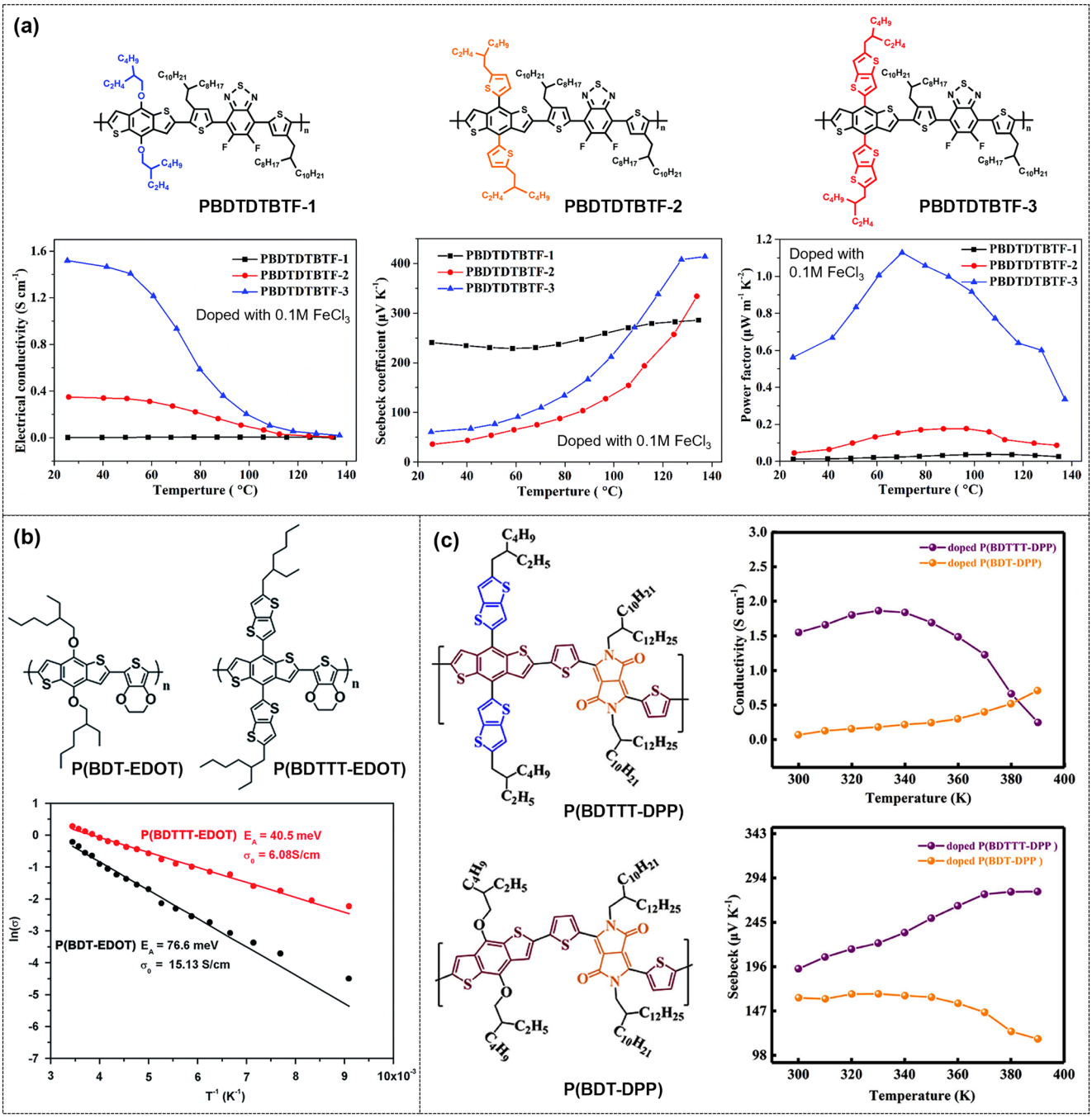


FIGURE 6 | BDT-based copolymers for p-type TE materials. (a) Comparison between PBDTDTBTF-1, PBDTDTBTF-2, and PBDTDTBTF-3 to assess the side chain effects on TE properties. Reproduced from 59 with permission (Copyright 2018, The Royal Society of Chemistry). (b) Comparison of electrical conductivity (σ) between P(BDT-EDOT) and P(BDTTT-EDOT) as a function of temperature (T). Reproduced from 60 with permission (Copyright 2019, The Royal Society of Chemistry). (c) Comparison of TE properties between P(BDTTT-DPP) and P(BDT-DPP) as a function of temperature. Reproduced from 58 with permission (Copyright 2021, American Chemical Society).

of P(BDTTT-EDOT) was reported as 2.19 $\mu W\,m^{-1}\,K^{-2}$ at room temperature, representing a fivefold improvement over P(BDT-EDOT). The PF of P(BDTTT-EDOT) increased significantly with rising temperature, reaching 101.3 $\mu W\,m^{-1}\,K^{-2}$ at 350 K [40].

The beneficial effects of 2D conjugation were similarly observed in D–A type polymers comprising BDT and DPP units (Figure 6c) [41]. The polymer P(BDTTT-DPP), which incorporated 2D conjugation, exhibited higher crystallinity compared to P(BDT-DPP), which lacked 2D conjugation. Additionally, the reduction in crystallinity upon doping with $FeCl_3$ was less pronounced in P(BDTTT-DPP) than in P(BDT-DPP). Notably, the lamellar stacking distance in P(BDTTT-DPP) was greater than that in P(BDT-DPP), facilitating more effective dopant infiltration during doping. This structural characteristic was interpreted as minimizing the extent of crystallinity disruption caused by dopant infiltration. When examining the temperature-dependent TE properties over the range of 300 K to 390 K, both polymers showed increases in electrical conductivity and Seebeck coefficient up to 340 K.

25673173, 2025, 10, Downloaded from https://onlinelibrary.wiley.com/doi/10.1002/eom2.70029 by Hansol Lee - Gachon University Global Campus , Wiley Online Library on [29/09/2025]. See the Terms and Conditions (https://onlinelibrary.wiley.com/terms-and-conditions) on Wiley Online Library for rules of use; OA articles are governed by the applicable Creative Commons License

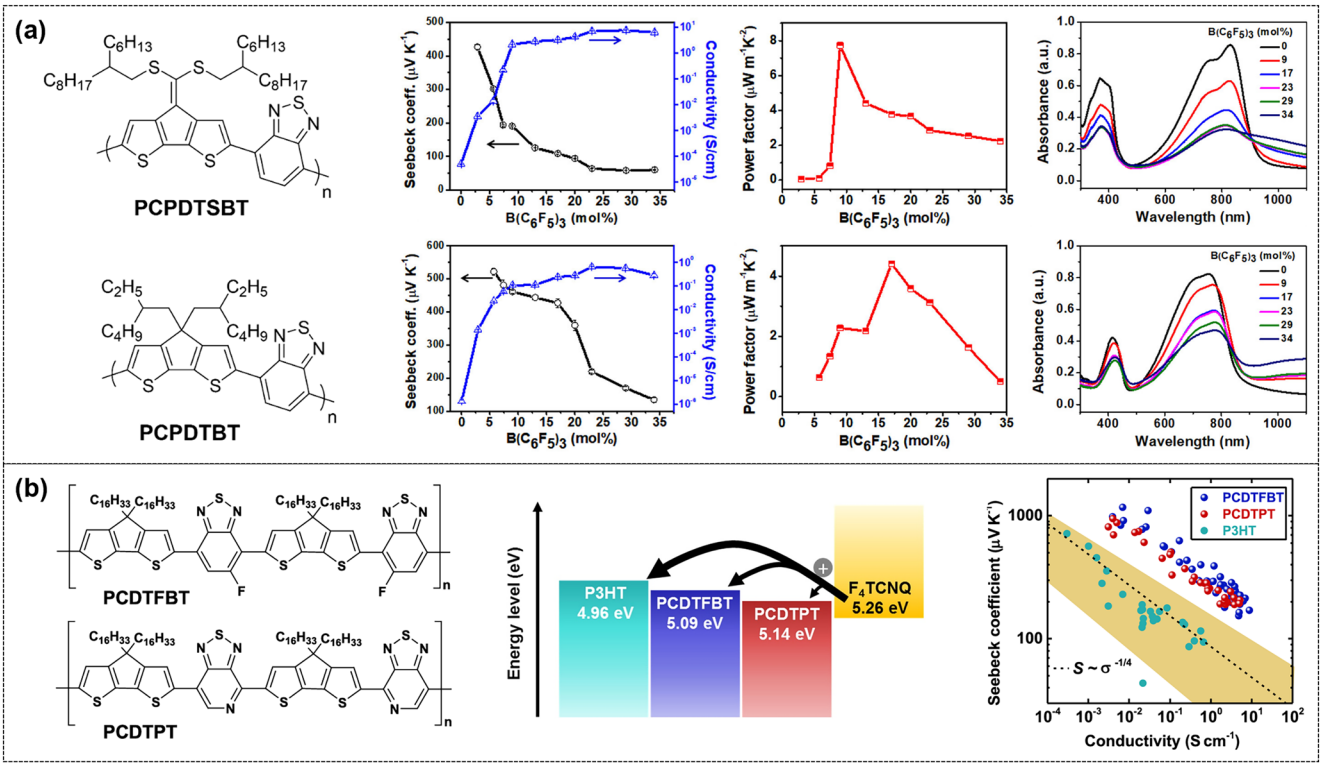


FIGURE 7 | CPDT-based copolymers for p-type TE materials. (a) Comparison of TE properties and absorption spectra between PCPDTSBT and PCPDTBT with respect to $B(C_6F_5)_3$ concentration. Reproduced from 61 with permission (Copyright 2018, American Chemical Society). (b) Comparison of TE properties between PCDTFBT, PCDTPT, and P3HT. Scheme of charge transfer efficiency from F4TCNQ to polymers with respect to the energy difference between the polymer HOMO and the F4TCNQ LUMO (Center). Reproduced from 63 with permission (Copyright 2019, Elsevier).

However, beyond this point, the two polymers exhibited distinct temperature-dependent behaviors. As the temperature continued to rise, P(BDTTT-DPP) showed a decrease in electrical conductivity and a continued increase in Seebeck coefficient, whereas P(BDT-DPP) exhibited a continuous increase in electrical conductivity accompanied by a decrease in Seebeck coefficient. Although the origin of this difference in temperature dependence was not fully clarified, it was assumed to stem from the structural differences between the two polymers. Consequently, P(BDTTT-DPP) achieved a PF of up to 6.50 $\mu W\,m^{-1}\,K^{-2}$ at room temperature, representing a 26-fold improvement compared to P(BDT-DPP). Additionally, within the measured temperature range, P(BDTTT-DPP) reached a maximum PF of 10.50 $\mu W\,m^{-1}\,K^{-2}$ at 350 K, while P(BDT-DPP) achieved a maximum PF of 0.95 $\mu W\,m^{-1}\,K^{-2}$ at 390 K [41].

2.1.7 | Conjugated Copolymers Containing Cyclopentadithiophene (CPDT)

The CPDT unit, composed of electron-rich dithiophene, is commonly employed in the design of D–A polymers due to its high planarity and favorable electronic properties [57]. The planar structure of the CPDT unit enables CPDT-based conjugated polymers to adopt a more ordered structure with higher crystallinity, which contributes to efficient charge transport and enhanced hole mobility [23]. Moreover, the methylene carbon in the CPDT unit possesses two acidic protons, allowing for facile functionalization. In addition, due to its lower resonance energy compared to benzene, CPDT more readily loses π electrons upon doping, making it well suited for application in TE polymers [23].

For D–A polymers incorporating CPDT as the donor unit and benzothiadiazole (BT) as the acceptor unit, the influence of CPDT's side chains on TE performance has been extensively studied [42]. Comparative studies of PCPDTBT, with an alkyl side chain on the CPDT unit, and PCPDTSBT, featuring a bis(alkylsulfanyl)methylene side chain, revealed significant differences in their properties (Figure 7a). The bis(alkylsulfanyl)methylene side chain in PCPDTSBT not only introduced a planar double bond but also enhanced molecular interactions through S–S interactions between sulfur atoms. These features contributed to a higher degree of crystallinity in PCPDTSBT compared to PCPDTBT. The stronger interchain interactions and higher crystallinity of PCPDTSBT compared to PCPDTBT were confirmed by their UV–vis absorption spectra, as evidenced by the more pronounced shoulder peaks and the smaller optical band gap observed for PCPDTSBT. It is noted that while the stronger interchain interaction of PCPDTSBT was beneficial for enhancing the ordering of the polymer film, it was less advantageous for doping efficiency, likely because the tighter interchain packing hindered the effective penetration of the dopant. When doped with $B(C_6F_5)_3$, PCPDTSBT exhibited an electrical conductivity of 7.47 $S\,cm^{-1}$ at a dopant concentration of 29 mol%, which is ten times higher than that of PCPDTBT (0.65 $S\,cm^{-1}$ at a dopant concentration of 23 mol%). PCPDTSBT achieved optimal TE performance at a relatively lower dopant concentration

25673173, 2025, 10, Downloaded from https://onlinelibrary.wiley.com/doi/10.1002/eom2.70029 by Hansol Lee - Gachon University Global Campus , Wiley Online Library on [29/09/2025]. See the Terms and Conditions (https://onlinelibrary.wiley.com/terms-and-conditions) on Wiley Online Library for rules of use; OA articles are governed by the applicable Creative Commons License

of 9 mol%, recording a maximum PF of 7.73 $\mu W\,m^{-1}\,K^{-2}$, while PCPDTBT showed a lower maximum PF of 4.41 $\mu W\,m^{-1}\,K^{-2}$ at a dopant concentration of 17 mol% [42]. Subsequent research optimized the $FeCl_3$ doping process for PCPDTSBT, leading to a remarkable increase in electrical conductivity to 206 $S\,cm^{-1}$ and a maximum PF of 49.8 $\mu W\,m^{-1}\,K^{-2}$ [64]. These results underscore the critical role of side-chain engineering in enhancing the TE properties of D–A polymers.

The TE performances of CPDT-based polymers were systematically investigated by incorporating pyridine thiadiazole (PT) as the acceptor unit (PCDTPT) or fluorinated benzothiadiazole (FBT) as the acceptor unit (PCDTFBT) (Figure 7b) [43]. Both polymers exhibit high planarity and exceptional carrier mobility, leading to excellent TE properties. Importantly, their crystalline structure remains largely intact after doping with F4TCNQ, preserving their key electronic characteristics. Even when mixed with dopants in solution, these polymers demonstrated minimal reductions in solubility, enabling the production of uniformly doped polymer films via solution mixing of dopant. PCDTFBT and PCDTPT exhibited lower HOMO energy levels than the benchmark homopolymer P3HT, with PCDTPT having the lower HOMO level of the two. It was observed that a lower HOMO energy level resulted in reduced doping efficiency, possibly due to the diminished energetic driving force for charge transfer from F4TCNQ. Nevertheless, the electrical conductivity and Seebeck coefficient of PCDTFBT and PCDTPT were significantly higher than those of P3HT. The maximum electrical conductivities of PCDTFBT and PCDTPT were 8.73 and 5.13 $S\,cm^{-1}$, respectively, which are approximately one order of magnitude higher than that of P3HT (0.61 $S\,cm^{-1}$). This was attributed to the superior charge transport ability of the two polymers, as mentioned earlier. As a result, in the double logarithmic plot of Seebeck coefficient versus electrical conductivity, the data points of PCDTFBT and PCDTPT were located above and to the right of those of P3HT, indicating improved TE properties. In this study, the maximum PFs were reported as 31.5 $\mu W\,m^{-1}\,K^{-2}$ for PCDTFBT, 21.8 $\mu W\,m^{-1}\,K^{-2}$ for PCDTPT, and 0.76 $\mu W\,m^{-1}\,K^{-2}$ for P3HT when doped with F4TCNQ [43].

Further research explored the influence of side-chain density on the doping efficiency of CPDT-based D–A polymers [65]. The D–A polymer P1 incorporates a CPDT donor unit in an A1–D–A2–D architecture, where the A1 unit (a DPP unit) was an acceptor unit equipped with long side chains whereas the A2 unit (a difluoro-benzothiadiazole, 2FBT) lacked side chains. This configuration created a large free volume between the polymer's side chains, facilitating dopant infiltration during the doping process. Consequently, P1 exhibited significantly enhanced doping efficiency compared to conventional D–A polymers. Additionally, a polymer P2, where the donor unit was modified from CPDT to cyclopentadithiophenyl thiophene (CPDTT), further improved doping efficiency. The additional thiophene in CPDTT increased the spacing between side chains, providing greater accessibility for dopants and resulting in even higher doping efficiency [65]. These findings highlight the critical role of side-chain engineering and polymer architecture in optimizing TE performance and doping efficiency for CPDT-based D–A polymers.

2.1.8 | Conjugated Copolymers Containing Dithienopyrrole (DTP) or Dithienosilole (DTS)

Like CPDT unit, DTP and DTS units possess a bridged dithiophene structure and are rich in electrons due to the presence of two thiophene rings, making them commonly used donor units in D–A type conjugated copolymers. Unlike CPDT, which features a carbon atom as the bridging atom between thiophenes, DTP and DTS incorporate nitrogen and silicon atoms, respectively. The DTP unit exhibits stronger electron-donating ability due to the delocalization of the nitrogen atom's lone pair electrons over the aromatic system [57], and also offers versatile opportunities for N-functionalization through the nitrogen site [66]. In the case of DTS, the C–Si bond is longer than the C–C bond, resulting in reduced steric hindrance, which can promote enhanced π–π stacking of DTS-containing polymers [67].

The TE properties of DTP-based copolymers have been extensively studied by combining DTP units with various acceptor units such as bithiophene, thienothiophene, and DPP units [12]. The D–A type polymer DPP-MeDTP, formed by copolymerizing DTP with DPP units, demonstrated markedly superior TE performance compared to the donor–donor polymers DTP-T2 and DTP-TT, which are synthesized by copolymerizing DTP with bithiophene (T2) or thienothiophene (TT) (Figure 8a). The enhanced performance of DPP-MeDTP is attributed to its higher planarity, leading to improved electrical conductivity. While the dopant molecules often degrade the crystallinity of CP upon doping, it was observed that DPP-MeDTP retained its crystalline structure during doping, unlike DTP-T2 and DTP-TT, which exhibited significant degradation in their crystallinities. Despite its relatively low doping efficiency, DPP-MeDTP achieved sufficient electrical conductivity to yield a peak power factor (PF) of 85.2 $\mu W\,m^{-1}\,K^{-2}$ when doped with F4TCNQ, a performance improvement of several-fold compared to DTP-T2 (12.4 $\mu W\,m^{-1}\,K^{-2}$) and DTP-TT (3.63 $\mu W\,m^{-1}\,K^{-2}$) [12].

Meanwhile, DTS was combined with 2FBT units to form a donor unit, while thiophene (PDFD-T), thienothiophene (PDFD-TT), and dithienothiophene (PDFD-DTT) were incorporated as donor units (Figure 8b) [44]. PDFD-TT and PDFD-DTT exhibited higher HOMO energy levels than PDFD-T due to their electron-richer donor units, resulting in greater doping efficiency and charge concentration upon doping with $FeCl_3$. However, these polymers suffered significant crystalline damage during doping, leading to a reduction in carrier mobility in the order of PDFD-T > PDFD-TT > PDFD-DTT. Consequently, PDFD-T exhibited the highest electrical conductivity and PF values. More specifically, under optimal conditions, PDFD-T achieved an electrical conductivity of 363.0 $S\,cm^{-1}$, a Seebeck coefficient of 46.8 $\mu V\,K^{-1}$, and a PF of 79.5 $\mu W\,m^{-1}\,K^{-2}$; PDFD-TT achieved an electrical conductivity of 118.1 $S\,cm^{-1}$, a Seebeck coefficient of 48.6 $\mu V\,K^{-1}$, and a PF of 28.3 $\mu W\,m^{-1}\,K^{-2}$; and PDFD-DTT achieved an electrical conductivity of 42.6 $S\,cm^{-1}$, a Seebeck coefficient of 43.7 $\mu V\,K^{-1}$, and a PF of 8.1 $\mu W\,m^{-1}\,K^{-2}$. Further investigations into PDFD-T revealed the effect of molecular weight on TE performance. Higher molecular weight PDFD-T retained its crystalline structure more effectively during doping, preserving charge transport pathways. As a result, while PDFD-T with high molecular weight achieved a PF of

25673173, 2025, 10, Downloaded from https://onlinelibrary.wiley.com/doi/10.1002/eom2.70029 by Hansol Lee - Gachon University Global Campus , Wiley Online Library on [29/09/2025]. See the Terms and Conditions (https://onlinelibrary.wiley.com/terms-and-conditions) on Wiley Online Library for rules of use; OA articles are governed by the applicable Creative Commons License

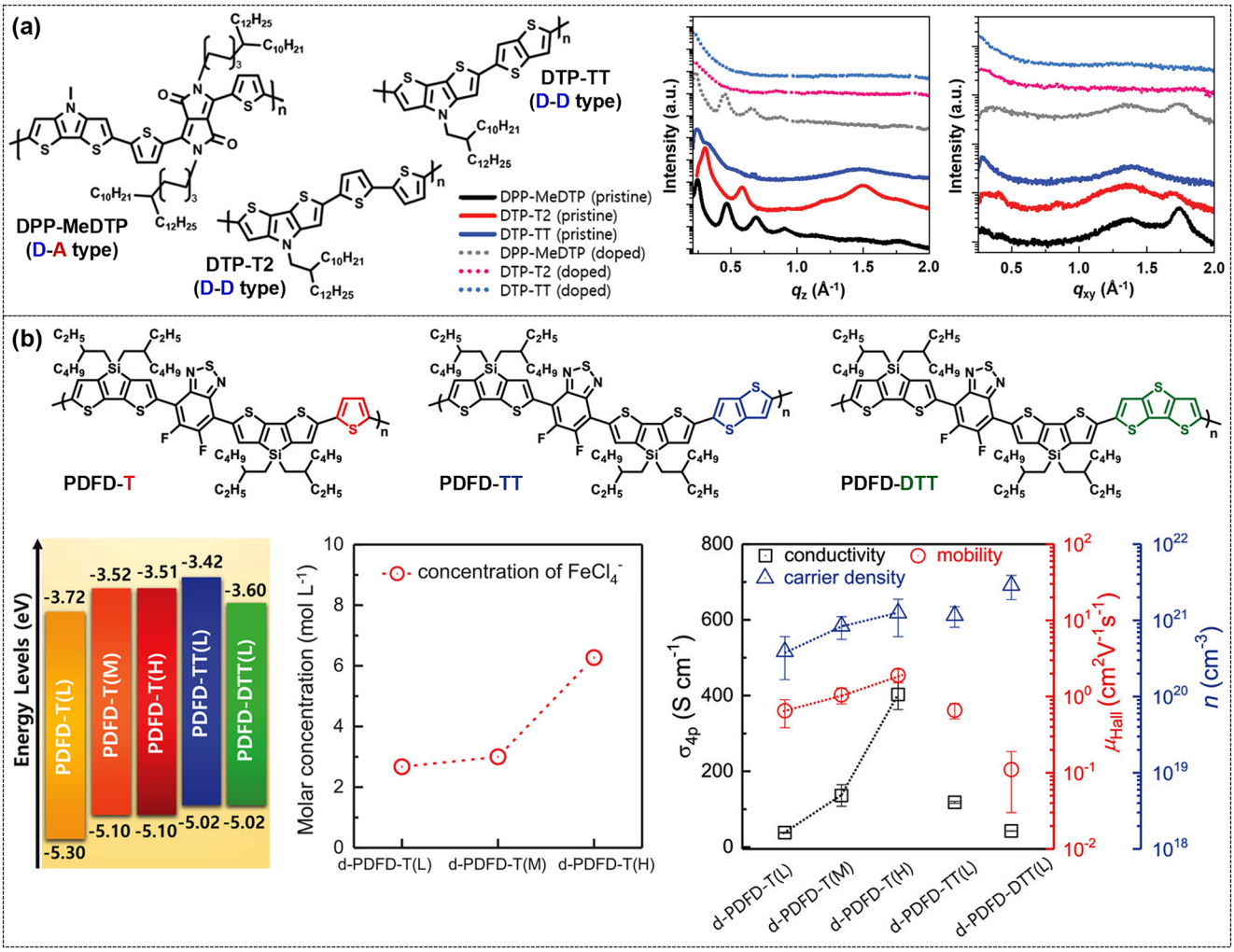


FIGURE 8 | DTP or DTS-based copolymers for p-type TE materials. (a) Comparison of microstructures between DPP-MeDTP, DTP-T2, and DTP-TT, with and without doping. Reproduced from 12 with permission (Copyright 2022, Wiley). (b) Comparison of energy bands and TE properties between PDFD-T, PDFD-TT and PDFD-DTT. The label (L), (M), and (H) indicate the low, medium, and high molecular weight, respectively (Center). Reproduced from 67 with permission (Copyright 2022, Wiley).

79.5 $\mu W\,m^{-1}\,K^{-2}$, PDFD-T with low molecular weight achieved an optimal PF of 31.8 $\mu W\,m^{-1}\,K^{-2}$, demonstrating the critical role of molecular weight in optimizing TE performance [44].

2.2 | N-Type CPs

To date, the TE performance of n-type polymers remains significantly inferior to that of their p-type counterparts [3]. A primary limitation of n-type TE polymers originates from the markedly lower doping efficiency, which leads to low electrical conductivity. While electrical conductivities exceeding 1000 $S\,cm^{-1}$ have been consistently reported for p-type polymers, n-type polymers have rarely surpassed conductivities of 1 $S\,cm^{-1}$, with only a limited number of polymers achieving such levels [68]. Both p-type and n-type polymers are capable of attaining high carrier mobilities exceeding 1 $cm^2\,V^{-1}\,s^{-1}$; therefore, the disparity in electrical conductivity is predominantly attributed to the lower charge density of n-type polymers, a direct consequence of their reduced doping efficiency. Moreover, the poor oxidative stability of n-type polymers and their dopants further hinders advancements in high-performance TE CPs [9]. Addressing these challenges is critical to bridging the performance gap between p-type and n-type TE materials.

Very recently, a number of insightful studies have achieved outstanding power factor values in n-type CPs. The strategies of these studies include the molecular design and optimization of the doping process. With demonstrated power factor around 100 $\mu W\,m^{-1}\,K^{-2}$, these studies revitalized the CP-based TE materials by offering the potential to realize high-performance TE p-n couples of CPs. The recent progress on the n-type TE CPs also provides insights into the material design and the doping process to further enhance the TE performance in both p- and n-type CPs (Table 2).

2.2.1 | Poly(Benzodifuran-Dione) (PBFDO)

While the TE properties of n-type CPs are still lower than those of p-type CPs, Tang et al. recently have made significant progress in poly(benzodifuran-dione) (PBFDO) (Figure 9a) [19]. PBFDO exhibited an ultrahigh conductivity over 2000 $S\,cm^{-1}$ due to high carrier concentration over 10^{22} cm^{-3}. Such a high

25673173, 2025, 10, Downloaded from https://onlinelibrary.wiley.com/doi/10.1002/eom2.70029 by Hansol Lee - Gachon University Global Campus , Wiley Online Library on [29/09/2025]. See the Terms and Conditions (https://onlinelibrary.wiley.com/terms-and-conditions) on Wiley Online Library for rules of use; OA articles are governed by the applicable Creative Commons License

TABLE 2 | Summary of key TE parameters of representative n-type conjugated polymers.

Polymer	Dopant	Maximum PF [$\mu W\,m^{-1}\,K^{-2}$]	References
PBFDO	—	90	[19]
P(NDIOD-T2)	N-DMBI	0.1	[18]
P(NDIOD-T2)	TDAE	0.012	[69]
p(gNDI-gT2)	N-DMBI	0.4	[70]
TEG-N2200	N-DMBI	0.4	[71]
P(NDI2OD-Tz2)	TDAE	1.5	[69]
PNDI2TEG-2Tz	N-DMBI	4.5	[72]
PNDI2C8TEG-2Tz	N-DMBI	16.5	[73]
pNB	N-DMBI	0.3	[74]
pNB-Tz	N-DMBI	9.9	[74]
pNB-TzDP	N-DMBI	53.4	[74]
BDPPV	N-DMBI	2.5	[75]
ClBDPPV	N-DMBI	17	[75]
FBDPPV	N-DMBI	28	[75]
UFBDPPV	N-DMBI	11.6	[76]
	TAM	80	[76]
LPPV-1	N-DMBI	1.96	[77]
	TAM	33.9	[76]
LPPV-2	N-DMBI	0.25	[77]
PDPH	N-DMBI	5.11×10^{-4}	[68]
PDPF	N-DMBI	4.65	[68]
P(TDPP-CT2)	N-DMBI	9.3	[78]
P(PzDPP-CT2)	N-DMBI	57.3	[78]
2DPP-2CNTVT	N-DMBI	115	[79]
BBL	TDAE	0.43	[80]
PI-BN	N-DMBI	0.02	[81]
A-A	N-DMBI	0.25	[82]
A-N	N-DMBI	1.6	[82]
N-N	N-DMBI	3.2	[82]
P2	N-DMBI	0.16	[83]
P-75	N-DMBI	13.2	[84]

degree of doping level can be achieved through in situ doping during the polymerization in a similar manner that a high degree of doping level was achieved in PEDOT:PSS. PBFDO was synthesized from H-BFDO monomer in the presence of duroquinone (TMQ) and idebenone. During the oxidative synthesis, BFDO suffers from not only polymerization but also reduction to have negative polarons, which were balanced by protons. Though PBFDO had no side chains, the resulting PBFDO was well dissolved in solvents with high dielectric constant because of its highly charged state. When a PBFDO solution was deposited to form a solid film, the absence of side chains and bulky dopant molecules enabled the PBFDO chains to form a tightly stacked structure, in which highly planar polymer backbones were stacked with minimal structural distortion. The PBFDO showed the Seebeck coefficient of $-21.02\,\mu V\,K^{-1}$, which corresponded to the power factor of $90\,\mu W\,m^{-1}\,K^{-2}$. This value is one of the highest power factors among n-type CPs to date. It was also demonstrated that, when one end of the TEG composed of PBFDO and PEDOT:PSS was attached to a hot plate, a maximum power output of 1940 nW was achieved at a hot plate temperature of 160°C.

In successive studies by J. Mei et al. [85, 86], the detailed synthetic mechanism of PBFDO and the variations in its electrical conductivity depending on different synthetic conditions were thoroughly investigated (Figure 9b). When $Cu(III)(OAc)_2$ was added to BFDO monomers, the removal of protons from furanone rings enabled both polymerization and n-type doping with a catalytic cycle under air conditions. Synthesis of PBFDO was performed under various reaction conditions, including catalyst loading, reaction temperature, and the type of additive used, and as a result, a significantly enhanced electrical conductivity of up to $6100\,S\,cm^{-1}$ was reported. This study also demonstrated that under certain reaction conditions, isomerization of the BFDO monomer can occur, leading to the formation of benzodipyranone (CCD). The BFDO monomer or 2-BFDO oligomer can experience chemical isomerization in the presence of water under heating. The CCD structure can construct a ladder polymer, which is more planar than the PBFDO, but the CCD structure cannot be doped during the synthesis. Recently, the incorporation of the CCD repeat unit in the PBFDO chain was reported to enhance the TE properties [87]. A transition from the BFDO to CCD form in the PBFDO chain decreased the doping level, thereby decreasing electrical conductivity. However, this transition also removed protons, which originally balanced the negatively charged polaron and severely distorted the polymer backbone. Therefore, the optimized degree of the transition effectively flattened the polymer backbone, increasing the carrier mobility. Moreover, the heterogeneous repeat units filtered the conduction of low-energy charge carriers, improving the Seebeck coefficient and, thereby, the power factor.

2.2.2 | CPs Containing Naphthalenediimide (NDI)

NDI unit features an electron-deficient aromatic core with two electron-withdrawing imide groups, resulting in a low-lying LUMO energy level that is favorable for efficient electron transport in n-type conjugated polymers. Moreover, the NDI unit can be readily synthesized from commercially available precursors, and its imide nitrogen atoms can be functionalized, which facilitates control over the polymer's solubility and film microstructure [88]. The 2,6-positions of the NDI core allow for highly regioselective bromination, enabling effective copolymerization with various aromatic moieties and extending π-conjugation [88]. These features allow for tunability of the electronic structure and interchain interactions

25673173, 2025, 10, Downloaded from https://onlinelibrary.wiley.com/doi/10.1002/eem2.70029 by Hansol Lee - Gachon University Global Campus , Wiley Online Library on [29/09/2025]. See the Terms and Conditions (https://onlinelibrary.wiley.com/terms-and-conditions) on Wiley Online Library for rules of use; OA articles are governed by the applicable Creative Commons License

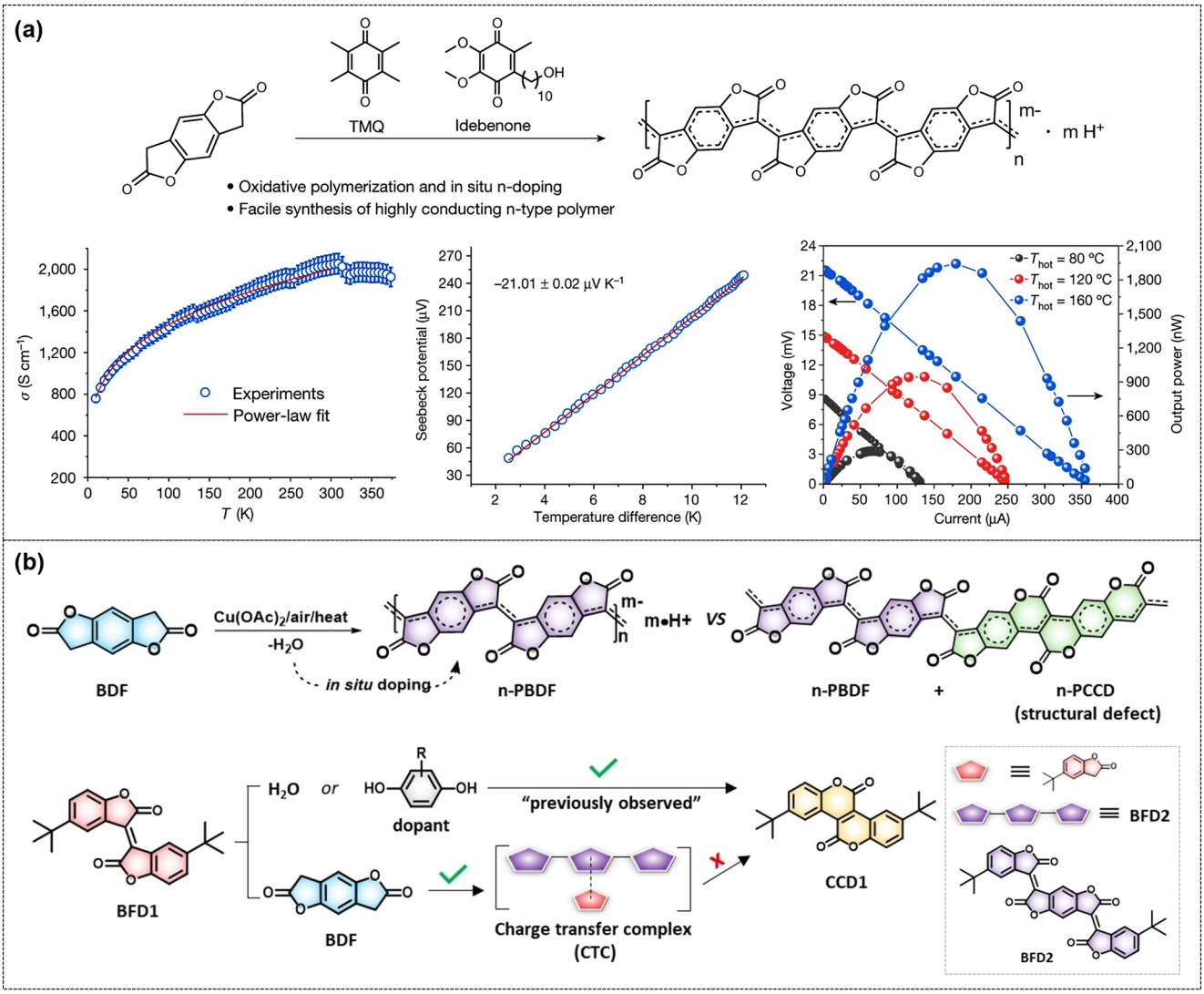


FIGURE 9 | PBFDO-based TE materials. (a) The synthetic strategies and the TE properties of PBFDO. Reproduced from 19 with permission (Copyright 2022, Springer Nature). (b) The evolution of structural defects during the synthesis of PBFDO (PBFD). BFDO (BFD) monomer can undergo chemical isomerization to CCD, which cannot be doped. Reproduced from 69 with permission (Copyright 2024, Wiley).

of NDI-based polymers. Owing to these advantages, the NDI unit has been widely utilized as a versatile building block in various organic electronic applications, including n-type TE materials.

In one of the early studies on NDI-based n-type TE polymers, P(NDIOD-T2), a D–A type conjugated copolymer composed of NDI and bithiophene (T2) units, was investigated. P(NDIOD-T2) is primarily doped using hydride transfer dopants, exhibiting electrical conductivities on the order of $10^{-3}\,S\,cm^{-1}$ and PF at the level of $0.1\,\mu W\,m^{-1}\,K^{-2}$ (Figure 10a) [3, 18]. Several factors contribute to the relatively low TE performance of P(NDIOD-T2): (1) poor miscibility with n-dopants, (2) charge carrier localization due to the large dihedral angle between NDI and T2 units, and (3) the low electron-accepting capability of the bithiophene donor unit [82]. Numerous efforts have been made to address these limitations and to enhance the TE performance of NDI-based polymers. P(NDIOD-T2), one of the most extensively studied NDI-based conjugated polymers in the field of organic electronics beyond thermoelectric devices, has been continuously used as a model polymer in follow-up studies aiming to overcome these limitations. Through this process, various molecular derivatives of P(NDIOD-T2) have been developed.

Improving miscibility between NDI-based polymers and n-type dopants, such as 4-(2,3-dihydro-1,3-dimethyl-1H-benzimidazol-2-yl)-N,N-dimethylbenzenamine (N-DMBI), has proven effective in increasing n-doping efficiency [70, 71]. In the absence of polar side chains, poor miscibility leads to dopant aggregation, reducing doping efficiency and electrical conductivity. However, introducing oligoethylene glycol-based polar side chains, as in p(gNDI-gT2), significantly improves miscibility, reducing dopant aggregation even at high dopant content (Figure 10b). As a result, p(gNDI-gT2) achieved a notable electrical conductivity of $0.3\,S\,cm^{-1}$ and a PF of $0.4\,\mu W\,m^{-1}\,K^{-2}$ [70]. Similarly, TEG-N2200, which replaced the alkyl side chain of P(NDIOD-T2) with a triethylene glycol side chain, achieved comparable performance with a maximum electrical conductivity of $0.17\,S\,cm^{-1}$ and a PF of $0.40\,\mu W\,m^{-1}\,K^{-2}$ (Figure 10c), as a result of the significantly improved miscibility with N-DMBI [71].

25673173, 2025, 10, Downloaded from https://onlinelibrary.wiley.com/doi/10.1002/eom2.70029 by Hansol Lee - Gachon University Global Campus , Wiley Online Library on [29/09/2025]. See the Terms and Conditions (https://onlinelibrary.wiley.com/terms-and-conditions) on Wiley Online Library for rules of use; OA articles are governed by the applicable Creative Commons License

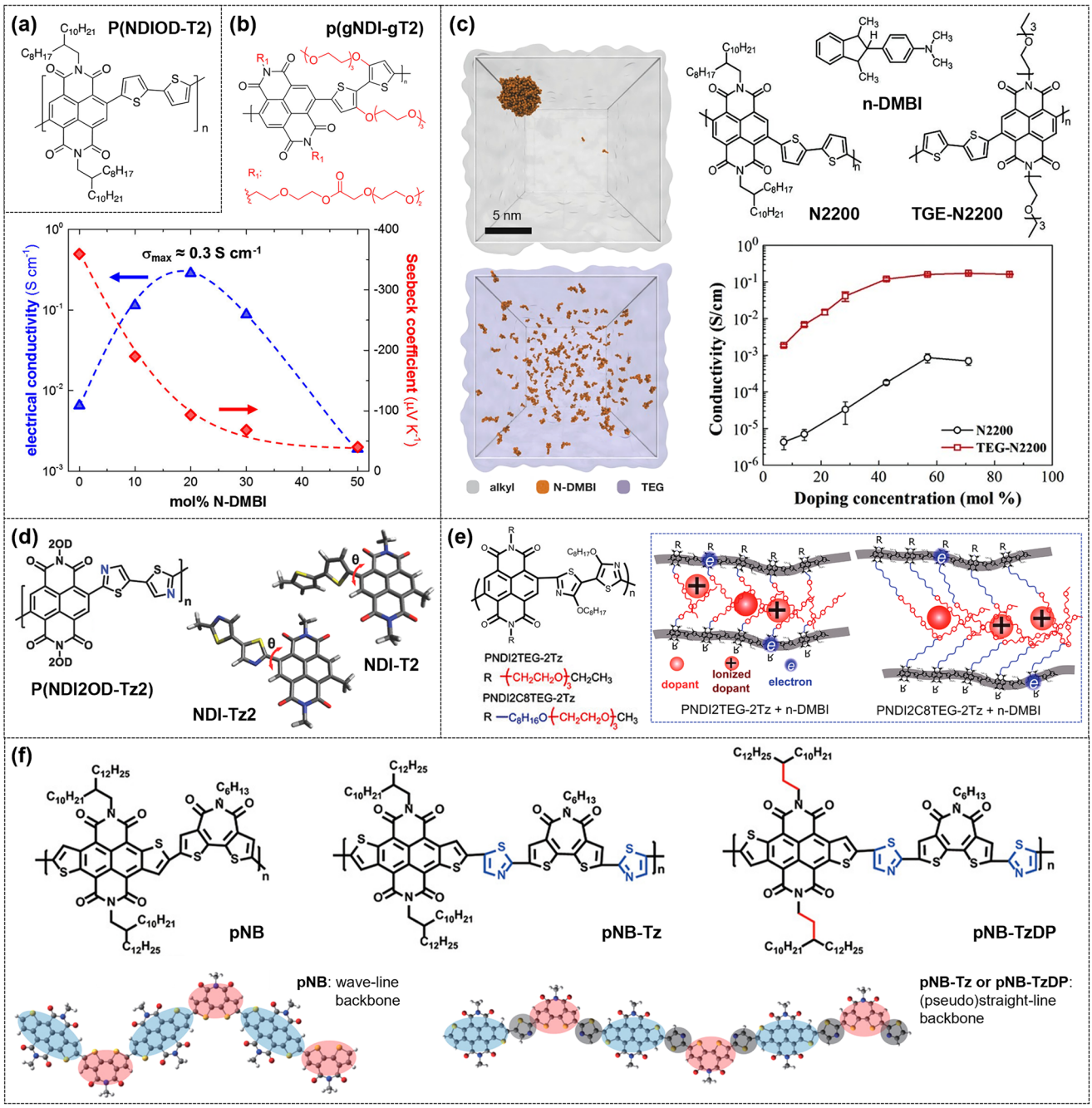


FIGURE 10 | NDI-based copolymers for n-type TE materials. (a) The chemical structure of P(NDIOD-T2). (b) The chemical structure and TE properties of P(gNDI-gT2). Reproduced from 74 with permission (Copyright 2018, American Chemical Society). (c) Comparison between N2200 and TEG-N2200. The miscibility of N-DMBI dopant molecules was improved by replacing alkyl side chain with TEG side chain (center), which improved the doping efficiency (Right). Reproduced from 75 with permission (Copyright 2018, Wiley). (d) The implemented N atom improved the planarity in P(NDI2OD-Tz2). Reproduced from 76 with permission (Copyright 2018, Wiley). (e) Comparison between PNDI2TEG-2Tz and PNDI2C8TEG-2Tz. Reproduced from 78 with permission (Copyright 2021, Wiley). (f) Comparison between pNB, pNB-Tz, and pNB-TzDP. Reproduced from 79 with permission (Copyright 2020, Wiley).

Substituting the bithiophene donor unit in P(NDIOD-T2) with a bithiazole unit formed the polymer P(NDI2OD-Tz2), which demonstrated improved TE properties (Figure 10d) [69]. The bithiazole unit reduced steric repulsion, enhanced chain rigidity and planarity, increased π–π stacking between polymer chains, and raised the polymer's electron affinity due to its electron-deficient nature. These structural improvements reduced charge carrier localization and facilitated charge transport. When doped with tetrakis(dimethylamino)ethylene (TDAE), P(NDI2OD-Tz2) exhibited an electrical conductivity of 0.1 S cm^{-1} and a PF of 1.5 μW m^{-1} K^{-2}, significantly outperforming P(NDIOD-T2), which showed a maximum PF of 0.012 μW m^{-1} K^{-2} [69].

Polymers combining polar side chains with bithiazole donor units have further advanced TE performance. PNDI2TEG-2Tz,

25673173, 2025, 10, Downloaded from https://onlinelibrary.wiley.com/doi/10.1002/eom2.70029 by Hansol Lee - Gachon University Global Campus , Wiley Online Library on [29/09/2025]. See the Terms and Conditions (https://onlinelibrary.wiley.com/terms-and-conditions) on Wiley Online Library for rules of use; OA articles are governed by the applicable Creative Commons License

which contains both polar side chains and a bithiazole donor unit, showed enhanced planarity and strong intermolecular interactions, achieving an electrical conductivity of 1.8 S cm^{-1} and a PF of 4.5 μW m^{-1} K^{-2} upon N-DMBI doping [72]. Moreover, PNDI2C8TEG-2Tz introduced an amphipathic side chain with a long alkyl spacer between the main chain and the ethylene glycol. This design reduced energetic disorder, increased the distance between ionized dopants and the main chain, and enhanced the Seebeck coefficient. Consequently, PNDI2C8TEG-2Tz achieved a PF of up to 16.5 μW m^{-1} K^{-2} when doped with N-DMBI (Figure 10e) [73].

Research on naphthodithiophenediimide (NDTI)-based polymers, such as pNB, pNB-Tz, and pNB-TzDP, has yielded promising results (Figure 10f) [74]. These acceptor–acceptor polymers integrate the NDTI unit with bithiopheneimide (pNB) or thiazole units (pNB-Tz and pNB-TzDP). The introduction of thiazole induced a more linear backbone conformation in pNB-Tz and pNB-TzDP, in contrast to the wave-like backbone of pNB. As a result, the incorporation of the thiazole unit led to increased chain linearity and enhanced intermolecular interactions in pNB-Tz and pNB-TzDP compared to pNB. Notably, pNB-TzDP with a bimodal crystal orientation (face-on and edge-on) exhibited optimized charge transport pathways and dopant penetration. The pNB-TzDP achieved an electrical conductivity of 11.6 S cm^{-1} and a PF of 53.4 μW m^{-1} K^{-2} when doped with N-DMBI, marking a significant advancement in n-type TE performance. For comparison, under optimized conditions, pNB exhibited a conductivity of 0.011 S cm^{-1} and a PF of 0.3 μW m^{-1} K^{-2}, while pNB-Tz showed a conductivity of 0.87 S cm^{-1} and a PF of 9.9 μW m^{-1} K^{-2} [74].

2.2.3 | CPs Containing Poly(*p*-Phenylene Vinylene) (PPV)

A derivative of PPV incorporating the benzodifurandione (BDP) unit is referred to as BDPPV and exhibits distinct n-type characteristics compared to conventional PPV, achieving a high carrier mobility of 1.1 cm^2 V^{-1} s^{-1} [89]. The excellent n-type transport properties of BDPPV are attributed to its molecular structure. The carbonyl groups introduced into the PPV backbone strongly withdraw electrons, thereby lowering the LUMO energy level of BDPPV. Additionally, these carbonyl groups form intramolecular hydrogen bonds with the hydrogen atoms on the adjacent benzene rings, which suppress torsion of the polymer chain and enhance backbone planarity. Owing to its outstanding n-type transport characteristics, studies have been conducted on n-type TE materials based on BDPPV and its derivatives. Comparative studies of BDPPV, ClBDPPV (chlorinated BDPPV), and FBDPPV (fluorinated BDPPV) revealed notable enhancements in TE properties upon halogenation (Figure 11a) [75]. The introduction of halogen atoms lowered the LUMO energy level, increasing the polymer's ability to accept C–H bonds and thereby improving n-doping efficiency with N-DMBI. As a result, the polymers exhibited significant differences in their electrical conductivity. BDPPV showed a maximum electrical conductivity of 0.26 S cm^{-1}, whereas ClBDPPV and FBDPPV achieved values exceeding 4 S cm^{-1}. Meanwhile, the Seebeck coefficients of all polymers decreased with increasing dopant concentration, with BDPPV showing a greater absolute value of Seebeck coefficient than the others. Among them, FBDPPV exhibited the highest TE performance, achieving a maximum power factor of 28 μW m^{-1} K^{-2} [75]. Subsequently, UFBDPPV advanced FBDPPV by applying an additional fluorine atom in the main chain. UFBDPPV achieved a maximum electrical conductivity and PF of 16 S cm^{-1} and 11.6 μW m^{-1} K^{-2}, respectively, when doped with N-DMBI. Remarkably, doping UFBDPPV with trisaminomethane (TAM) significantly improved its TE performance, yielding a maximum electrical conductivity and PF of 22.5 S cm^{-1} and 80 μW m^{-1} K^{-2}, respectively (Figure 11b). This dramatic enhancement was attributed to the chemical characteristics of TAM: it minimally perturbs the polymer backbone conformation and ordering, and its cation strong affinity for the side chains rather than the backbone [76].

Ladder-type polymers, designed to minimize main-chain twisting and to enhance planarity, have also shown promise for n-type TE applications. LPPV, a ladder-type polymer derived from PPV, features a highly robust and planar structure due to the incorporation of fused electron-deficient units (Figure 11c) [77]. This design reduces structural disorder by maintaining the shape of polymer chains through intramolecular hydrogen bonding between hydrogens and carbonyl groups within the chain. The resulting high planarity facilitates charge carrier delocalization along extended chain segments, enabling efficient intrachain charge transport. When comparing LPPV-1 and LPPV-2, which are LPPVs with different alkyl side chain lengths, LPPV-1 with the shorter side chain exhibited enhanced crystallinity. After doping with N-DMBI, LPPV-1 achieved a maximum electrical conductivity of 1.1 S cm^{-1} and a PF of 1.96 μW m^{-1} K^{-2}, whereas LPPV-2 achieved a maximum electrical conductivity of 0.07 S cm^{-1} and a PF of 0.25 μW m^{-1} K^{-2} [77]. Further improvements were observed when TAM was used as the dopant, significantly increasing the electrical conductivity and resulting in a PF of 33.9 μW m^{-1} K^{-2} [76]. These findings underscore the potential of ladder-type polymers and dopant engineering in advancing the TE performance of n-type conjugated materials.

2.2.4 | CPs Containing DPP

The DPP unit, as previously discussed in Section 2.1.3, has been extensively utilized in both p-type and n-type TE CPs, highlighting its versatility in TE device applications. Contrary to the conventional understanding that high planarity is critical for achieving high electrical conductivity in CPs, recent findings suggest that a twisted chain structure may offer advantages for doping and conductivity enhancement. For instance, the n-doped polymer P(BTP-DPP), composed of DPP and biindenothiophenylidene (BTP) units, was compared with the highly planar P(NDIOD-T2) (Figure 12a) [90]. While P(NDIOD-T2) exhibits high carrier mobility due to its linear structure, its doping efficiency is relatively low. In contrast, the twisted chain structure of P(BTP-DPP) creates sufficient free volume for effective dopant penetration. Effective doping of P(BTP-DPP) by ruthenium pentamethylcyclopentadienyl mesitylene dimer, $(RuCp^*mes)_2$ was confirmed by UPS measurements, which showed that P(BTP-DPP) became heavily doped even at relatively low dopant loadings. As a result, while P(NDIOD-T2) exhibited an electrical conductivity of approximately 10^{-4} to 10^{-5} S cm^{-1} when doped with $(RuCp^*mes)_2$, P(BTP-DPP) achieved a significantly higher electrical conductivity of 0.45 S cm^{-1} [90].

25673173, 2025, 10, Downloaded from https://onlinelibrary.wiley.com/doi/10.1002/eom2.70029 by Hansol Lee - Gachon University Global Campus , Wiley Online Library on [29/09/2025]. See the Terms and Conditions (https://onlinelibrary.wiley.com/terms-and-conditions) on Wiley Online Library for rules of use; OA articles are governed by the applicable Creative Commons License

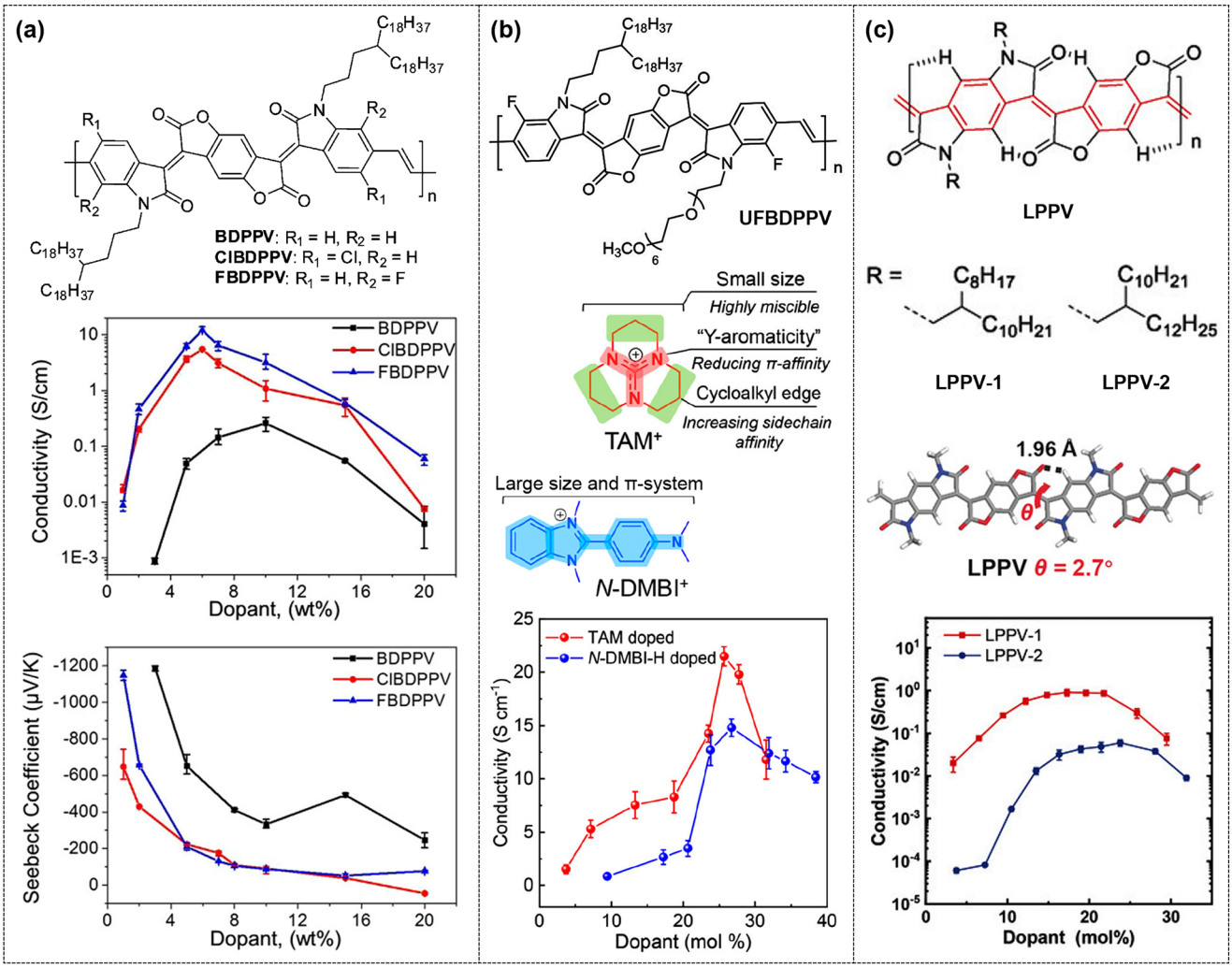


FIGURE 11 | PPV-based copolymers for n-type TE materials. (a) Effects of implemented Cl atom (CLBDPPV) and F atom (FBDPPV) on TE properties, as a function of dopant concentration. Reproduced from 81 with permission (Copyright 2015, American Chemical Society). (b) Comparison between TAM and N-DMBI for n-type dopants in UFBDPPV. Reproduced from 82 with permission (Copyright 2020, American Chemical Society). (c) Hydrogen bonding-induced ladder-type PPV-based (LPPV) polymers. Reproduced from 83 with permission (Copyright 2019, Wiley).

The effect of fluorination on the TE performance of DPP-based donor–acceptor (D–A) polymers has also been investigated [68]. In a comparative study between PDPH, which lacks fluorine atoms on the donor unit, and PDPF (Figure 12b), which incorporates fluorine, fluorination was found to enhance n-doping efficiency without compromising electron mobility. Moreover, PDPF exhibited a higher energy barrier for backbone torsion compared to PDPH, which was attributed to the formation of C–H···F and C–H···O interactions induced by the fluorine atoms in PDPF. These interactions made the polymer backbone more rigid and planar and were believed to enable more effective intrachain charge transport in PDPF than in PDPH. The electron-accepting properties introduced by fluorine also improved molecular orientation, shifting PDPF from a predominantly edge-on orientation (as observed in PDPH) to a bimodal orientation comprising both edge-on and face-on configurations. This change increased miscibility with dopants, contributing to significantly higher electrical conductivity and PF of PDPF compared to those of PDPH. While PDPH exhibited a maximum electrical conductivity of $1.01\times10^{-3}\,S\,cm^{-1}$ and a PF of $5.11\times10^{-4}\,\mu W\,m^{-1}\,K^{-2}$, PDPF showed much improved values, with a maximum electrical conductivity of $1.30\,S\,cm^{-1}$ and a PF of $4.65\,\mu W\,m^{-1}\,K^{-2}$ [90].

The TE properties of DPP-based polymers were further explored by varying the flanking units. A D–A polymer, P(PzDPP-CT2), incorporating pyrazine-flanked DPP as the acceptor unit and dicyanobithiophene as the donor unit, was compared to P(TDPP-CT2), which uses thiophene-flanked DPP instead (Figure 12c) [78]. The pyrazine unit's ability to form hydrogen bonds within the polymer chain enhanced the planarity of P(PzDPP-CT2), leading to a shorter π–π stacking distance and improved carrier mobility. Consequently, P(PzDPP-CT2) outperformed P(TDPP-CT2), achieving a maximum electrical conductivity of $8.4\,S\,cm^{-1}$ and a PF of $57.3\,\mu W\,m^{-1}\,K^{-2}$ when doped with N-DMBI. The maximum electrical conductivity and PF of P(TDPP-CT2) were $0.39\,S\,cm^{-1}$ and $9.3\,\mu W\,m^{-1}\,K^{-2}$, respectively, for reference [78]. These results underscore the critical role of flanking unit engineering in optimizing the TE properties of DPP-based CPs, highlighting the multifaceted strategies available for enhancing the TE performance of DPP-based polymers.

25673173, 2025, 10, Downloaded from https://onlinelibrary.wiley.com/doi/10.1002/eom2.70029 by Hansol Lee - Gachon University Global Campus , Wiley Online Library on [29/09/2025]. See the Terms and Conditions (https://onlinelibrary.wiley.com/terms-and-conditions) on Wiley Online Library for rules of use; OA articles are governed by the applicable Creative Commons License

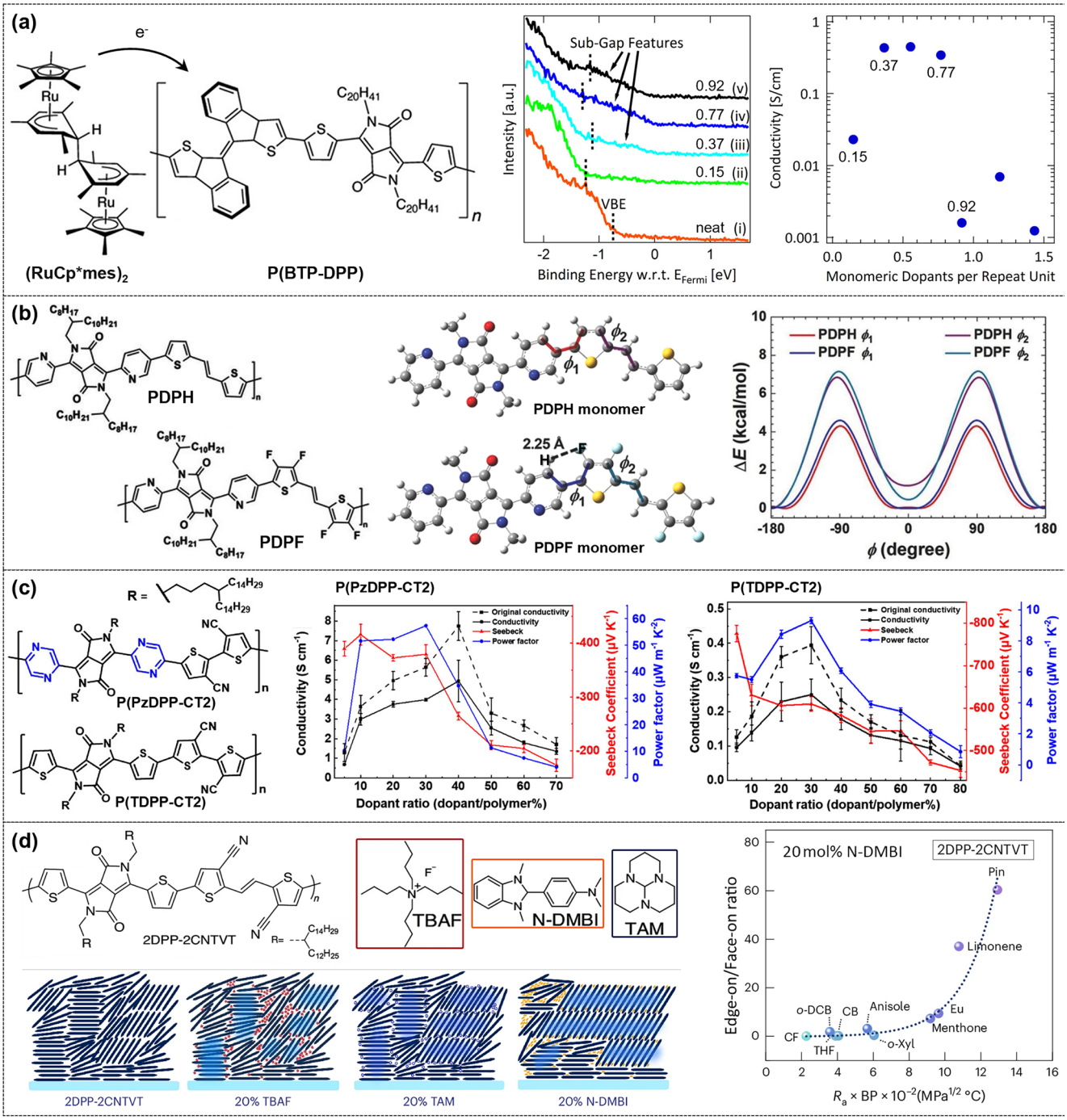


FIGURE 12 | DPP-based copolymers for n-type TE materials. (a) Chemical structure of P(BTP-DPP) and its LUMO and HOMO levels with respect to the molar ratio of dopant. Reproduced from 84 with permission (Copyright 2017, American Chemical Society). (b) Replacing protons in PDPH with F atoms (PDPF) increased the rotational potential energy through H-F interactions. Reproduced from 68 with permission (Copyright 2018, Wiley). (c) Comparison of TE properties between P(PzDPP-CT2) and P(TDPP-CT2). Reproduced from 85 with permission (Copyright 2019, American Chemical Society). (d) The effect of Hansen distance (R_a) and the boiling point (BP) of the solvents on crystalline ordering of 2DPP-2CNTVT and the dopant intercalation. Reproduced from 86 with permission (Copyright 2025, Springer Nature).

Recently, Villalva et al. reported that engineered optimization of the solvent condition and the dopant choice can dramatically improve the power factor in 2DPP-2CNTVT, incorporating DPP as the acceptor unit and dicyanobithiophene-vinylene as the donor unit (Figure 12d) [79]. The Hansen distances (R_a) between the chemical species were quantified in 3-dimensional Hansen solubility parameters-based space with axes representing dispersive, polar, and hydrogen-bonding intermolecular forces. The R_a between the solvent and the polymer was compared with that between the dopant and the polymer to evaluate the ability of the dopant to intercalate the polymer aggregates in the solvent. Among the dopants used in this study, N-DMBI showed the smallest R_a with 2DPP-2NTVT, indicating the strongest affinity with the polymer. The use of the solvent with large R_a to the polymers caused segregation of 2DPP-2NTVT, whereas solvents with the small R_a to the polymer did not allow dopant

25673173, 2025, 10, Downloaded from https://onlinelibrary.wiley.com/doi/10.1002/eom2.70029 by Hansol Lee - Gachon University Global Campus , Wiley Online Library on [29/09/2025]. See the Terms and Conditions (https://onlinelibrary.wiley.com/terms-and-conditions) on Wiley Online Library for rules of use; OA articles are governed by the applicable Creative Commons License

intercalation. Chlorobenzene (CB) was a good solvent for 2DPP-2CNTVT, but it was not for N-DMBI. Meanwhile, N-DMBI was miscible with 2DPP-2CNTVT. Therefore, the intercalation of N-DMBI into 2DPP-2CNTVT was strongly induced, causing the aggregation of 2DPP-2CNTVT:N-DMBI in the solvent state. The aggregated 2DPP-2CNTVT:N-DMBI was likely to form an edge-on configuration due to the interaction with the substrate, resulting in highly-doped, edge-on crystallites that exhibited a high power factor of 115 $\mu W m^{-1} K^{-2}$ ($ZT = 0.17$) at room temperature with a simultaneous increase in both the Seebeck coefficient and the conductivity compared to the other dopants and solvents. The study revealed the critical role of complex interactions between the dopant, the solvent, and the polymer in determining the doping efficiency and the microstructure of the polymer and their effects on the TE tradeoffs.

2.2.5 | Other n-Type CPs

In addition to the aforementioned classes of materials, various other conjugated polymers with diverse structures have also been explored for the development of n-type TE conjugated polymers. The ladder-type, non-twisting polymer BBL has been recognized for its exceptionally long charge delocalization length compared to other n-type polymers, such as P(NDI2OD-T2), attributed to its high planarity and absence of twists (Figure 13a).

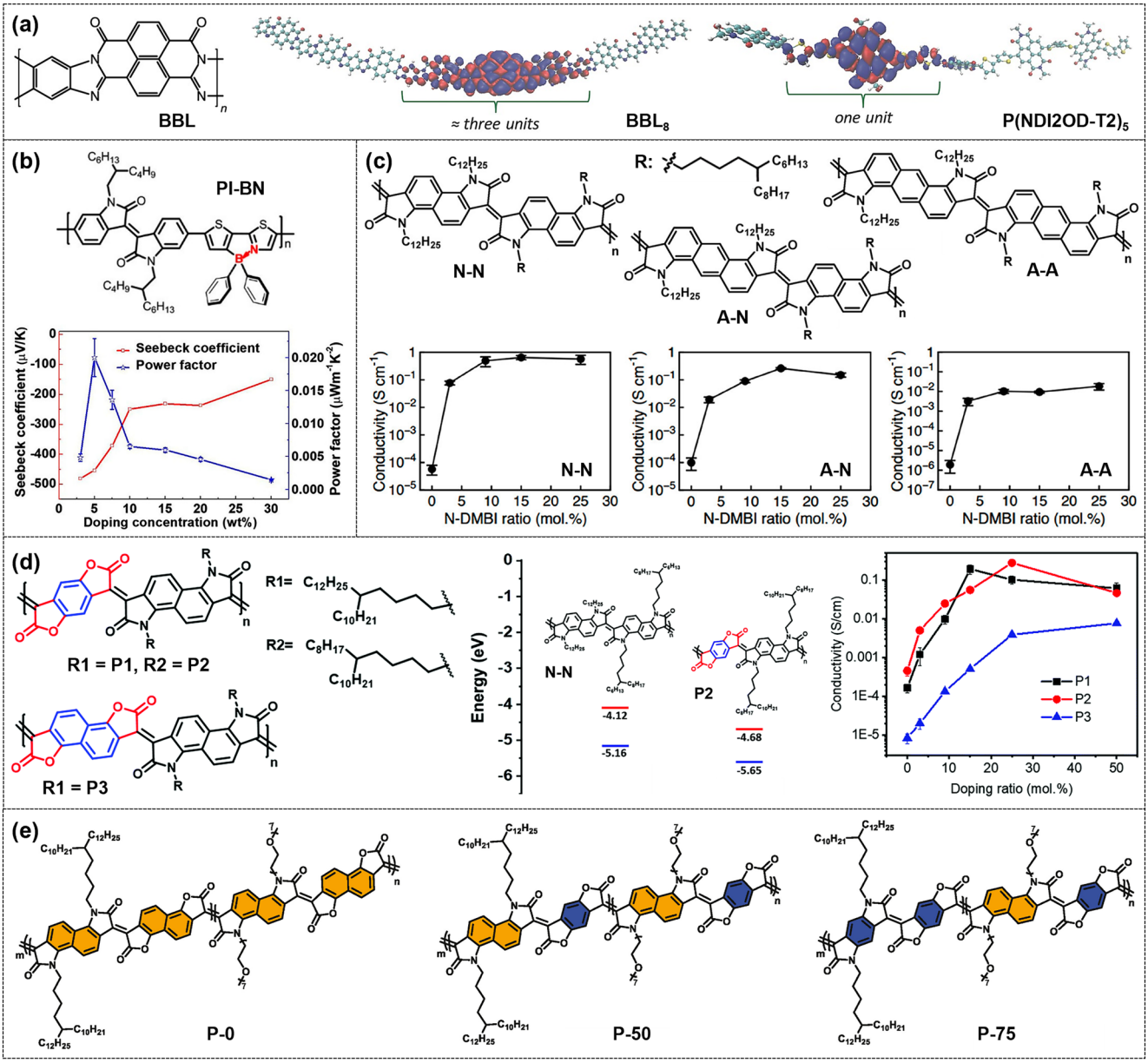


FIGURE 13 | Other CPs for n-type TE materials. (a) Comparison of charge delocalization in BBL and P(NDI2OD-T2). Reproduced from 87 with permission (Copyright 2016, Wiley). (b) Chemical structure and the TE properties of PI-BN. Reproduced from 88 with permission (Copyright 2020, American Chemical Society). (c) Chemical structures of N-N, A-N, and A-A polymers. Reproduced from 73 with permission (Copyright 2021, American Chemical Society). (d) Chemical structures and accompanied LUMO and HOMO levels of N-N polymer and its derivatives P1, P2, and P3. Reproduced from 89 with permission (Copyright 2020, The Royal Society of Chemistry). (e) Chemical structures of P-0, P-50, and P-75 polymers, where the number indicates the degree of benzene rings in the repeat unit. Reproduced from 90 with permission (Copyright 2022, Wiley).

25673173, 2025, 10, Downloaded from https://onlinelibrary.wiley.com/doi/10.1002/eom2.70029 by Hansol Lee - Gachon University Global Campus , Wiley Online Library on [29/09/2025]. See the Terms and Conditions (https://onlinelibrary.wiley.com/terms-and-conditions) on Wiley Online Library for rules of use; OA articles are governed by the applicable Creative Commons License

This feature plays a crucial role in achieving high electrical conductivity. When doped with TDAE, BBL demonstrated a power factor PF of 0.43 $\mu W\,m^{-1}\,K^{-2}$, showcasing its potential for n-type TE applications [80].

Efforts to improve TE performance have explored the incorporation of boron–nitrogen coordination bonds (B ← N) into D–A polymers (Figure 13b). The D–A polymer PI-BN, composed of Isoindigo (IID) units and B ← N-bridged thienylthiazole (BNTT) units, exhibited favorable n-doping characteristics due to the energy-level reduction of both the HOMO and LUMO upon introduction of the B ← N unit [81]. Adding a benzene group to the boron atom further reduced crystallinity, significantly improving miscibility with dopants. Unlike PI-BT, a polymer with a structure similar to PI-BN but containing a bithiophene unit instead of the BNTT unit, not be doped by N-DMBI, PI-BN could be doped effectively with N-DMBI. At the optimal doping concentration of 5 wt%, it achieved an electrical conductivity of $9.7\times10^{-4}\,S\,cm^{-1}$, a Seebeck coefficient of $-453.8\,\mu V\,K^{-1}$, and a PF of 0.02 $\mu W\,m^{-1}\,K^{-2}$ [81].

The effect of acene core size in fused lactam-based acceptor–acceptor polymers was also investigated [82]. These polymers, devoid of donor units, were expected to exhibit higher n-doping efficiency. As the acene core size in the main chain decreased from anthracene-anthracene (A-A) to anthracene-naphthalene (A-N) and then to naphthalene-naphthalene (N-N), the LUMO energy level was progressively lowered, enhancing n-doping by N-DMBI (Figure 13c). The reduced acene core size also improved electron delocalization, resulting in higher electron mobility. Among these, the N-N polymer displayed the highest electrical conductivity of 0.65 $S\,cm^{-1}$ and a PF of 3.2 $\mu W\,m^{-1}\,K^{-2}$.

Modifications to the lactam-based N-N polymer by introducing bis-lactone units yielded an alternating lactam–lactone chain structure. The lactone units, being more electron-deficient than lactam units, further reduced the LUMO energy level, enhancing the oxidation stability of the polymer–dopant system (Figure 13d). The resulting polymer P2 achieved an electrical conductivity of 0.28 $S\,cm^{-1}$ and a PF of 0.16 $\mu W\,m^{-1}\,K^{-2}$ when doped with N-DMBI [83]. Further studies investigated the impact of varying lactone content in alternating lactam–lactone polymers. Increasing the benzene content in the polymer chain from 0% to 75% raised the lactone unit content (Figure 13e), lowering the LUMO energy level and enhancing chain planarity and charge dispersion. These changes improved charge transfer properties and reduced the activation energy for charge transport. The polymer P-75, with 75% benzene content, exhibited the highest performance, achieving an electrical conductivity of 12 $S\,cm^{-1}$ and a PF of 13.2 $\mu W\,m^{-1}\,K^{-2}$ when doped with N-DMBI [84].

2.3 | Stability Issues in CP-Based TE Materials

To enable the practical application of TE devices based on CPs, it is essential to ensure the long-term stability of CP-based TE materials. The most critical factor in achieving long-term stability is the ability to maintain their optimized doped state over time. Unfortunately, securing the doping stability of TE polymers remains an unresolved challenge. Therefore, this section briefly reviews representative studies aimed at improving the long-term stability of p-type and n-type conjugated polymer TE materials.

2.3.1 | Thermal Stability of p-Type CP-Based TE Materials

In the case of p-type TE polymers, their low HOMO energy levels prevent them from being highly reactive with moisture or oxygen in the air. As a result, the air stability of p-type TE polymers is relatively higher compared to that of n-type TE polymers [91]. Therefore, in p-type TE polymers, the primary focus has been improving the thermal stability of these materials. When thermal stress is applied, it can promote thermal diffusion of the dopant, leading to dopant molecules escaping from the polymer film, aggregating, or undergoing thermal decomposition of the dopant anion [92–94]. These processes can cause dedoping of the polymer, ultimately resulting in a decrease in electrical conductivity and TE performance.

Some studies have demonstrated that the thermal stability of p-type TE polymers can be enhanced through side chain design. J. Li et al. compared the thermal stability of a polythiophene-based polymer with polar side chains, poly(thiophene-3-[2-(2-methoxy-ethoxy)ethoxy]-2,5-diyl) (S-P3MEET), and P3HT, a polythiophene-based polymer with nonpolar hexyl substituents, when doped with F4TCNQ (Figure 14a) [92]. It was found that the F4TCNQ anion binds more strongly to the polar side chains of S-P3MEET than to the nonpolar side chains of P3HT. Additionally, the melting temperature of the side chains in S-P3MEET increased by ~30°C. As a result, after thermal annealing at 210°C, F4TCNQ remained in the polymer film of S-P3MEET, whereas in the case of P3HT, F4TCNQ gradually diffused out even at much lower temperatures close to room temperature. This study clearly demonstrated that polar side chains can effectively stabilize dopant anions, allowing them to remain in place even under thermal stress. A similar study was also conducted by R. Kroon et al. [95] In their study, they compared the thermal stability of F4TCNQ-doped poly[3,3′-bis(2-(2-(2-(2-methoxyethoxy)ethoxy)ethoxy)ethoxy)-2,2′-bithiophene-alt-thiophene] (p(g42T-T)), a polythiophene-based polymer with oligo ethylene glycol side chains (Figure 14a), with that of P3HT. When measuring the electrical conductivity of the two doped polymers while gradually increasing the temperature over time, a decrease in conductivity was observed for P3HT at temperatures below 100°C, whereas no decrease was observed for p(g42T-T) even up to 150°C (Figure 14b). This enhanced thermal stability of p(g42T-T) was also attributed to the strong binding between its polar side chains and F4TCNQ.

Meanwhile, a recent study reported that removing side chains from polymers can enhance the thermal stability of p-type TE polymers. F. Zhong et al. synthesized poly(4-(4-(dodecyldimethylsilyl)-5-(thieno[3,2-b]thiophen2-yl)thiophen-2-yl)-7-(4-(dodecyldimethylsilyl)thiophen-2-yl)benzo[c][1,2,5]thiadiazole) (SiBT-TT), a benzothiadiazole-based conjugated copolymer whose side chains can be removed through thermal-assisted rapid acid cleavage, and investigated its thermal stability upon $FeCl_3$ doping (Figure 14c) [96]. In this study, the side chains of SiBT-TT were thermally

25673173, 2025, 10, Downloaded from https://onlinelibrary.wiley.com/doi/10.1002/eom2.70029 by Hansol Lee - Gachon University Global Campus , Wiley Online Library on [29/09/2025]. See the Terms and Conditions (https://onlinelibrary.wiley.com/terms-and-conditions) on Wiley Online Library for rules of use; OA articles are governed by the applicable Creative Commons License

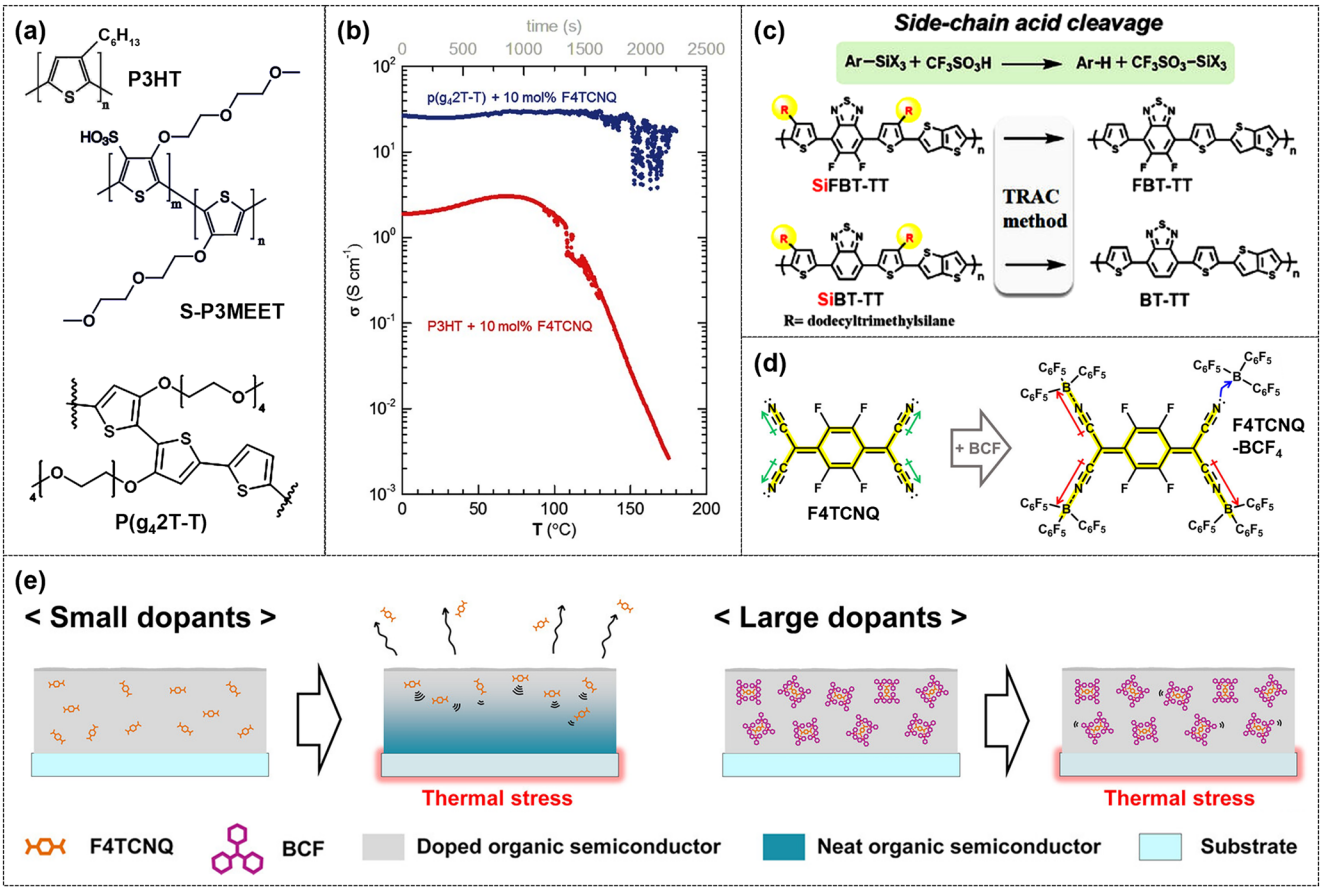


FIGURE 14 | (a) Molecular structures of P3HT, S-P3MEET, and p(g42T-T). (b) Electrical conductivity of F4TCNQ-doped p(g42T-T) (blue) and P3HT (red) during heating in air. Reproduced from 95 with permission (Copyright 2017, Wiley) (c) Chemical mechanism of side-chain acid cleavage and chemical structure of polymers SiFBT-TT, FBT-TT, SiBT-TT, and BT-TT. Reproduced from 96 with permission (Copyright 2025, Wiley) (d) Lewis pairing of F4TCNQ with BCF molecules. (e) Thermal diffusion comparison between small (F4TCNQ) and large (F4TCNQ–BCF4) dopants. Reproduced from 94 with permission (Copyright 2023, Wiley).

cleaved with the assistance of TfOH, yielding a side-chain-free polymer called (BT-TT). When $FeCl_3$-doped SiBT-TT and BT-TT were heated at 100°C for 1000 min, the electrical conductivity and PF of SiBT-TT gradually decreased with increasing heating time. In contrast, BT-TT showed no decrease in either electrical conductivity or PF, demonstrating excellent thermal stability. This high thermal stability stands in stark contrast to previous reports that $FeCl_3$-doped polymers generally exhibit poor thermal stability above 65°C due to aggregation and decomposition of $FeCl_3$ [93]. The high thermal stability of BT-TT was attributed to the absence of side chains, which reduced thermal motion of the polymer backbone and suppressed dopant diffusion. In addition, the absence of side chains allowed BT-TT to form a denser and more ordered packing structure than SiBT-TT, helping to maintain a stable polymer network even during thermal annealing, which was also suggested to contribute to its superior thermal stability.

Recently, studies have also reported that, in addition to tuning the polymer structure, modifying the dopant can enhance the thermal stability of p-type TE polymers. E. H. Suh et al. combined a CN-functionalized conjugated dopant with a Lewis acid molecule to create a Lewis-paired CN group, which was then used as a p-dopant [94]. In the Lewis-paired CN group, the CN group is bonded to the Lewis acid through a Lewis acid–base reaction, significantly enhancing the electron-withdrawing nature of the CN group. This enhancement made the dopant a much stronger p-dopant. In the case of F4TCNQ, which has four CN groups, it could bind with up to four tris(pentafluorophenyl)borane (BCF) molecules (Figure 14d). The resulting F4TCNQ-BCF Lewis-paired dopant exhibited strongly suppressed thermal diffusion within the p-type polymer PDPP3T due to its large molecular size (Figure 14e). As a result, the doped PDPP3T maintained stable electrical conductivity even after 42 h of thermal annealing at 80 to 120°C. Similar results were also obtained by O. Zapata-Arteaga et al., where BCF:F4TCNQ-doped P3HT exhibited a much slower thermally induced decrease in electrical conductivity compared to when either BCF or F4TCNQ was used alone for doping [97].

2.3.2 | Air Stability of n-Type CP-Based TE Materials

Unlike p-type TE polymers, n-type TE polymers exhibit high reactivity with oxygen and moisture in the air due to their high LUMO energy levels. As a result, n-type TE polymers generally possess relatively poor air stability. It has been proposed that for an n-doped CP to be fully stable in ambient conditions, the polymer's electron affinity must be greater than 4.7 eV [91]. n-Type dopants also face similar issues. For dopants that induce n-doping via direct electron transfer from the HOMO of the dopant

25673173, 2025, 10, Downloaded from https://onlinelibrary.wiley.com/doi/10.1002/eom2.70029 by Hansol Lee - Gachon University Global Campus , Wiley Online Library on [29/09/2025]. See the Terms and Conditions (https://onlinelibrary.wiley.com/terms-and-conditions) on Wiley Online Library for rules of use; OA articles are governed by the applicable Creative Commons License

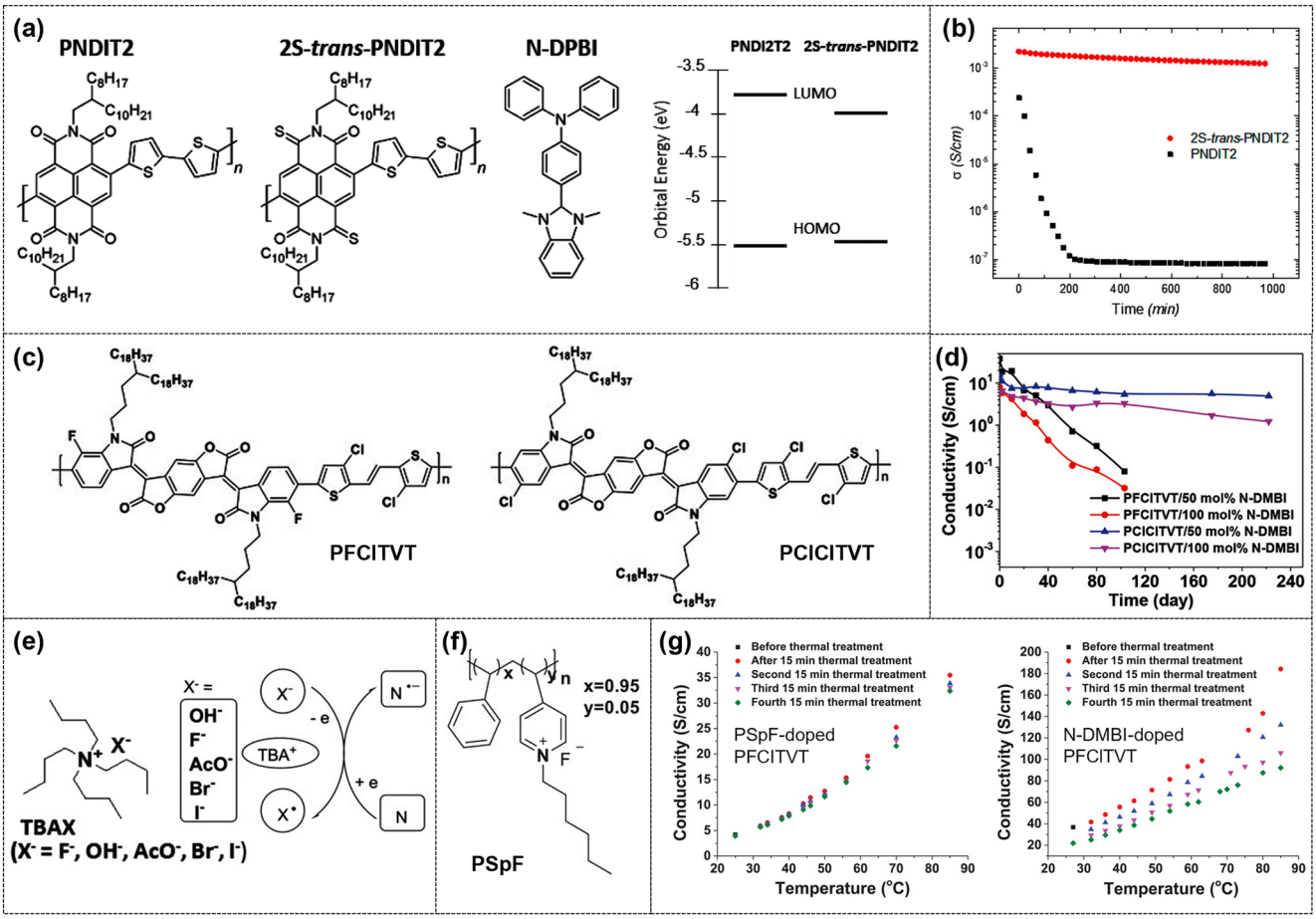


FIGURE 15 | (a) Molecular structures of the polymers PNDIT2 and 2S-trans-PNDIT2, the dopant N-DPBI, and comparison of the HOMO and LUMO energy levels of the two polymers. (b) Comparison of air stability between N-DPBI doped 2S-trans-PNDIT2 and PNDIT2. Reproduced from 100 with permission (Copyright 2018, American Chemical Society) (c) Molecular structures of the polymers PFClTVT and PClClTVT. (d) Comparison of air stability between N-DMBI doped PFClTVT and PClClTVT. Reproduced from 101 with permission (Copyright 2021, Wiley) (e) Molecular structure and n-doping mechanism of the n-dopant TBAX. (f) Molecular structure of the n-type copolymer dopant PSpF. (g) Comparison of thermal air stability between PSpF-doped PFClTVT (left) and N-DMBI-doped PFClTVT (right). Reproduced from 110 with permission (Copyright 2022, Wiley).

to the LUMO of the CP, their high HOMO and LUMO energy levels make them vulnerable to oxidation by oxygen or moisture in the air [91, 98–99]. Therefore, in order to improve the air stability of n-type CP-based TE materials, research is being conducted on the development of air-stable n-type polymers as well as air-stable n-type dopants.

The most straightforward approach to improving the air stability of n-type polymers is to further lower their LUMO energy levels. D. Nava et al. demonstrated that lowering the LUMO level through thionation in NDI-based n-type polymers has a dramatic effect on enhancing air stability [100]. They compared PNDIT2, an n-type conjugated polymer composed of NDI and bithiophene units, with 2S-trans-PNDIT2, in which two carbonyl oxygen atoms of the NDI unit were substituted with sulfur (Figure 15a). After doping both polymers with the N-DPBI dopant, they evaluated their air stability. Thionation of the NDI unit resulted in a lower LUMO energy level for 2S-trans-PNDIT2: while PNDIT2 had a LUMO energy level of −3.75 eV, that of 2S-trans-PNDIT2 was −3.96 eV. When the doped polymer films were exposed to ambient air at 50% relative humidity, the electrical conductivity of PNDIT2 decreased sharply, reaching a level similar to that of the pristine polymer within 200 min. In contrast, the electrical conductivity of 2S-trans-PNDIT2 decreased to only about half its original value even after 1000 min., demonstrating significantly enhanced air stability (Figure 15b).

Meanwhile, it has been suggested that the air stability of n-type TE polymers can vary depending on the crystalline structure and thickness of the polymer film, as these factors influence the ease with which O_2 and H_2O from the atmosphere can penetrate into the film. For example, J. Han et al. synthesized the n-type polymers PFClTVT and PClClTVT, in which fluorinated-benzodifurandione-based oligoviologen (BDOPV) and chlorinated-BDOPV serve as the acceptor units, respectively, with dichlorodithienylethene (ClTVT) as the donor unit (Figure 15c), and examined their air stability after doping with N-DMBI [101]. Despite having nearly identical LUMO energy levels, the more crystalline polymer, PClClTVT, exhibited a slower decrease in electrical conductivity over time, indicating improved air stability (Figure 15d). This enhanced stability was attributed to the denser film structure resulting from its higher crystallinity, which more effectively blocked the penetration of O_2 and H_2O. C.-Y. Yang et al. investigated the air stability of TAM-doped FBDPPV and found that the polymer film exhibited

25673173, 2025, 10, Downloaded from https://onlinelibrary.wiley.com/doi/10.1002/eom2.70029 by Hansol Lee - Gachon University Global Campus , Wiley Online Library on [29/09/2025]. See the Terms and Conditions (https://onlinelibrary.wiley.com/terms-and-conditions) on Wiley Online Library for rules of use; OA articles are governed by the applicable Creative Commons License

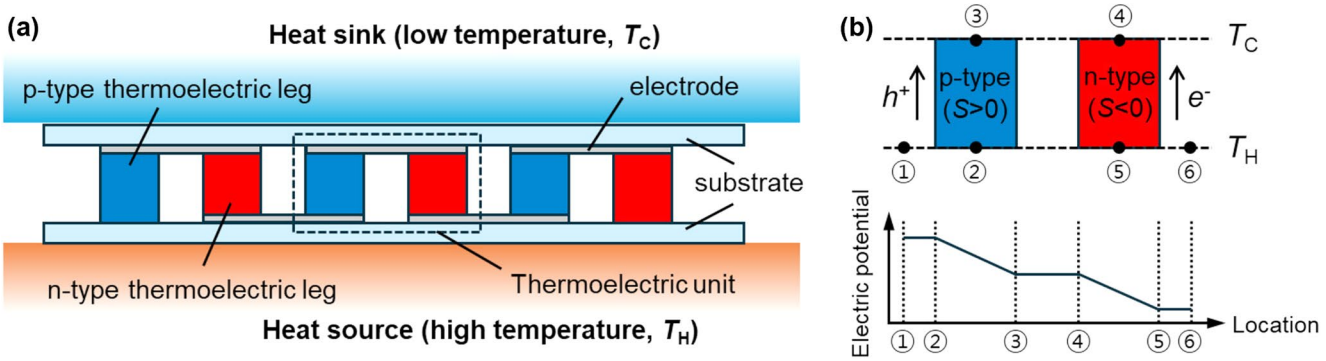


FIGURE 16 | (a) Convention TEG structure with p-type and n-type TE legs connected in series. (b) The charge transport in TE legs with accompanying electric potential profile.

excellent air stability when the thickness was 10 μm, whereas significant air instability was observed when the film was only 10 nm thick [102]. This difference was explained by the self-encapsulation effect of the upper polymer layers in the thicker film, which served to block the penetration of O_2 and H_2O into the film interior.

To address the air stability issue of n-type dopants, new dopants have been developed that can induce effective n-doping without possessing a high HOMO energy level. One representative n-doping mechanism is hydride transfer, and dopants such as N-DMBI and TAM are well-known hydride donors that n-dope polymers through this mechanism [102–105]. Since these dopants do not rely on direct electron transfer from their HOMO to the polymer's LUMO, they can still achieve effective n-doping even without a HOMO level significantly higher than the polymer's LUMO. As a result, improved air stability can be obtained. However, even for the widely used N-DMBI, it has been reported that it can react with molecular oxygen to form an amide derivative [106]. This amide product reduces doping efficiency and acts as an impurity, leading to decreased electrical conductivity [106].

In addition to direct electron transfer or hydride transfer mechanisms, dopants that induce n-doping via anions have also been reported. These dopants exist in the form of salts, and it is believed that the anions in the salts interact with the π* orbitals of the polymer semiconductor to transfer electrons [107, 108]. However, the detailed mechanism remains incompletely understood. A representative class of such dopants includes tetrabutylammonium salts (TBAX salts, where $X = F^-$, OH^-, AcO^-, Br^-, I^-) (Figure 15e) [109]. Recently, an n-type copolymer dopant, polystyrene–poly(4-vinyl-N-hexylpyridinium fluoride) (PSpF), was developed as an n-dopant that follows this doping mechanism while also offering enhanced air stability (Figure 15f) [110]. PSpF contains an ammonium cation and fluoride anion on the pyridine side chain, enabling n-doping of polymers through interaction with the fluoride anion. When the air stability of PSpF-doped PFClTVT was compared with that of N-DMBI-doped PFClTVT, the PSpF-doped PFClTVT exhibited significantly superior stability (Figure 15g). This enhanced stability was attributed to the polystyrene fragments in PSpF, which likely suppressed the penetration of O_2 and H_2O into the film.

3 | Flexible TEGs

Figure 16a schematically illustrates the structure of a conventional TEG, where a series of repeating TE units generates an electrical potential with alternating directions under a given temperature difference T_H–T_C (Figure 16b). Each TE unit consists of p-type and/or n-type TE material legs with electrodes attached at both ends. These units are generally classified into two types: p-n leg structures and single-leg structures. The p-n leg structure includes a pair of p-type and n-type TE legs, whereas the single-leg structure contains only one type of leg, either p-type or n-type. In practical applications, the p-n leg structure is more commonly employed.

Multiple TE units are interconnected through electrodes and mounted on a substrate. The substrate not only maintains the mechanical integrity of the module by holding the units in place but also plays a crucial role in heat transfer, which includes both the absorption of thermal energy from the high-temperature heat source and the dissipation of residual heat to the cold side. In the typical p-n leg structure, the TE legs are positioned and connected between two substrates, which are in direct contact with the hot and cold sides, respectively. The legs are alternately connected in series via electrodes that link the p-type and n-type elements.

To maximize the electrical power output of a TEG under a given hot-side and cold-side temperature gradient, the most critical factor is the use of high-performance TE materials in the legs. However, the design of the module also substantially influences overall efficiency. For instance, to preserve the maximum temperature gradient across the p-type and n-type legs, it is essential to minimize temperature drops caused by the thermal resistance of the substrates and electrodes. Similarly, thermal losses at the interfaces between the TE legs and the electrodes should be minimized. Furthermore, to reduce electrical energy losses, both the electrical contact resistance at these interfaces and the intrinsic resistance of the electrodes must be kept as low as possible.

The CP-based TE materials, which can possess inherent mechanical flexibility, have enabled deformable TEGs such as flexible and stretchable TEGs. In deformable TEGs, not only is the TE conversion efficiency crucial, but also its flexibility

25673173, 2025, 10, Downloaded from https://onlinelibrary.wiley.com/doi/10.1002/eom2.70029 by Hansol Lee - Gachon University Global Campus , Wiley Online Library on [29/09/2025]. See the Terms and Conditions (https://onlinelibrary.wiley.com/terms-and-conditions) on Wiley Online Library for rules of use; OA articles are governed by the applicable Creative Commons License

is a crucial requirement. Therefore, additional measures must be taken to ensure flexibility when selecting materials and designing the module structure. The flexibility of a TEG is primarily achieved by using inherently flexible TE materials. However, CP-based TE materials with high inherent flexibility often exhibit lower TE performance because reducing the persistence length of the chain backbone and increasing free volume to retain high flexibility is likely to cause poor backbone planarity and weak interchain interaction, both of which deteriorate charge transport. Therefore, various strategies such as flexible substrate [5, 111] and/or thin film processing [112, 113] are adopted to complement the limited flexibility of high-performance CP-based TE materials. In the following content, studies on flexible TEGs are categorized based on the structure of the modules. Representative structures include the Π-type structure, Y-type structure, rolled-up structure, and textile structure, each with its own unique characteristics, advantages, and disadvantages.

3.1 | Π-Type Structure

The Π-type structure is the most common and widely used configuration for fabricating TEGs. The term "Π-type" refers to a TE unit in which a pair of p-type and n-type legs are connected to a shared electrode, forming a structure reminiscent of the Greek letter "Π". A Π-type TEG typically comprises multiple such units connected in series. This architecture is relatively straightforward to fabricate using conventional deposition, printing, or patterning techniques, and is readily scalable for large-area applications [5, 111, 114–115]. However, the relatively wide spacing between individual TE units restricts packing density, thereby limiting the effective area available for power generation [116].

Bubnova et al. focused on optimizing the ZT for the conducting polymer PEDOT-Tos, achieving $ZT = 0.25$ at room temperature [117]. PEDOT-Tos was also demonstrated as TEG, which comprised 54 TE couples of PEDOT-Tos as the p-type TE leg and the organic small molecule tetrathiofulvlene-7,7,8,8-tetracyanoquinodimethane (TTF-TCNQ) as the n-type TE leg (Figure 17a). The periodic cavities were formed on the SU-8 layer through photolithography, then filled with p- or n-type TE materials. The fabricated TEG exhibited a low packing density of 0.47 in area, resulting in a low power density of 0.23 nW $cm^{-2} K^{-2}$. A hypothetical power density of 0.46 nW $cm^{-2} K^{-2}$ was suggested in this work, assuming a packing density of 0.94, but such a high packing density was not demonstrated.

Similarly, Sun et al. provided one of the earliest demonstrations of a fully organic Π-type TEG constructed from both p-type and n-type coordination polymers (Figure 17b) [17]. They synthesized a series of poly(metal 1,1,2,2-ethenetetrathiolate) compounds, identifying poly[Na_x(Ni-ett)] as n-type and poly[Cu_x(Cu-ett)] as p-type TE materials. By integrating these materials, the authors fabricated a Π-type TEG consisting of 35 thermocouple pairs arranged in a traditional series configuration. The module achieved an output power of 750 μW demonstrating the viability of organic TE materials despite their traditionally lower conductivity and performance. This work also left the possibility of further enhancement, as the TEG had a low packing density of 0.4. The work on poly(metal 1,1,2,2-ethenetetrathiolate) compound was further extended through developing a bulk Π-type TEG that employed Cu(I)-ethylenetetrathiolate (Cu(I)-ett) as the p-type leg and poly[K_x(Ni-ett)] as the n-type leg (Figure 17c) [118]. The TE properties of Cu(I)-ett were optimized via chemical oxidation and reduction, yielding a maximum power factor of 118.2 μW $m^{-1} K^{-2}$ and a ZT of 0.060 at 400 K. A complete Π-type device was fabricated using these materials, generating an open-circuit voltage of 1.51 V and a short-circuit current of 2.71 mA under a 60 K temperature gradient. The device delivered a peak output power exceeding 1 mW and was capable of powering a liquid crystal display (LCD) calculator, offering a demonstration of real-world applicability. This study highlighted the potential of hybrid metal–organic coordination polymers and emphasized the importance of oxidation state tuning and interface engineering in enhancing TE performance within Π-type architectures.

Zhang et al. presented PEDOT:PSS TE composites supported by a microstructured polyurethane (PU) frame [119]. However, the focus of this work remained on multifunctional sensing (pressure and temperature) rather than power generation because of the poor TE output of PEDOT:PSS-based TE composites. The TEG was demonstrated by incorporating only p-type TE legs without n-type TE legs (Figure 17d). The structure of the TEG was, therefore, not explicitly Π-type TEG, providing insights into single-type TEG for self-powered sensor applications, where the extent of power output is just a part of theevaluation.

More recently, Lin et al. reported a flexible, lightweight Π-type TEG based on hybrid composites of inorganic Bi_2Te_3 nanoparticles and the conducting polymer PEDOT:PSS (Figure 17e) [120]. The device was structured with serially connected p-type and n-type legs embedded between polyimide (PI) films, forming a sandwich configuration. The Π-type layout was used to optimize electrical connectivity and voltage generation. At a ΔT of 45 K, the device achieved an output power of 9.0 mW, a specific power of 2.3 mW g^{-1}, and an areal power density of 6.5 W m^{-2}. The hybridized TE material retained the high TE performance of Bi_2Te_3, a traditional inorganic TE material. However, it failed to retain the solution-processability and inherent flexibility of PEDOT:PSS, necessitating a high-cost fabrication process such as hot pressing and the use of flexible supporting layers (PI films), which endowed the TEG with limited flexibility that exhibited a minimum bending radius of 20 mm.

From a microfabrication perspective, Massetti et al. introduced a monolithic micro-TEG (μTEG) fabricated entirely using digital direct writing techniques, including femtosecond laser micromachining and inkjet printing (Figure 17f) [121]. The TE legs—comprising PEDOT:PSS (p-type) and a doped fullerene derivative (n-type)—were embedded into a plastic substrate featuring a conical cavity structure to enhance thermal gradients. Despite the microscale dimensions, the Π-type structure was preserved, with TE couples connected electrically in series and thermally in parallel. The μTEG achieved a power density of 30.5 nW cm^{-2} at a ΔT of 25 K, making it suitable for powering distributed IoT sensors.

Extending the automatic fabrication process using inkjet printing techniques, a fully stretchable Π-type TEG that

25673173, 2025, 10, Downloaded from https://onlinelibrary.wiley.com/doi/10.1002/eom2.70029 by Hansol Lee - Gachon University Global Campus , Wiley Online Library on [29/09/2025]. See the Terms and Conditions (https://onlinelibrary.wiley.com/terms-and-conditions) on Wiley Online Library for rules of use; OA articles are governed by the applicable Creative Commons License

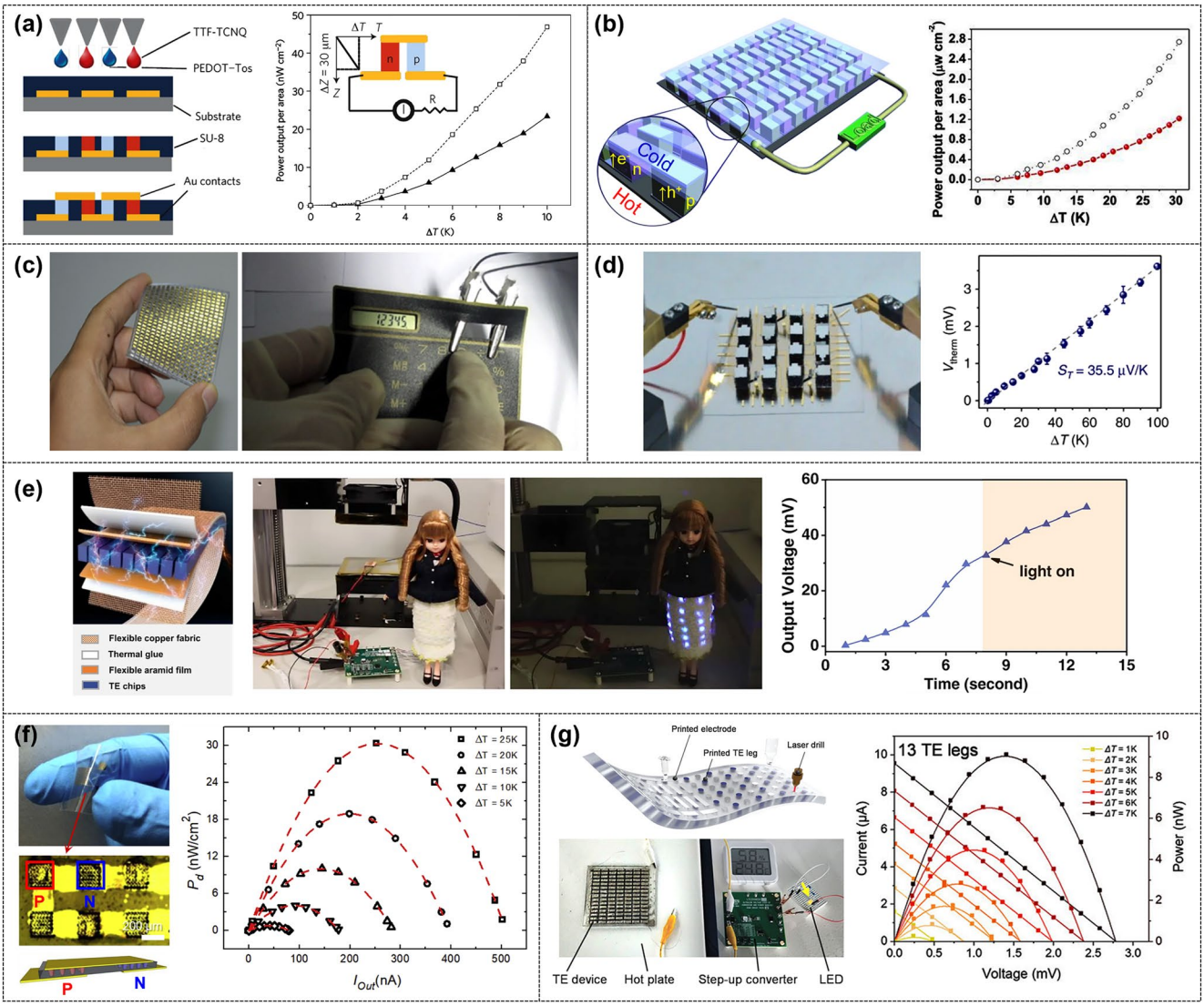


FIGURE 17 | (a) A Π-type TEG comprising 54 PEDOT-Tos/TTF-TCNQ TE couples. The fabricated TEG exhibited a packing density of 0.47 in area (▲), while the hypothetical maximum packing density was expected to be 0.94 (□). Reproduced from 117 with permission (Copyright 2011, Springer Nature). (b) A Π-type TEG comprising 35 poly[Cu_x(Cu-ett)]/ poly[Na_x(Ni-ett)] TE couples. The fabricated TEG exhibited a packing density of 0.4 in area (●), while the hypothetical maximum packing density was expected to be 0.94 (○). Reproduced from 17 with permission (Copyright 2012, Wiley). (c) A TEG comprising 220 Cu(I)-ett complex/poly[K_x(Ni-ett)] TE couples, which generated sufficiently large power to operate a calculator ($\Delta T = 60$ K). Reproduced from 118 with permission (Copyright 2014, Elsevier). (d) A TEG of 16 TE legs, where microstructured PU frame was coated by PEDOT:PSS. Measured output voltage as function of ΔT for a single TE leg. Reproduced from 119 with permission (Copyright 2015, Springer Nature). (e) A TEG comprising 32 TE pillars that was obtained by hot pressing of n- and p-type Bi_2Te_3/PEDOT:PSS composites. Applying a hot and cold plate on the TEG increases ΔT across the TEG over time, turning LEDs on after 8 s with output voltage 30 mV (ΔT = ~8.5 K). Reproduced from 120 with permission (Copyright 2022, Springer Nature). (f) A TEG comprising 128 micro-scale PEDOT:PSS/PTEG-1 TE couples. The TE couples were inkjet-printed on microcavities on PEN film, then connected by inkjet printing of Ag electrode patterns. The fabricated TEG generated an electric power density $P_d = 30$ nW cm^{-2} at $\Delta T = 25$ K. Reproduced from 121 with permission (Copyright 2020, Elsevier). (g) A stretchable TEG comprising 13 PEDOT:PSS/SEBS TE legs and 105 silver electrode legs. The TEG exhibited a high power density (0.32 nW cm^{-2}K^{-2}), which can turn on LED on hot plate ($T = 70$°C) in ambient air condition without external heat sink. Reproduced from 20 with permission (Copyright 2025, Wiley).

maintained excellent mechanical and electrical stability under deformation with a high power density was demonstrated (Figure 17g) [20]. Using solution-processed organic materials, p-type TE legs were embedded along with electrode patterns into an elastomeric matrix. A stepwise curing strategy enabled the formation of elastomeric networks while preserving TE properties. The resulting stretchable TEG retained 90% of its maximum power output under 40% strain and remained stable after 200 stretching cycles, demonstrating both mechanical robustness and long-term durability. The Π-type architecture facilitated through-plane heat flow, enabling direct harvesting of body heat. The device achieved a power density of 0.32 nW cm^{-2}K^{-2}, among the highest reported for stretchable TEGs. This study demonstrated the adaptability of Π-type structures for deformable, skin-compatible electronics.

25673173, 2025, 10, Downloaded from https://onlinelibrary.wiley.com/doi/10.1002/eem2.70029 by Hansol Lee - Gachon University Global Campus , Wiley Online Library on [29/09/2025]. See the Terms and Conditions (https://onlinelibrary.wiley.com/terms-and-conditions) on Wiley Online Library for rules of use; OA articles are governed by the applicable Creative Commons License

3.2 | Y-Type Structure

To achieve high flexibility in TE modules, it is advantageous for the module to be thin. However, in the conventional vertical Π-type TEG, reducing the module thickness inherently reduces the thickness of the TE legs [122]. This, in turn, diminishes the temperature gradient across the TE material, thereby compromising its performance. That is, enhancing flexibility by reducing thickness results in a trade-off with TE efficiency. To overcome this inherent compromise and simultaneously improve both flexibility and TE performance, Y-type flexible TEGs have been developed.

The Y-type structure introduces guide columns to support thin TE films, where one side is in contact with the heat source (hot side) and the other with the cold side. Heat flows vertically through these guide columns while traveling laterally through the TE legs. This design results in a heat flow path parallel to the substrate within the TE material, similar to a lateral Π-type configuration, while preserving the vertical alignment of hot and cold sides characteristic of the vertical Π-type structure. Since the TE films lie flat, their length can be extended to increase the temperature gradient without affecting the overall thickness of the module, making this architecture particularly well-suited for enhancing flexibility without sacrificing performance.

Pataki et al. developed a rolled Y-type organic micro-TEG (μTEG) featuring PEDOT:PSS and a stable n-type polymer poly(benzimidazobenzophenanthroline): poly(ethyleneimine) (BBL:PEI), deposited alternately using inkjet and spray-coating techniques (Figure 18a) [123]. This TEG achieved a very high-density design which incorporated 1842 TE pairs per cm^2. The rolled architecture preserved the lateral alignment of the TE films, with alternating p-n segments forming the core of the TEG, where a thin parylene C substrate enabled rolling of the TEG into a cylinder with radii of curvature ranging from 3.5 to 0.2 mm. The μTEG produced 0.15 $\mu W\,cm^{-2}$ under a 50 K temperature gradient, and simulations indicated that geometric optimization could yield $>1\,\mu W\,cm^{-2}$ at a ΔT of 50 K. This study underscores the advantage of planar Y-type architectures in achieving high voltage and power outputs in compact, flexible devices.

Huang et al. embedded Y-type TEG structures into photothermoelectric (PTE) devices using drop-casted films of poly[Cu_x(Cu-ett)]:PVDF (p-type), which exhibited superb light absorption at wavelengths in the near-infrared (NIR) range (Figure 18b) [124]. The fabricated device utilized the planar, lateral arrangement of TE films in series, featuring Seebeck voltage under near-infrared (NIR) illumination. The position of the NIR laser spot developed differences in the temperature gradient along with the TE films, establishing Seebeck voltages with different directions. While the study focused on the photothermal response, the successful implementation of Y-type layouts demonstrated their viability for multifunctional sensing and energy harvesting from both light and heat.

Yang et al. synthesized a triaminomethane (TAM) n-dopant and implemented it in the doping of poly(p-phenylene vinylene) (FBDPPV) to yield n-type TE material FBDPPV:TAM. Incorporating PEDOT:PSS as p-type TE material, an all-polymer TEG using a lateral configuration was demonstrated (Figure 18c) [102]. Both legs were patterned through drop coating TE solutions onto a patterned SU-8 template on a polyethylene terephthalate (PET) substrate. The resulting device achieved a power output of 77 nW and exhibited compatibility with thick (10 μm) films without performance degradation, highlighting its robustness. This represented the first demonstration of an all-polymer flexible TEG using a Y-type configuration with both leg types derived from a common polymer matrix, enabled by miscible doping and uniform film morphology. This structure was readily adopted for other solution-processible TE materials. Using a single polymer backbone based on thiophene-fused benzodifurandione oligo(p-phenylenevinylene) (TBDOPV), the TEG fabrication process was even more simplified by doping the polymer films into both p- and n-type using $FeCl_3$ and N-DMBI, respectively (Figure 18d) [125]. The TEG achieved power factors exceeding $200\,\mu W\,m^{-1}\,K^{-2}$ for n-type and over $100\,\mu W\,m^{-1}\,K^{-2}$ for p-type films, resulting in a record output of 404 nW.

Liu et al. designed a stretchable TEG by integrating p-type and n-type carbon nanotube paper (CNTP) films on a hydrogel substrate (Figure 18e) [126]. The films, arranged laterally and connected in series in a Y-type configuration, were incorporated into a wavy structure that enabled up to 300% stretchability with minimal performance degradation—maintaining over 90% of the original output. This mechanical resilience was attributed to the hydrogel's self-healing properties and the structural flexibility of the wavy design, supporting the suitability of Y-type architectures for wearable applications.

Brunetti et al. also reported a fully printed organic TEG was fabricated using PEDOT:PSS as the p-type and PBFDO as the n-type material (Figure 18f) [21]. The TE materials were patterned via a combination of inkjet and screen printing on an ultrathin, flexible parylene substrate in a lateral layout, forming a Y-type configuration. Each p-n junction contributed to electrical series connectivity within the origami-inspired architecture, which integrated 21 TE pairs. The device achieved a record normalized power density of 0.718 nW $cm^{-2}\,K^{-2}$ because of high TE performances of p-type PEDOT:PSS and n-type PBFDO films. Stability testing demonstrated reliable operation across a broad temperature range (−8°C to 200°C) and high humidity (up to 90%), confirming the robustness for harsh environments of the fabricated TEG.

3.3 | Textile Structure

TE generation using body heat presents a convenient and sustainable method for powering portable and wearable electronic devices. To facilitate this, fiber-based TEGs have been proposed and developed. When integrated into garments or wearable electronics, these fiber-based TEGs significantly enhance portability and offer excellent flexibility, enabling comfortable wear without impeding user movement [113]. The fiber-based TEGs, therefore, have often been demonstrated as textile-structured TEGs by direct printing of TE materials onto textile substrates or coating individual fibers with TE materials to form TE threads, which are then woven into fabrics or sewn onto textiles.

25673173, 2025, 10, Downloaded from https://onlinelibrary.wiley.com/doi/10.1002/eom2.70029 by Hansol Lee - Gachon University Global Campus , Wiley Online Library on [29/09/2025]. See the Terms and Conditions (https://onlinelibrary.wiley.com/terms-and-conditions) on Wiley Online Library for rules of use; OA articles are governed by the applicable Creative Commons License

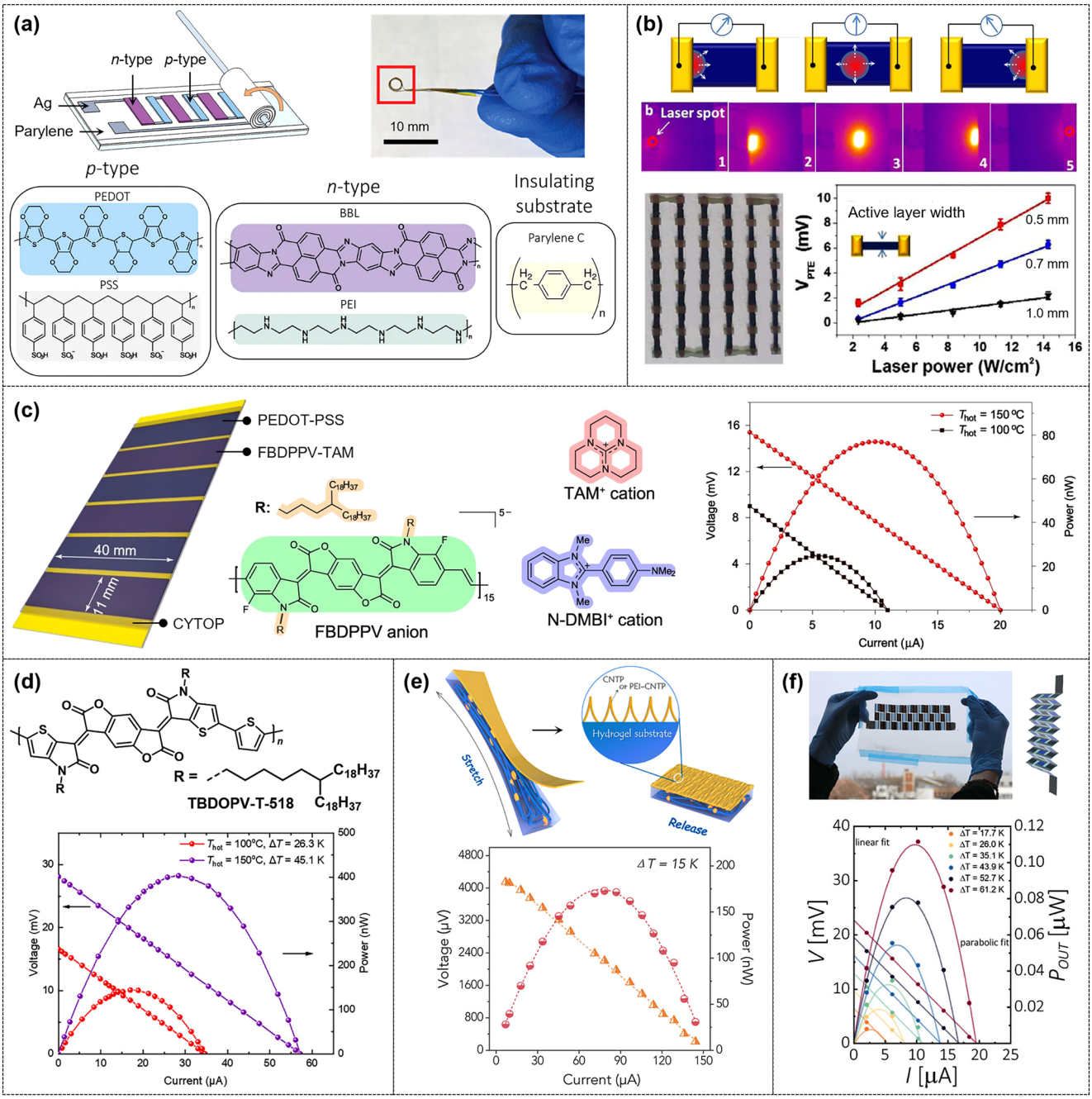


FIGURE 18 | (a) A Y-type TEG comprising PEDOT:PSS film as p-type TE pattern and BBL or PEI as n-type TE pattern on perylene C substrate. Reproduced from 123 with permission (Copyright 2024, Wiley). (b) A TEG comprising poly[Cu_x(Cu-ett)]:PVDF films as TE patterns for NIR detection. The position of laser was proved by the direction and the extent of photothermoelectric (PTE) Seebeck voltage, which exhibited linear correlation with applied laser power. Reproduced from 124 with permission (Copyright 2015, American Chemical Society). (c) A TEG with corrugated Y-type structure that comprised PEDOT:PSS and FBDPPV-TAM films as p- and n-type TE patterns, respectively. Reproduced from 102 with permission (Copyright 2020, Springer Nature). (d) A TEG with corrugated Y-type structure that comprised TBDOPY-T-518/$FeCl_3$ and TBDOPY-T-518/N-DMBI films as p- and n-type TE patterns, respectively. Reproduced from 125 with permission (Copyright 2023, AAAS). (e) A stretchable TEG comprising p-type CNTP and n-type PEI-CNTP on self-healable hydrogel substrate. Reproduced from 126 with permission (Copyright 2021, Chinese Chemical Society). (f) A fully printed TEG comprising p-type PEDOT:PSS and n-type PBFDO patterns. Reproduced from 21 with permission (Copyright 2025, Wiley).

Lund et al. designed an embroidered textile TEG using conductive sewing threads composed of PEDOT:PSS for TE generation and silver-coated polyamide for wiring. These threads were embroidered through layers of wool felt to form vertical thermocouple legs (Figure 19a) [127]. A single TE leg was constructed by sewing multiple numbers of conductive threads coated by PEDOT:PSS or silver. Thereby, PEDOT:PSS and conductive zones were alternatively formed on a wool felt. For the coercive TE generation, conductive paste was printed to form the top and bottom electrodes for series connection of PEDOT:PSS

25673173, 2025, 10, Downloaded from https://onlinelibrary.wiley.com/doi/10.1002/eem2.70029 by Hansol Lee - Gachon University Global Campus , Wiley Online Library on [29/09/2025]. See the Terms and Conditions (https://onlinelibrary.wiley.com/terms-and-conditions) on Wiley Online Library for rules of use; OA articles are governed by the applicable Creative Commons License

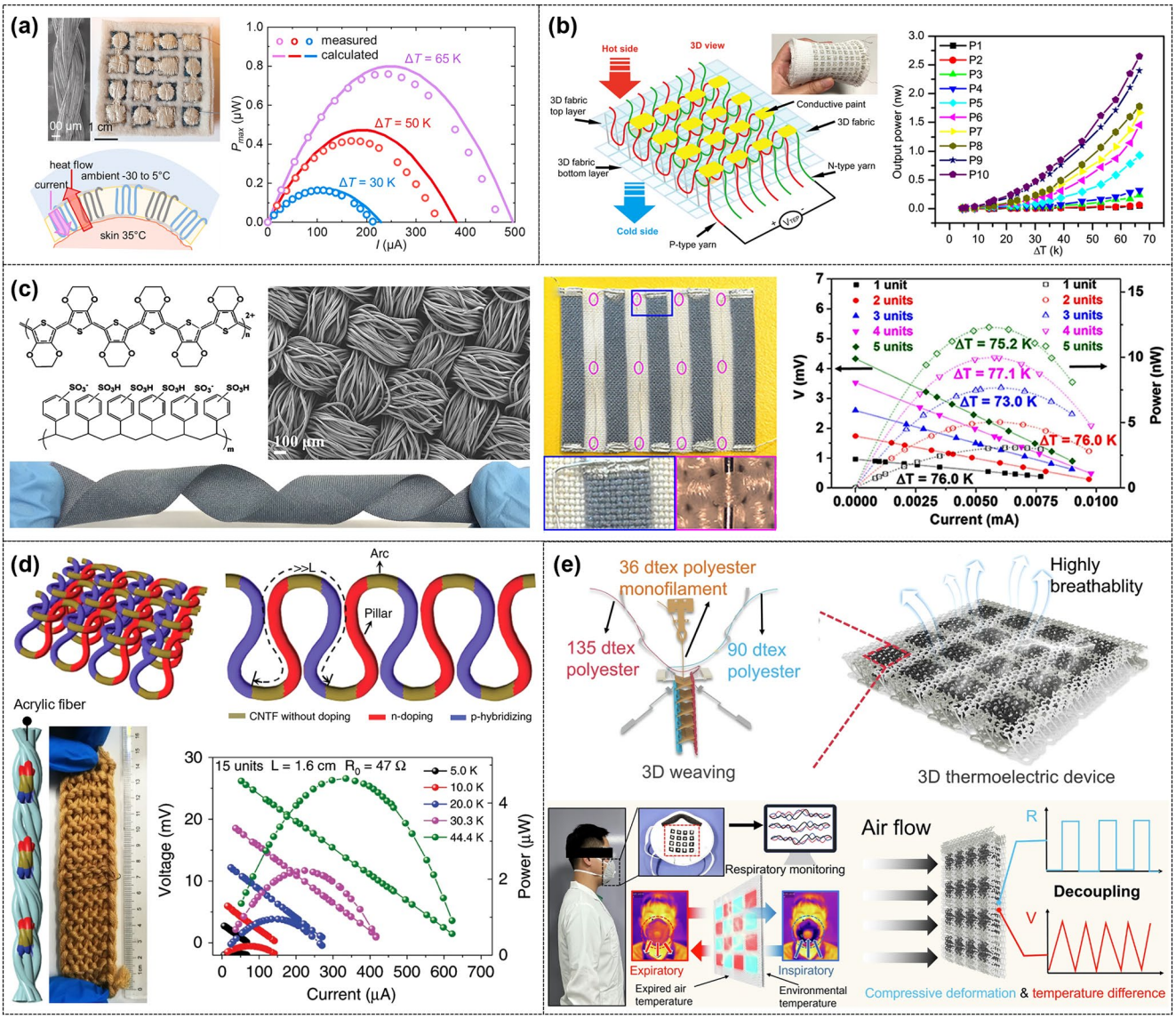


FIGURE 19 | (a) A textile TEG woven by PEDOT:PSS coated silk thread (SEM images) and silver plated polyamide thread on felted wool fabric. Reproduced from 127 with permission (Copyright 2020, Elsevier). (b) A textile TEG fabricated by weaving p-type PEDOT:PSS/MWCNT yarn and n-type N-MWCNT yarn on the locknit spacer fabric. Reproduced from 128 with permission (Copyright 2017, IOP Publishing). (c) A textile TEG comprising PEDOT:PSS-soaked polyester fabrics. Fabric TE patterns were electrically connected by weaving them on uncoated polyester fabric (blue square, left inset of the center photograph) with silver wire (pink ellipses, right inset of the center photograph). Reproduced from 129 with permission (Copyright 2015, Springer Nature). (d) A textile TEG fabricated by 3-dimensionally weaving CNTF wrapped by an acrylic fiber along spacer fabric. CNTF periodically featuring p-type and n-type characteristics via hybridization with PEDOT:PSS and n-doping, respectively. Reproduced from 22 with permission (Copyright 2020, Springer Nature). (e) A textile TEG based on 3-dimensionally woven spacer fabric. Oleylamine-doped CNT yarn (n-type) and PEDOT:PSS/CNT yarn (p-type) were woven along with the spacer fabric to yield TE patterns. The TEG was sensitive to both heat and deformation (pressure), which proved by voltage output and resistance change, respectively. Reproduced from 130 with permission (Copyright 2025, Springer Nature).

and conductive zones, resulting in a textile-based, out-of-plane TEG. With eight thermocouples, the device produced up to 1.2 μW at a ΔT of 65 K, illustrating the potential of polymer-based yarns for wearable energy harvesting within textile-integrated systems.

Wu and Hu proposed a textile TEG prototype based on a 3D locknit spacer fabric substrate. Nonionic waterborne polyurethane (NWPU)/multiwalled CNT (MWCNT) composites were used to coat polyester yarns [128]. For a p-type coating agent, PEDOT:PSS was added to form NWPU/PEDOT:PSS/MWCNT composite solution, and n-doped MWCNT (N-CMWCNT) was used to form NWPU/N-MWCNT composite solution for the n-type coating agent. Polyester yarns were coated with TE composites through dip coating, then embroidered into the fabric and connected in series (Figure 19b). The sandwich-like structure enabled the formation of thermal gradients across the fabric's thickness. While the power output remained relatively low, the prototype demonstrated the feasibility of 3D fabric architectures for wearable TE energy harvesting and highlighted the potential

25673173, 2025, 10, Downloaded from https://onlinelibrary.wiley.com/doi/10.1002/eom2.70029 by Hansol Lee - Gachon University Global Campus , Wiley Online Library on [29/09/2025]. See the Terms and Conditions (https://onlinelibrary.wiley.com/terms-and-conditions) on Wiley Online Library for rules of use; OA articles are governed by the applicable Creative Commons License

for performance improvements through advanced materials and interface engineering.

Du et al. demonstrated a TEG comprising commercial polyester fabric strips, which were directly coated with PEDOT:PSS (Figure 19c) [129]. The coated fabric strips were stitched onto a polyester fabric and then electrically connected in series by waving fine metal wires. Although the study focused primarily on p-type behavior and simple strip configurations, it introduced a breathable, air-permeable fabric generator concept, capable of producing approximately 4.3 mV at a ΔT of 75.2 K.

Sun et al. developed a TE fabric using alternately doped CNT fibers—p-type fibers hybridized with PEDOT:PSS and n-type fibers doped with oleylamine (Figure 19d) [22]. These fibers were passivated by acrylic fiber wrapping, so the threads can be interwoven into a textile architecture, which achieved improved heat flow for high TE performance as well as an improved mechanical strength. The resulting fabric exhibited remarkable stretchability (~80%), retained performance under mechanical deformation, and achieved a peak power density of 70 mW m^{-2} at a temperature difference of 44 K. This design is particularly noteworthy as the first to demonstrate fully woven TE modules that are simultaneously flexible, stretchable, and high-performing.

He et al. introduced a three-dimensional (3D) textile TE fabric based on a knitted spacer fabric structure, incorporating p- and n-type doped TE yarns via industrial knitting techniques (Figure 19e) [130]. The 3D architecture, reinforced by spandex spacer yarns, preserved static air pockets that sustained a stable temperature gradient across the fabric thickness. The CNT-based TE yarns, doped with oleylamine (n-type) and PEDOT:PSS (p-type), exhibited excellent durability (over 10 000 mechanical cycles), rapid thermal response (20 ms), and high air permeability (1300 mm s^{-1}), supporting efficient body-heat-driven operation. Leveraging its air-breathable feature, the 3D TE fabric was applied to a mask for respiratory monitoring. The temperature difference across the TE fabric was reverted for expiratory and inspiratory air flow, yielding voltage output changes. The expiratory air flow also compressed the TE fabric, decreasing the electrical resistance. Integrating the resistance and voltage output changes, effective respiratory monitoring using the 3D TE fabric was demonstrated (Table 3).

3.4 | Challenges and Prospects

Flexible TEGs have emerged as promising candidates for self-powered wearable electronics, ambient energy harvesters, and lightweight thermal sensors. Despite rapid advances in material development, their deployment in real-world applications still faces key challenges related to mechanical durability, device integration, cost-effectiveness, and scalable manufacturing. To bridge the gap between molecular design and device fabrication, it is essential to evaluate flexible TEGs in the context of their device architectures, Π-type, Y-type, and textile-based configurations.

Π-type flexible TEGs, consisting of alternating p-type and n-type legs connected electrically in series and thermally in parallel, are widely adapted from conventional rigid TEG architectures. Their compact vertical geometry allows low internal resistance, favoring high power output when modest temperature gradients are available. Therefore, Π-type flexible TEGs are particularly attractive for compact modules designed to harvest heat from flat surfaces such as human skin, electronics packages, or conformal heaters. However, their practical application in flexible platforms remains limited due to poor mechanical deformability, as interfacial delamination under bending stress arises with mismatches of modulus in layered assembly. The mechanical deformation of Π-type structure requires TE and electrode materials to be stretchable, which often degrades the TE performance significantly. With limited mechanical flexibility, Π-type structure is typically incompatible with stretchable or curved surfaces, and consistent thermal contact with both heat source and sink becomes difficult in dynamic or wearable environments. From a manufacturing perspective, their multilayer stacking and vertical alignment demand precise fabrication steps, increasing complexity and cost relative to in-plane designs. The requirement of p-n pairs for high power density also inhibits the practical application of Π-type TEGs, as the n-type CPs possess environmental stability issues, which should be addressed using material engineering strategies, such as in situ doping, developing environmentally stable n-type dopants, and passivation [19, 76, 131–132].

Y-type TEGs adopt a planar radial architecture in which p-type and n-type TE legs extend laterally from a shared junction or interconnect, allowing efficient in-plane thermal gradient utilization. This configuration is especially well-suited for applications where the heat source is distributed over a surface or where lateral temperature gradient naturally exists. However, the thermal gradient often arises from a heated or cooled surface, forming an out-of-plane temperature gradient. Therefore, Y-type TEGs were often folded to exploit the out-of-plane temperature gradient, because Y-type devices offer superior mechanical flexibility compared to Π-type TEGs. Y-type TEGs are also inherently compatible with printing-based fabrication techniques, making them promising candidates for scalable integration into soft electronics and large-area energy harvesting systems. The radial layout also facilitates more compact electrical interconnections while avoiding complex vertical stacking. However, Y-type devices typically suffer from longer current paths and increased internal resistance compared to Π-type structures, potentially limiting output current under high-impedance conditions. Cross-scale optimization strategies for Y-type devices include designing anisotropically conducting legs that optimize thermal and electrical conduction along the length of the conductor, as well as implementing nanostructure to optimize the trade-off relation between the Seebeck coefficient and the electrical conductivity [133–135]. From a fabrication standpoint, the use of inkjet or screen printing with orthogonally patterned masks enables selective deposition of complementary TE materials, while flexible encapsulation materials can provide protection against moisture and mechanical fatigue. Y-type TEGs can become a strong candidate for wearable and conformable TE applications, if their inherently low electrical conductivity and power output are overcome by bridging molecular design, material engineering, and scalable processing.

Textile-based TEGs represent a highly promising platform for wearable and conformal energy harvesting due to their inherent

25673173, 2025, 10, Downloaded from https://onlinelibrary.wiley.com/doi/10.1002/eem2.70029 by Hansol Lee - Gachon University Global Campus , Wiley Online Library on [29/09/2025]. See the Terms and Conditions (https://onlinelibrary.wiley.com/terms-and-conditions) on Wiley Online Library for rules of use; OA articles are governed by the applicable Creative Commons License

TABLE 3 | Summary of key features of various TEGs.

Device architecture	p-type material	n-type material	Fabrication method	Normalized power density ($\mu W\,cm^{-2}\,K^{-2}$)	Mechanical deformability	References
Π-type	PEDOT-Tos	TTF-TCNQ	Synthesis of precursor in photolithographed template	0.23	None	[117]
Π-type	poly[Na_x(Ni-ett)]	poly[Cu_x (Cu-ett)]	Compressed TE leg adhered to substrate	0.44	None	[17]
Π-type	poly[K_x(Ni-ett)]	poly[Cu_x (Cu-ett)]	Compressed TE leg adhered to substrate	0.0011	Flexible	[118]
Π-type	PEDOT:PSS	—	Stamp-printing on microstructured frame	0.013	Flexible	[119]
Π-type	Bi_2Te_3/ PEDOT:PSS	Bi_2Te_3/ PEDOT:PSS	Hot-pressed TE leg	475.6	Flexible	[120]
Π-type	PEDOT:PSS/ SEBS	—	Ink-jet printing on laser-drilled substrate	0.32	Stretchable	[20]
Π-type	PEDOT:PSS	PTEG-1	Ink-jet printing of μTEG	0.049	Flexible	[121]
Y-type	PEDOT:PSS	BBL:PEI	Spray coating over shadow mask	0.061	Flexible	[123]
Y-type	poly[Cu_x(Cu-ett)]/ PVDF		Drop-casting over shadow mask	—	Flexible	[124]
Y-type	PEDOT:PSS	FBDPPV:TAM	Drop-casting over photolithographed SU-8 mask	0.0026	Flexible	[102]
Y-type	TBDOPV:$FeCl_3$	TBDOPV:N-DMBI	Drop-casting	0.014	Flexible	[125]
Y-type	CNTP	PEI/CNTP	Dip-coating of CNTP-based frame	0.048	Stretchable	[126]
Y-type	PEDOT:PSS	PBFDO	Screen-printing	0.72	Flexible	[21]
Textile	PEDOT:PSS	—	Sewing threads coated by TE materials	0.010	Flexible	[127]
Textile	PEDOT:PSS	N-MWCNT	Sewing polyest yarns coated by TE materials	0.0001	Flexible	[128]
Textile	PEDOT:PSS	—	Dip-coating of polyester fabric template	0.0002	Flexible	[129]

(Continues)

25673173, 2025, 10, Downloaded from https://onlinelibrary.wiley.com/doi/10.1002/eom2.70029 by Hansol Lee - Gachon University Global Campus , Wiley Online Library on [29/09/2025]. See the Terms and Conditions (https://onlinelibrary.wiley.com/terms-and-conditions) on Wiley Online Library for rules of use; OA articles are governed by the applicable Creative Commons License

TABLE 3 | (Continued)

Device architecture	p-type material	n-type material	Fabrication method	Normalized power density ($\mu W\,cm^{-2}\,K^{-2}$)	Mechanical deformability	References
Textile	PEDOT:PSS	n-CNT	Sewing CNT fibers dip-coated/ electro-sprayed by TE materials	1.47	Stretchable	[22]
Textile	Oleylamine-CNT	PEDOT:PSS	Dip-coating of wrap-knitted fabric	0.045	Flexible	[130]

softness, breathability, and compatibility with human motion. These devices are typically fabricated by integrating TE yarns or fibers composed of p-type and n-type materials into woven, knitted, or embroidered textile structures. Their core advantage lies in mechanical robustness under repetitive deformation, making them ideal for body heat harvesting and integration into garments, bandages, or seating fabrics. Unlike Π- or Y-type structures, textile-based TEGs can maintain intimate and continuous contact with irregular, moving surfaces, ensuring persistent thermal contact in real-world scenarios. However, they face several limitations: their areal power output is generally lower due to low packing density and limited thermal gradient, and maintaining stable electrical and thermal junctions at fiber crossings is technically challenging. Furthermore, maintaining high TE performance of TE materials in fiber or yarn form remains a major barrier to commercialization. At the material level, incorporating flexible binders or ionic crosslinkers can enhance inter-fiber adhesion and reduce interfacial resistance. Scalable fiber coating or extrusion techniques allow precise control over doping levels and fiber morphology, while textile engineering approaches, such as hierarchical weaving, directional knitting, or embroidery with embedded heat-flow guidance, can be used to enhance the packing density and contact stability. Altogether, textile-based TEGs offer a unique pathway toward self-powered smart garments and skin-mountable electronics, where conformability and mechanical endurance are prioritized over absolute power density.

To realize practical flexible TEGs based on CPs, each device architecture must be matched with its optimal application scenario and supported by cross-scale strategies that bridge molecular design with device integration. Π-type devices, while capable of high power density through vertical stacking, face limitations in mechanical compliance and multilayer integration complexity, making them suitable for planar or skin-mounted applications. Y-type configurations allow easier planar integration and good conformability but often suffer from low packing density and limited thermal isolation. Textile-based TEGs offer excellent stretchability and comfort for wearables, but their performance is hindered by poor electrical interconnectivity and limited temperature gradient across fiber junctions. These limitations should be addressed by material engineering strategies to bridge molecular design with device integration. Several material engineering strategies have emerged to address such challenges. First, the intrinsic instability of n-type CPs, often caused by redox sensitivity and poor air stability, can be mitigated through compositionally graded composites and core–shell structured packaging [132, 136]. These methods protect the oxidation-vulnerable polymer core from ambient degradation, thereby enhancing operational durability. To overcome the low power factor due to inefficient charge transport, the introduction of hierarchical nanostructures in CP matrices enhances carrier mobility and energy filtering, leading to simultaneous improvement in electrical conductivity and Seebeck coefficient [135]. Mechanical failure under strain, a key limitation in wearable and stretchable devices, can be mitigated by constructing diverse conducting networks using hybrid fillers such as carbon nanotubes, Ag nanowires, or graphene within the polymer matrix. These networks maintain electrical pathways even under mechanical deformation [137]. Engineering anisotropic conduction properties can also improve the TE properties of CPs. In layered Bi_2Te_3, orthogonal thermal and electrical pathways enable directional heat transfer suppression and effective electrical conduction across TE legs [133]. Such techniques can be adopted to CP for high TE performance. When matched with the characteristics of each device type, bridging molecular design and device integration through material engineering can unlock the full potential of CP-based TEGs for applications in wearable electronics, biomedical systems, and autonomous energy devices.

4 | Conclusions

This review comprehensively summarizes recent advances in CP-based TE materials, with particular attention to molecular design strategies, doping mechanisms, and their implications for flexible and stretchable TEG architectures. The reviewed studies highlight that achieving high TE performance in CPs requires the careful balancing of several interdependent factors: backbone planarity, charge carrier delocalization, dopant compatibility, and microstructural stability upon doping.

For TE applications, CPs must be doped to attain a semi-metallic state, where TE performance is maximized. However, doping CPs involves the addition of a considerable amount of molecular dopant, which disrupts polymer crystallinity or aggregates into electrically insulating domains. Therefore, it is essential to design both the polymer structure and the doping processes for efficient doping. Doping processes can be categorized as in situ doping during polymerization and ex-situ doping after polymer formation. Ex-situ doping using molecular dopants exhibits

25673173, 2025, 10, Downloaded from https://onlinelibrary.wiley.com/doi/10.1002/eom2.70029 by Hansol Lee - Gachon University Global Campus , Wiley Online Library on [29/09/2025]. See the Terms and Conditions (https://onlinelibrary.wiley.com/terms-and-conditions) on Wiley Online Library for rules of use; OA articles are governed by the applicable Creative Commons License

inherent limitations in doping efficiency, as long side chains are often required to ensure compatibility with both dopants and solvents. While these long, flexible side chains improve miscibility and allow dopant intercalation between CP lamellae, they also hinder dopant–polymer interactions at elevated doping levels and form insulating layers that impede charge transport.

Recent progress in TE CPs has addressed many side-chain-related issues by improving backbone planarity, incorporating cleavable side chains, or optimizing miscibility between the dopant, solvent, and polymer. Nonetheless, relatively low electrical conductivities ($<1000\,S\,cm^{-1}$) suggest that dopant intercalation into polymer crystallites remains limited at high doping levels due to repulsion between ionized dopants, side-chain interference, and steric hindrance in tightly packed crystalline domains. Further optimization of ex-situ doping, in tandem with rational dopant and polymer design, could improve TE performance by overcoming these challenges. However, the doping level is likely constrained in ex-situ approaches, as enhancements in backbone rigidity and planarity necessary for crystallinity tend to hinder dopant intercalation. The overall TE performance, in terms of power factor and ZT, has advanced to values rivaling those of traditional inorganic TE materials. However, these high ZT values in CPs primarily stem from high Seebeck coefficients and low thermal conductivities, while improvements in electrical conductivity remain modest, potentially limiting practical applications.

A breakthrough in doping efficiency was achieved through in situ doping during polymerization. PEDOT:PSS, a representative conducting polymer, exhibits electrical conductivities ranging from 1000 to $4000\,S\,cm^{-1}$, comparable to that of indium tin oxide electrodes. Such high conductivity arises from enhanced doping efficiency, typically one polaron per three repeat units. Given that the polaron delocalization length in PEDOT chains spans 2 to 3 repeat units, nearly every repeat unit in PEDOT:PSS is charged. This high doping efficiency is achieved via in situ processes where the strong oxidant used for oxidative polymerization of EDOT also dopes the polymer by oxidizing the monomer to its charged state. The resulting ionized oxidants are chemically unstable and are replaced by PSS through ion exchange during polymerization.

In addition, n-type CPs have also been polymerized with in situ doping, achieving high doping levels up to 90% of repeat units charged in PBFDO. PBFDO polymerization involves catalytic cycles in which the oxidant is reduced to initiate polymerization, then is oxidized back with the reduction of H-BFDO to $BFDO^{-}$. The successful synthesis of PBFDO demonstrates the universal feasibility of in situ doping for both p- and n-type CPs. It should be noted that the monomer or oligomer is doped during in situ doping, allowing the formation of charged polymer backbones without side chains. The absence of side chains facilitates close dopant–monomer interactions, leading to a high density of charged repeat units, which endow the polymerized CP chain with solubility in polar solvents (e.g., water for PEDOT:PSS, DMSO for PBFDO) without the need for side chains. Currently, PEDOT:PSS and PBFDO have been successfully synthesized via in situ doping, and further development could yield TE materials with significantly improved electrical conductivities, complementing the ex-situ doping.

However, improving material properties alone is insufficient. Realizing high-performance TEGs also requires precise structural design and material integration into device architectures. The inherent flexibility of CPs enables the fabrication of Π-type, Y-type, and textile-based flexible TEGs. These designs allow effective thermal gradients and mechanical adaptability, essential for wearable and deformable energy-harvesting applications. Yet, CP-based TE materials often exhibit reduced mechanical compliance because of rigid backbone structure and high crystallinity.

Advanced approaches to decouple trade-offs among TE parameters through targeted material design and process engineering are vital. Going forward, bridging the gap between material innovation and device realization necessitates a more integrated strategy. CPs designed for high ZT should be evaluated not only for intrinsic properties but also for compatibility with device fabrication, mechanical durability, and long-term operational stability. Future research should focus on scalable processing techniques, interfacial engineering to reduce contact resistance, and multilayered architectures that optimize both thermal and electrical transport. Ultimately, the interplay among molecular design, doping strategy, and device architecture will define the next generation of organic TEs. The future of CP-based TEGs depends on co-optimizing these factors to achieve systems that are efficient, flexible, and manufacturable at scale for applications such as wearable electronics, distributed IoT systems, and sustainable energy harvesting.

Author Contributions

All the authors take full responsibility for the content of this review and approved its submission. **Daegun Kim:** investigation, validation, data curation, writing – review and editing. **Hoimin Kim:** data curation, formal analysis, visualization. **Jeong-Min Seo:** data curation, visualization. **Il Jeon:** validation, project administration, supervision. **Hansol Lee:** validation, data curation, writing – original draft, writing – review and editing. **Boseok Kang:** conceptualization, funding acquisition, project administration, resources, supervision, writing – review and editing.

Acknowledgments

This work was supported by the National Research Foundation of Korea (NRF) grant funded by the Korea government (MSIT) (RS-2023-NR076607, RS-2025-00516030, RS-2025-25413074, and RS-2025-23523476). This research was also supported by the Nano and Material Technology Development Program through the NRF funded by the Ministry of Science and ICT (Grant No. RS-2024-00403639).

Conflicts of Interest

The authors declare no conflicts of interest.

References

1. R. Kroon, D. A. Mengistie, D. Kiefer, et al., "Thermoelectric Plastics: From Design to Synthesis, Processing and Structure–Property Relationships," *Chemical Society Reviews* 45 (2016): 6147–6164.

2. S. Gogoc and P. Data, "Organic Thermoelectric Materials as the Waste Heat Remedy," *Molecules* 27 (2022): 1016.

3. M. Goel, C. D. Heinrich, G. Krauss, and M. Thelakkat, "Principles of Structural Design of Conjugated Polymers Showing Excellent Charge

25673173, 2025, 10, Downloaded from https://onlinelibrary.wiley.com/doi/10.1002/eom2.70029 by Hansol Lee - Gachon University Global Campus , Wiley Online Library on [29/09/2025]. See the Terms and Conditions (https://onlinelibrary.wiley.com/terms-and-conditions) on Wiley Online Library for rules of use; OA articles are governed by the applicable Creative Commons License

Transport Toward Thermoelectrics and Bioelectronics Applications," *Macromolecular Rapid Communications* 40 (2019): 1800915.

4. K. A. Peterson, E. M. Thomas, and M. L. Chabinyc, "Thermoelectric Properties of Semiconducting Polymers," *Annual Review of Materials Research* 50 (2020): 551–574.

5. Y. Jia, Q. Jiang, H. Sun, et al., "Wearable Thermoelectric Materials and Devices for Self-Powered Electronic Systems," *Advanced Materials* 33 (2021): 2102990.

6. Y. He, Q. Wei, N. An, C. Meng, and Z. Hu, "Organic Small-Molecule Electrodes: Emerging Organic Composite Materials in Supercapacitors for Efficient Energy Storage," *Molecules* 27 (2022): 7692.

7. D. Rodriquez, S. Savagatrup, E. Valle, et al., "Mechanical Properties of Solution-Processed Small-Molecule Semiconductor Films," *ACS Applied Materials & Interfaces* 8 (2016): 11649–11657.

8. A. Tripathi, Y. Lee, S. Lee, and H. Y. Woo, "Recent Advances in n-Type Organic Thermoelectric Materials, Dopants, and Doping Strategies," *Journal of Materials Chemistry C* 10 (2022): 6114–6140.

9. S. Lee, S. Kim, A. Pathak, et al., "Recent Progress in Organic Thermoelectric Materials and Devices," *Macromolecular Research* 28 (2020): 531–552.

10. D. Scheunemann and M. Kemerink, "Non-Wiedemann-Franz Behavior of the Thermal Conductivity of Organic Semiconductors," *Physical Review B* 101 (2020): 075206.

11. W. Zhao, J. Ding, Y. Zou, C.-a. Di, and D. Zhu, "Chemical Doping of Organic Semiconductors for Thermoelectric Applications," *Chemical Society Reviews* 49 (2020): 7210–7228.

12. H. Lee, H. Li, Y.-S. Kim, et al., "Novel Dithienopyrrole-Based Conjugated Copolymers: Importance of Backbone Planarity in Achieving High Electrical Conductivity and Thermoelectric Performance," *Macromolecular Rapid Communications* 43 (2022): 2200277.

13. H. Yan, T. Ohta, and N. Toshima, "Stretched Polyaniline Films Doped by (±)-10-Camphorsulfonic Acid: Anisotropy and Improvement of Thermoelectric Properties," *Macromolecular Materials and Engineering* 286 (2001): 139–142.

14. G. H. Kim, L. Shao, K. Zhang, and K. P. Pipe, "Engineered Doping of Organic Semiconductors for Enhanced Thermoelectric Efficiency," *Nature Materials* 12 (2013): 719–723.

15. J. Ding, Z. Liu, W. Zhao, et al., "Selenium-Substituted Diketopyrrolopyrrole Polymer for High-Performance p-Type Organic Thermoelectric Materials," *Angewandte Chemie International Edition* 58 (2019): 18994–18999.

16. S. Wang, W. Zhu, I. E. Jacobs, et al., "Enhancing the Thermoelectric Properties of Conjugated Polymers by Suppressing Dopant-Induced Disorder," *Advanced Materials* 36 (2024): 2314062.

17. Y. Sun, P. Sheng, C. Di, et al., "Organic Thermoelectric Materials and Devices Based on p- and n-Type Poly(Metal 1,1,2,2-Ethenetetrathiolate) s," *Advanced Materials* 24 (2012): 932–937.

18. R. A. Schlitz, F. G. Brunetti, A. M. Glaudell, et al., "Solubility-Limited Extrinsic n-Type Doping of a High Electron Mobility Polymer for Thermoelectric Applications," *Advanced Materials* 26 (2014): 2825–2830.

19. H. Tang, Y. Liang, C. Liu, et al., "A Solution-Processed n-Type Conducting Polymer With Ultrahigh Conductivity," *Nature* 611 (2022): 271–277.

20. D. Kim, M.-E. Kim, H. Kim, et al., "Stepwise Curing Induced all-Stretchable Thermoelectric Generator of High Power Density," *Small* 21 (2025): 2406662.

21. I. Brunetti, N. James Pataki, D. R. Hinojosa, et al., "A Scalable Fully Printed Organic Thermoelectric Generator for Harsh Environments Enabled by a Stable n-Type Polymer," *Advanced Materials Technologies* 10 (2025): 2400968.

22. T. Sun, B. Zhou, Q. Zheng, L. Wang, W. Jiang, and G. J. Snyder, "Stretchable Fabric Generates Electric Power From Woven Thermoelectric Fibers," *Nature Communications* 11 (2020): 572.

23. S. Pyo, Y. Im, and H. Kim, "Cyclopentadithiophene-Based Conjugated Polymers for Organic Thermoelectric Devices and Other Applications," *Organic Polymer Material Research* 5 (2023): 1–10.

24. Z. Fan, P. Li, D. Du, and J. Ouyang, "Significantly Enhanced Thermoelectric Properties of PEDOT:PSS Films Through Sequential Post-Treatments With Common Acids and Bases," *Advanced Energy Materials* 7 (2017): 1602116.

25. D. Ju, D. Kim, H. Yook, J. W. Han, and K. Cho, "Controlling Electrostatic Interaction in PEDOT:PSS to Overcome Thermoelectric Tradeoff Relation," *Advanced Functional Materials* 29 (2019): 1905590.

26. D. Ju, J. Kim, H. Yook, J. W. Han, and K. Cho, "Engineering Counter-Ion-Induced Disorder of a Highly Doped Conjugated Polymer for High Thermoelectric Performance," *Nano Energy* 90 (2021): 106604.

27. J. Hynynen, D. Kiefer, and C. Müller, "Influence of Crystallinity on the Thermoelectric Power Factor of P3HT Vapour-Doped With F4TCNQ," *RSC Advances* 8 (2018): 1593–1599.

28. A. Hamidi-Sakr, L. Biniek, J.-L. Bantignies, et al., "A Versatile Method to Fabricate Highly in-Plane Aligned Conducting Polymer Films With Anisotropic Charge Transport and Thermoelectric Properties: The Key Role of Alkyl Side Chain Layers on the Doping Mechanism," *Advanced Functional Materials* 27 (2017): 1700173.

29. V. Vijayakumar, Y. Zhong, V. Untilova, et al., "Bringing Conducting Polymers to High Order: Toward Conductivities Beyond 105 S Cm^{-1} and Thermoelectric Power Factors of 2 mW m^{-1} K^{-2}," *Advanced Energy Materials* 9 (2019): 1900266.

30. I. H. Jung, C. T. Hong, U.-H. Lee, Y. H. Kang, K.-S. Jang, and S. Y. Cho, "High Thermoelectric Power Factor of a Diketopyrrolopyrrole-Based Low Bandgap Polymer via Finely Tuned Doping Engineering," *Scientific Reports* 7 (2017): 44704.

31. N. Y. Kim, T. S. Lee, D. Y. Lee, et al., "Enhanced Doping Efficiency and Thermoelectric Performance of Diketopyrrolopyrrole-Based Conjugated Polymers With Extended Thiophene Donors," *Journal of Materials Chemistry C* 9 (2021): 340–347.

32. Z. Liu, Y. Hu, P. Li, J. Wen, J. He, and X. Gao, "Enhancement of the Thermoelectric Performance of DPP Based Polymers by Introducing One 3,4-Ethylenedioxythiophene Electron-Rich Building Block," *Journal of Materials Chemistry C* 8 (2020): 10859–10867.

33. F. Zhong, X. Yin, Z. Chen, C. Gao, and L. Wang, "Significantly Reduced Thermal-Activation Energy for Hole Transport via Simple Donor Engineering: Understanding the Role of Molecular Parameters for Thermoelectric Behaviors," *ACS Applied Materials & Interfaces* 12 (2020): 26276–26285.

34. T. S. Lee, S. B. Lee, D.-Y. Choi, et al., "Doping and Thermoelectric Behaviors of Donor-Acceptor Polymers With Extended Planar Backbone," *Macromolecular Research* 29 (2021): 887–894.

35. S. E. Yoon, Y. Kang, S. Y. Noh, et al., "High Efficiency Doping of Conjugated Polymer for Investigation of Intercorrelation of Thermoelectric Effects With Electrical and Morphological Properties," *ACS Applied Materials & Interfaces* 12 (2020): 1151–1158.

36. J. M. Han, S. E. Yoon, K. H. Jung, et al., "Dopant-Dependent Thermoelectric Performance of Indoloindole-Selenophene Based Conjugated Polymer," *Chemical Engineering Journal* 431 (2022): 133779.

37. T. Liu, D. Xie, J. Xu, and C. Pan, "Structure and Doping Optimization of IDT-Based Copolymers for Thermoelectrics," *Polymers* 12 (2020): 1463.

38. D. Xie, J. Xiao, Q. Li, T. Liu, J. Xu, and G. Shao, "Backbone Effects on the Thermoelectric Properties of Ultra-Small Bandgap Conjugated Polymers," *Polymers* 13 (2021): 2486.

25673173, 2025, 10, Downloaded from https://onlinelibrary.wiley.com/doi/10.1002/eom2.70029 by Hansol Lee - Gachon University Global Campus , Wiley Online Library on [29/09/2025]. See the Terms and Conditions (https://onlinelibrary.wiley.com/terms-and-conditions) on Wiley Online Library for rules of use; OA articles are governed by the applicable Creative Commons License

39. L. Wang, C. Pan, Z. Chen, X. Zhou, C. Gao, and L. Wang, "A Study of the Thermoelectric Properties of Benzo[1,2-*b*:4,5-*b*']Dithiophene–Based Donor–Acceptor Conjugated Polymers," *Polymer Chemistry* 9 (2018): 4440–4447.

40. X. Zhou, C. Pan, C. Gao, et al., "Thermoelectrics of Two-Dimensional Conjugated Benzodithiophene-Based Polymers: Density-Of-States Enhancement and Semi-Metallic Behavior," *Journal of Materials Chemistry A* 7 (2019): 10422–10430.

41. B. Li, X. Li, F. Yang, et al., "Enhanced Thermoelectric Performance of a Donor–Acceptor-Based Two-Dimensional Conjugated Polymer With High Crystallinity," *ACS Applied Energy Materials* 4 (2021): 4662–4671.

42. J. Lee, J. Kim, T. L. Nguyen, et al., "A Planar Cyclopentadithiophene–Benzothiadiazole-Based Copolymer With sp^2-Hybridized Bis(Alkylsulfanyl)methylene Substituents for Organic Thermoelectric Devices," *Macromolecules* 51 (2018): 3360–3368.

43. E. H. Suh, Y. J. Jeong, J. G. Oh, et al., "Doping of Donor-Acceptor Polymers With Long Side Chains via Solution Mixing for Advancing Thermoelectric Properties," *Nano Energy* 58 (2019): 585–595.

44. S. E. Yoon, B. Kim, S. Y. Chun, et al., "Impact of Molecular Weight on Molecular Doping Efficiency of Conjugated Polymers and Resulting Thermoelectric Performances," *Advanced Functional Materials* 32 (2022): 2202929.

45. J. Rivnay, S. Inal, B. A. Collins, et al., "Structural Control of Mixed Ionic and Electronic Transport in Conducting Polymers," *Nature Communications* 7 (2016): 11287.

46. N. Kim, S. Kee, S. H. Lee, et al., "Highly Conductive PEDOT:PSS Nanofibrils Induced by Solution-Processed Crystallization," *Advanced Materials* 26 (2014): 2268–2272.

47. E. Lim, A. M. Glaudell, R. Miller, and M. L. Chabinyc, "The Role of Ordering on the Thermoelectric Properties of Blends of Regioregular and Regiorandom Poly(3-Hexylthiophene)," *Advanced Electronic Materials* 5 (2019): 1800915.

48. J. Shanahan, L. Yan, Y. Olanrewaju, et al., "Acid-Triggered Side Chain Cleavage Leads to Doped Conjugated Polymers of High Conductivity," *Journal of the American Chemical Society* 146 (2024): 32243–32248.

49. J. Min, D. Kim, S. G. Han, et al., "Position-Induced Efficient Doping for Highly Doped Organic Thermoelectric Materials," *Advanced Electronic Materials* 8 (2022): 2101142.

50. G. Zuo, X. Liu, M. Fahlman, and M. Kemerink, "High Seebeck Coefficient in Mixtures of Conjugated Polymers," *Advanced Functional Materials* 28 (2018): 1703280.

51. J. Sun, M. L. Yeh, B. J. Jung, et al., "Simultaneous Increase in Seebeck Coefficient and Conductivity in a Doped Poly(Alkylthiophene) Blend With Defined Density of States," *Macromolecules* 43 (2010): 2897–2903.

52. M. Grzybowski and D. T. Gryko, "Diketopyrrolopyrroles: Synthesis, Reactivity, and Optical Properties," *Advanced Optical Materials* 3 (2015): 280–320.

53. W. Zhuang, S. Wang, Q. Tao, et al., "Synthesis and Electronic Properties of Diketopyrrolopyrrole-Based Polymers With and Without Ring-Fusion," *Macromolecules* 54 (2021): 970–980.

54. N. Luo, G. Zhang, and Z. Liu, "Keep Glowing and Going: Recent Progress in Diketopyrrolopyrrole Synthesis Towards Organic Optoelectronic Materials," *Organic Chemistry Frontiers* 8 (2021): 4560–4581.

55. K. Gmucová, "Structural Properties Versus Electronic Structure of Donor-Acceptor Alternating Copolymers: A Review," *Synthetic Metals* 274 (2021): 116718.

56. S. Wang, G. Zuo, J. Kim, and H. Sirringhaus, "Progress of Conjugated Polymers as Emerging Thermoelectric Materials," *Progress in Polymer Science* 129 (2022): 101548.

57. Z. G. Zhang and J. Wang, "Structures and Properties of Conjugated Donor–Acceptor Copolymers for Solar Cell Applications," *Journal of Materials Chemistry* 22 (2012): 4178–4187.

58. J. Park, S. E. Yoon, Y. Kang, I. Lee, J. H. Kim, and B.-G. Kim, "Doping Characteristics of Isoindoloindole-Based Conjugated Polymer Toward Robust Transformable Organic Conductor," *Organic Electronics* 75 (2019): 105435.

59. I. Cho, S. K. Park, B. Kang, et al., "Design, Synthesis, and Versatile Processing of Indolo[3,2-b]Indole-Based π-Conjugated Molecules for High-Performance Organic Field-Effect Transistors," *Advanced Functional Materials* 26 (2016): 2966–2973.

60. S. A. Samsoniya and M. V. Trapaidze, "The Chemistry of Indoloindoles," *Russian Chemical Reviews* 76 (2007): 313–326.

61. S. E. Yoon, J. Park, J. E. Kwon, et al., "Improvement of Electrical Conductivity in Conjugated Polymers Through Cascade Doping With Small-Molecular Dopants," *Advanced Materials* 32 (2020): 2005129.

62. C. Liang and H. Wang, "Indacenodithiophene-Based D-A Conjugated Polymers for Application in Polymer Solar Cells," *Organic Electronics* 50 (2017): 443–457.

63. W. Khelifi and C. K. Luscombe, "Recent Developments in Indacenodithiophene and Indacenodithienothiophene-Based Donor-Acceptor Conjugated Polymers: From Design to Device Performance in Organic Electronics," *Progress in Polymer Science* 151 (2024): 101804.

64. Y. Lee, J. Park, J. Son, H. Y. Woo, and J. Kwak, "Degenerately Doped Semi-Crystalline Polymers for High Performance Thermoelectrics," *Advanced Functional Materials* 31 (2021): 2006900.

65. G.-H. Nam, C. Sun, D. S. Chung, and Y.-H. Kim, "Enhancing Doping Efficiency of Diketopyrrolopyrrole-Copolymers by Introducing Sparse Intramolecular Alkyl Chain Spacing," *Macromolecules* 54 (2021): 7870–7879.

66. S. C. Rasmussen and S. J. Evenson, "Dithieno[3,2-b:2′,3′-D]Pyrrole-Based Materials: Synthesis and Application to Organic Electronics," *Progress in Polymer Science* 38 (2013): 1773–1804.

67. Y. Geng, J. Cong, K. Tajima, Q. Zeng, and E. Zhou, "Synthesis and Properties of D–A Copolymers Based on Dithienopyrrole and Benzothiadiazole With Various Numbers of Thienyl Units as Spacers," *Polymer Chemistry* 5 (2014): 6797–6803.

68. C.-Y. Yang, W.-L. Jin, J. Wang, et al., "Enhancing the n-Type Conductivity and Thermoelectric Performance of Donor–Acceptor Copolymers Through Donor Engineering," *Advanced Materials* 30 (2018): 1802850.

69. S. Wang, H. Sun, T. Erdmann, et al., "A Chemically Doped Naphthalenediimide-Bithiazole Polymer for n-Type Organic Thermoelectrics," *Advanced Materials* 30 (2018): 1801898.

70. D. Kiefer, A. Giovannitti, H. Sun, et al., "Enhanced n-Doping Efficiency of a Naphthalenediimide-Based Copolymer Through Polar Side Chains for Organic Thermoelectrics," *ACS Energy Letters* 3 (2018): 278–285.

71. J. Liu, L. Qiu, R. Alessandri, et al., "Enhancing Molecular n-Type Doping of Donor–Acceptor Copolymers by Tailoring Side Chains," *Advanced Materials* 30 (2018): 1704630.

72. J. Liu, G. Ye, B. V. D. Zee, et al., "N-Type Organic Thermoelectrics of Donor–Acceptor Copolymers: Improved Power Factor by Molecular Tailoring of the Density of States," *Advanced Materials* 30 (2018): 1804290.

73. J. Liu, G. Ye, H. G. O. Potgieser, et al., "Amphipathic Side Chain of a Conjugated Polymer Optimizes Dopant Location Toward Efficient n-Type Organic Thermoelectrics," *Advanced Materials* 33 (2021): 2006694.

74. Y. Wang and K. Takimiya, "Naphthodithiophenediimide–Bithiopheneimide Copolymers for High-Performance n-Type Organic

25673173, 2025, 10, Downloaded from https://onlinelibrary.wiley.com/doi/10.1002/eom2.70029 by Hansol Lee - Gachon University Global Campus , Wiley Online Library on [29/09/2025]. See the Terms and Conditions (https://onlinelibrary.wiley.com/terms-and-conditions) on Wiley Online Library for rules of use; OA articles are governed by the applicable Creative Commons License

Thermoelectrics: Significant Impact of Backbone Orientation on Conductivity and Thermoelectric Performance," *Advanced Materials* 32 (2020): 2002060.

75. K. Shi, F. Zhang, C.-A. Di, et al., "Toward High Performance n-Type Thermoelectric Materials by Rational Modification of BDPPV Backbones," *Journal of the American Chemical Society* 137 (2015): 6979–6982.

76. Y. Lu, Z.-D. Yu, Y. Liu, et al., "The Critical Role of Dopant Cations in Electrical Conductivity and Thermoelectric Performance of n-Doped Polymers," *Journal of the American Chemical Society* 142 (2020): 15340–15348.

77. Y. Lu, Z.-D. Yu, R.-Z. Zhang, et al., "Rigid Coplanar Polymers for Stable n-Type Polymer Thermoelectrics," *Angewandte Chemie International Edition* 58 (2019): 11390–11394.

78. X. Yan, M. Xiong, J.-T. Li, et al., "Pyrazine-Flanked Diketopyrrolopyrrole (DPP): A New Polymer Building Block for High-Performance n-Type Organic Thermoelectrics," *Journal of the American Chemical Society* 141 (2019): 20215–20221.

79. D. Rosas Villalva, D. Derewjanko, Y. Zhang, et al., "Intermolecular-Force-Driven Anisotropy Breaks the Thermoelectric Trade-Off in n-Type Conjugated Polymers," *Nature Materials* 24 (2025): 1236–1244.

80. S. Wang, H. Sun, U. Ail, et al., "Thermoelectric Properties of Solution-Processed n-Doped Ladder-Type Conducting Polymers," *Advanced Materials* 28 (2016): 10764–10771.

81. C. Dong, B. Meng, J. Liu, and L. Wang, "B ← N Unit Enables n-Doping of Conjugated Polymers for Thermoelectric Application," *ACS Applied Materials & Interfaces* 12 (2020): 10428–10433.

82. H. Chen, M. Moser, S. Wang, et al., "Acene Ring Size Optimization in Fused Lactam Polymers Enabling High n-Type Organic Thermoelectric Performance," *Journal of the American Chemical Society* 143 (2021): 260–268.

83. M. Alsufyani, R. K. Hallani, S. Wang, et al., "The Effect of Aromatic Ring Size in Electron Deficient Semiconducting Polymers for n-Type Organic Thermoelectrics," *Journal of Materials Chemistry C* 8 (2020): 15150–15157.

84. M. Alsufyani, M.-A. Stoeckel, X. Chen, et al., "Lactone Backbone Density in Rigid Electron-Deficient Semiconducting Polymers Enabling High n-Type Organic Thermoelectric Performance," *Angewandte Chemie International Edition* 61 (2022): e202113078.

85. J. Hwang, Q. Zhao, M. Ahmed, et al., "Reductive Doping Inhibits the Formation of Isomerization-Derived Structural Defects in n-Doped Poly(Benzodifurandione) (n-PBDF)," *Angewandte Chemie International Edition* 63 (2024): e202401465.

86. Z. Ke, A. Abtahi, J. Hwang, et al., "Highly Conductive and Solution-Processable n-Doped Transparent Organic Conductor," *Journal of the American Chemical Society* 145 (2023): 3706–3715.

87. H. Ji, J. G. Lee, H. Lee, D. Kim, and K. Cho, "High-Performance Organic Thermoelectric Materials Based on n-Type Conjugated Polymers via Chemical Isomerization-Induced Charge Transport Modulation," *Materials Horizons* (2025).

88. N. Zhou and A. Facchetti, "Naphthalenediimide (NDI) Polymers for all-Polymer Photovoltaics," *Materials Today* 21 (2018): 377–390.

89. T. Lei, J.-H. Dou, X.-Y. Cao, J.-Y. Wang, and J. Pei, "Electron-Deficient Poly(p-Phenylene Vinylene) Provides Electron Mobility Over 1 $cm^2 V^{-1} s^{-1}$ Under Ambient Conditions," *Journal of the American Chemical Society* 135 (2013): 12168–12171.

90. E. E. Perry, C.-Y. Chiu, K. Moudgil, et al., "High Conductivity in a Nonplanar n-Doped Ambipolar Semiconducting Polymer," *Chemistry of Materials* 29 (2017): 9742–9750.

91. C. G. Tang, K. Hou, and W. L. Leong, "The Quest for Air Stability in Organic Semiconductors," *Chemistry of Materials* 36 (2024): 28–53.

92. J. Li, C. W. Rochester, I. E. Jacobs, et al., "The Effect of Thermal Annealing on Dopant Site Choice in Conjugated Polymers," *Organic Electronics* 33 (2016): 23–31.

93. S.-A. Chen, J.-M. Ni, and M.-Y. Hua, "Thermal Undoping Behavior of $FeCl_3$-Doped Poly(3-Octylthiophene)," *Journal of Polymer Research* 4 (1997): 261–265.

94. E. H. Suh, S. B. Kim, J. Jung, and J. Jang, "Extremely Electron-Withdrawing Lewis-Paired CN Groups for Organic p-Dopants," *Angewandte Chemie International Edition* 62 (2023): e202304245.

95. R. Kroon, D. Kiefer, D. Stegerer, L. Yu, M. Sommer, and C. Müller, "Polar Side Chains Enhance Processability, Electrical Conductivity, and Thermal Stability of a Molecularly p-Doped Polythiophene," *Advanced Materials* 29 (2017): 1700930.

96. F. Zhong, Y. Zheng, J. Song, L. Chen, and H. Li, "Side-Chain-Free Benzothiadiazole-Based Thermoelectric Polymers With Enhanced Electrical Conductivity and Thermal Stability by Acid Cleavage," *Advanced Functional Materials* (2025): 2507113.

97. O. Zapata-Arteaga, A. Perevedentsev, M. Prete, et al., "A Universal, Highly Stable Dopant System for Organic Semiconductors Based on Lewis-Paired Dopant Complexes," *ACS Energy Letters* 9 (2024): 3567–3577.

98. H. E. Winberg, J. E. Carnahan, D. D. Coffman, and M. Brown, "Tetraaminoethylenes," *Journal of the American Chemical Society* 87 (1965): 2055–2056.

99. K. Xu, H. Sun, T.-P. Ruoko, et al., "Ground-State Electron Transfer in all-Polymer Donor–Acceptor Heterojunctions," *Nature Materials* 19 (2020): 738–744.

100. D. Nava, Y. Shin, M. Massetti, et al., "Drastic Improvement of Air Stability in an n-Type Doped Naphthalene-Diimide Polymer by Thionation," *ACS Applied Energy Materials* 1 (2018): 4626–4634.

101. J. Han, H. Fan, Q. Zhang, Q. Hu, T. P. Russell, and H. E. Katz, "Dichlorinated Dithienylethene-Based Copolymers for Air-Stable n-Type Conductivity and Thermoelectricity," *Advanced Functional Materials* 31 (2021): 2005901.

102. C.-Y. Yang, Y.-F. Ding, D. Huang, et al., "A Thermally Activated and Highly Miscible Dopant for n-Type Organic Thermoelectrics," *Nature Communications* 11 (2020): 3292.

103. F. Pallini, S. Mattiello, N. Manfredi, et al., "Direct Detection of Molecular Hydrogen Upon p- And n-Doping of Organic Semiconductors With Complex Oxidants or Reductants," *Journal of Materials Chemistry A* 11 (2023): 8192–8201.

104. B. D. Naab, S. Guo, S. Olthof, et al., "Mechanistic Study on the Solution-Phase n-Doping of 1,3-Dimethyl-2-Aryl-2,3-Dihydro-1H-Benz oimidazole Derivatives," *Journal of the American Chemical Society* 135 (2013): 15018–15025.

105. C. Xu and D. Wang, "Electron Transfer Driving Force as the Criterion for Efficient n-Doping of Organic Semiconductors With DMBI-H Derivatives," *Journal of Materials Chemistry A* 11 (2023): 15416–15425.

106. O. Bardagot, C. Aumaître, A. Monmagnon, J. Pécaut, P.-A. Bayle, and R. Demadrille, "Revisiting Doping Mechanisms of n-Type Organic Materials With n-DMBI for Thermoelectric Applications: Photo-Activation, Thermal Activation, and Air Stability," *Applied Physics Letters* 118 (2021): 203904.

107. C.-Z. Li, C.-C. Chueh, F. Ding, et al., "Doping of Fullerenes via Anion-Induced Electron Transfer and Its Implication for Surfactant Facilitated High Performance Polymer Solar Cells," *Advanced Materials* 25 (2013): 4425–4430.

108. B. Zhao, C.-Z. Li, S.-Q. Liu, et al., "A Conductive Liquid Crystal via Facile Doping of an n-Type Benzodifurandione Derivative," *Journal of Materials Chemistry A* 3 (2015): 6929–6934.

109. X. Zhao, D. Madan, Y. Cheng, et al., "High Conductivity and Electron-Transfer Validation in an n-Type Fluoride-Anion-Doped

25673173, 2025, 10, Downloaded from https://onlinelibrary.wiley.com/doi/10.1002/eem2.70029 by Hansol Lee - Gachon University Global Campus , Wiley Online Library on [29/09/2025]. See the Terms and Conditions (https://onlinelibrary.wiley.com/terms-and-conditions) on Wiley Online Library for rules of use; OA articles are governed by the applicable Creative Commons License

Polymer for Thermoelectrics in Air," *Advanced Materials* 29 (2017): 1606928.

110. J. Han, E. Tiernan, T. Lee, et al., "A New Polystyrene–Poly(Vinylpyridinium) Ionic Copolymer Dopant for n-Type all-Polymer Thermoelectrics With High and Stable Conductivity Relative to the Seebeck Coefficient Giving High Power Factor," *Advanced Materials* 34 (2022): 2201062.

111. Y. Wang, L. Yang, X.-L. Shi, et al., "Flexible Thermoelectric Materials and Generators: Challenges and Innovations," *Advanced Materials* 31 (2019): 1807916.

112. S. J. Kim, J. H. We, and B. J. Cho, "A Wearable Thermoelectric Generator Fabricated on a Glass Fabric," *Energy & Environmental Science* 7 (2014): 1959–1965.

113. Y. Li, J. Zeng, Y. Zhao, et al., "Fabric-Based Flexible Thermoelectric Generators: Design Methods and Prospects," *Frontiers in Materials* 9 (2022): 1046883.

114. J. Zang, J. Chen, Z. Chen, et al., "Printed Flexible Thermoelectric Materials and Devices," *Journal of Materials Chemistry A* 9 (2021): 19439–19464.

115. M. Burton, G. Howells, J. Atoyo, and M. Carnie, "Printed Thermoelectrics," *Advanced Materials* 34 (2022): 2108183.

116. W. Zhou, Q. Fan, Q. Zhang, et al., "High-Performance and Compact-Designed Flexible Thermoelectric Modules Enabled by a Reticulate Carbon Nanotube Architecture," *Nature Communications* 8 (2017): 14886.

117. O. Bubnova, Z. U. Khan, A. Malti, et al., "Optimization of the Thermoelectric Figure of Merit in the Conducting Polymer Poly(3,4-Ethylenedioxythiophene)," *Nature Materials* 10 (2011): 429–433.

118. P. Sheng, Y. Sun, F. Jiao, C. Di, W. Xu, and D. Zhu, "A Novel Cuprous Ethylenetetrathiolate Coordination Polymer: Structure Characterization, Thermoelectric Property Optimization and a Bulk Thermogenerator Demonstration," *Synthetic Metals* 193 (2014): 1–7.

119. F. Zhang, Y. Zang, D. Huang, C.-a. Di, and D. Zhu, "Flexible and Self-Powered Temperature-Pressure Dual-Parameter Sensors Using Microstructure-Frame-Supported Organic Thermoelectric Materials," *Nature Communications* 6 (2015): 8356.

120. S. Lin, L. Zhang, W. Zeng, et al., "Flexible Thermoelectric Generator With High Seebeck Coefficients Made From Polymer Composites and Heat-Sink Fabrics," *Communications Materials* 3 (2022): 44.

121. M. Massetti, S. Bonfadini, D. Nava, et al., "Fully Direct Written Organic Micro-Thermoelectric Generators Embedded in a Plastic Foil," *Nano Energy* 75 (2020): 104983.

122. X. Yuan, P. Qiu, C. Sun, et al., "Extraordinary Self-Powered Y-Shaped Flexible Film Thermoelectric Device for Wearables," *Energy & Environmental Science* 17 (2024): 4968–4976.

123. N. J. Pataki, N. Zahabi, Q. Li, et al., "A Rolled Organic Thermoelectric Generator With High Thermocouple Density," *Advanced Functional Materials* 34 (2024): 2400982.

124. D. Huang, Y. Zou, F. Jiao, et al., "Interface-Located Photothermoelectric Effect of Organic Thermoelectric Materials in Enabling NIR Detection," *ACS Applied Materials & Interfaces* 7 (2015): 8968–8973.

125. Z.-D. Yu, Y. Lu, Z.-Y. Wang, et al., "High n-Type and p-Type Conductivities and Power Factors Achieved in a Single Conjugated Polymer," *Science Advances* 9 (2023): eadf3495.

126. Z. Liu, X. Wang, S. Wei, et al., "A Wavy-Structured Highly Stretchable Thermoelectric Generator With Stable Energy Output and Self-Rescuing Capability," *CCS Chemistry* 3 (2021): 2404–2414.

127. A. Lund, Y. Tian, S. Darabi, and C. Müller, "A Polymer-Based Textile Thermoelectric Generator for Wearable Energy Harvesting," *Journal of Power Sources* 480 (2020): 228836.

128. Q. Wu and J. Hu, "A Novel Design for a Wearable Thermoelectric Generator Based on 3D Fabric Structure," *Smart Materials and Structures* 26 (2017): 045037.

129. Y. Du, K. Cai, S. Chen, et al., "Thermoelectric Fabrics: Toward Power Generating Clothing," *Scientific Reports* 5 (2015): 6411.

130. X. He, X.-L. Shi, X. Wu, et al., "Three-Dimensional Flexible Thermoelectric Fabrics for Smart Wearables," *Nature Communications* 16 (2025): 2523.

131. C.-Y. Chang and C.-C. Wang, "Enhanced Stability and Performance of Air-Processed Perovskite Solar Cells via Defect Passivation With a Thiazole-Bridged Diketopyrrolopyrrole-Based π-Conjugated Polymer," *Journal of Materials Chemistry A* 8 (2020): 8593–8604.

132. V. Lotocki, A. M. Battaglia, N. Moon, H. M. Titi, and D. S. Seferos, "Conjugated Core–Shell Bottlebrush Polymers That Exhibit Crystallization-Driven Self-Assembly," *Chemical Science* 16 (2025): 920–932.

133. C. V. Manzano, B. Abad, M. Muñoz Rojo, et al., "Anisotropic Effects on the Thermoelectric Properties of Highly Oriented Electrodeposited Bi_2Te_3 Films," *Scientific Reports* 6 (2016): 19129.

134. D. Kim, S. B. Lee, M.-J. Kim, et al., "Low-Temperature Alignment of Conjugated Polymers by Plasticizer-Aided Physical Rubbing," *Small Methods* 7 (2023): 2300256.

135. K. Zhang, Y. Zhang, and S. Wang, "Enhancing Thermoelectric Properties of Organic Composites Through Hierarchical Nanostructures," *Scientific Reports* 3 (2013): 3448.

136. C. Ou, L. Zhang, Q. Jing, V. Narayan, and S. Kar-Narayan, "Compositionally Graded Organic–Inorganic Nanocomposites for Enhanced Thermoelectric Performance," *Advanced Electronic Materials* 6 (2020): 1900720.

137. Y. Zhang, S. Liu, J. J. Koh, and C. He, "Construction of a Hierarchical Multiscale Conducting Network for Enhanced Thermoelectric Response in Organic PEDOT:PSS Based Nanocomposites," *Journal of Materiomics* 7 (2021): 34–39.

Biographies



Daegun Kim is an assistant professor in the School of Chemical, Biological and Battery Engineering at Gachon University. He received his B.S. (2015) and Ph.D. (2021) in Chemical Engineering from Pohang University of Science and Technology (POSTECH). After gaining experience as a staff engineer at Samsung Electronics for three years, he joined the faculty at Gachon University. His research interests cover organic-based electronic materials and their applications, including transistors, sensors, and thermoelectric devices.



Hoimin Kim is a Ph.D. candidate at the SKKU Advanced Institute of Nanotechnology (SAINT), Sungkyunkwan University (SKKU), located in Suwon, Korea. He received his B.S. in Chemical Engineering from SKKU in 2021. His current research focuses on organic thermoelectric materials and their application in module fabrication, as well as exploring novel organic doping strategies.

25673173, 2025, 10, Downloaded from https://onlinelibrary.wiley.com/doi/10.1002/eom2.70029 by Hansol Lee - Gachon University Global Campus , Wiley Online Library on [29/09/2025]. See the Terms and Conditions (https://onlinelibrary.wiley.com/terms-and-conditions) on Wiley Online Library for rules of use; OA articles are governed by the applicable Creative Commons License



Il Jeon read Chemistry for Bachelors and Masters degrees at Oxford University. Upon graduation in 2008, he worked as the youngest senior researcher at LG Display for 5 years. In 2016, he received a Ph.D. degree from the University of Tokyo. After working as a JSPS fellow, he became an Assistant Professor at the same university. Later, he joined Sungkyunkwan University (SKKU) as a Full Professor and achieved an Early-Tenured Professorship. Currently, he serves as the Centre Director of SKKU Global Research Centre (SGRC) and Vice Provost of International Affairs. He has, thus far, published more than 120 lead-authored SCI papers.



Hansol Lee is an assistant professor in the School of Chemical, Biological and Battery Engineering at Gachon University, Korea. He received his B.S. (2013) and Ph.D. (2019) degrees in Chemical Engineering from Pohang University of Science and Technology (POSTECH). Following his doctoral studies, he worked as a postdoctoral researcher at the Center for Advanced Soft Electronics (2019–2021) and the Polymer Research Institute at POSTECH (2021–2022). His research focuses on polymeric materials for soft electronics, organic-based optoelectronic and energy conversion devices, and the chemical doping of conjugated polymers.



Boseok Kang is an Associate Professor in the SKKU Advanced Institute of Nanotechnology at Sungkyunkwan University (SKKU), Korea. He received a Ph.D. degree from Pohang University of Science and Technology (POSTECH) in Chemical Engineering (2015). He was a postdoctoral researcher at the Global Frontier Research Center for Advanced Soft Electronics (2016–2019) and in Cavendish Laboratory at University of Cambridge (2018–2019), and then joined the faculty at SKKU in 2019. His current research interests are various nanoscale phenomena occurred in organic electronic and energy devices.

25673173, 2025, 10, Downloaded from https://onlinelibrary.wiley.com/doi/10.1002/eem2.70029 by Hansol Lee - Gachon University Global Campus , Wiley Online Library on [29/09/2025]. See the Terms and Conditions (https://onlinelibrary.wiley.com/terms-and-conditions) on Wiley Online Library for rules of use; OA articles are governed by the applicable Creative Commons License